Molecular Mechanisms of Drug Transport at the Blood-CSF Barrier Revealed by Live Tissue Imaging and Quantitative Fluorescence Microscopy

Austin Sun

A dissertation

submitted in partial fulfillment of the

requirements for the degree of

Doctor of Philosophy

University of Washington

2023

Reading Committee:

Joanne Wang, Chair

Edward Kelly

Rodney Ho

Program Authorized to Offer Degree:

Pharmaceutics

University of Washington

Abstract

Molecular Mechanisms of Drug Transport at the Blood-CSF Barrier Revealed by Live Tissue Imaging and Quantitative Fluorescence Microscopy

Austin Sun

Chair of the Supervisory Committee:
Joanne Wang
Department of Pharmaceutics

The blood-cerebrospinal fluid barrier (BCSFB) is formed by the choroid plexus epithelial (CPE) cells, which express several polyspecific membrane transporters that contribute towards clearance of xenobiotic and endogenous compounds from the cerebrospinal fluid (CSF). However, BCSFB transporters are poorly characterized with respect to function, activity, and pharmacokinetic significance. Previous approaches using fluorescence microscopy to study BCSFB transport in intact choroid plexus tissues were poorly validated and more qualitative in nature due to the lack of real time quantitative methods for image analysis. This dissertation research is aimed to develop and validate an approach to study BCSFB transport activity through live tissue imaging and quantitative fluorescence microscopy, and subsequently utilize this approach and other biochemical approaches to elucidate the molecular mechanisms and

functional significance of organic anion transporting polypeptides (OATPs), breast cancer resistance protein (Bcrp), and P-glycoprotein (P-gp) at the BCSFB.

To better assess the transepithelial transport process at the blood-CSF barrier, I developed and validated a quantitative confocal microscopy approach to study CSF-to-blood organic anion and organic cation transport processes at the murine BCSFB in real time. Real time quantification of fluorescence occurring at different tissue compartments can enable the deconvolution of transport kinetics occurring at the apical (CSF-facing) and basolateral (blood-facing) membranes of the BCSFB. This approach was demonstrated to be consistent, reproducible, and capable of tracking transepithelial transport at the BCSFB with temporal and spatial resolution. I showed that large organic anion probes, 8-fluorescein-cAMP (fluo-cAMP) and fluorescein methotrexate (FL-MTX), are efficiently transported from the CSF compartment into the CPE cells and subsequently effluxed into the subepithelial space. Transport of the large organic anion probes were rate limited by the apical uptake transport, presumed to be mediated by OATPs. In contrast, the small organic cation and plasma membrane monoamine transporter (PMAT) substrate IDT307, was transported into CPE cells and retained. A novel parameter, choroid plexus efflux index (CPEI), was proposed to distinguish between transepithelial flux and CPE cell accumulation. The approach presented is valuable for the characterization of compartment specific accumulation of substrates, perpetrator drug interactions, and rate-determining steps in transepithelial transport at the BCSFB.

To elucidate the molecular mechanisms of OATP-mediated organic anion clearance at the blood-CSF barrier, I utilized the recently developed quantitative fluorescence microscopy approach alongside other biochemical approaches to probe OATP1A expression, localization, and function. Using RT-PCR and supporting literature data, we found that OATP1A5 is the

primary OATP1A isoform expressed on the apical, CSF-facing membrane Using quantitative fluorescence microscopy, I demonstrated that the fluorescent organic anions, sulforhodamine101 (SR101), FL-MTX, and fluo-cAMP were efficiently transported across the blood-CSF barrier. Transepithelial transport of these compounds across the CPE cells was abolished in Oatp1a/1b$^{-/-}$ mice, suggesting OATP1A5 is the primary contributor to large organic anion uptake in mice. Using transporter-expressing cell lines, the fluorescent probes were confirmed to be substrates of mouse OATP1A5 and its human homolog OATP1A2, corroborating our findings in the isolated CP and suggesting an overlap in function between mouse OATP1A5 and human OATP1A2. Immunofluorescence staining revealed the presence of OATP1A2 protein at the apical membrane in human CP tissues. Based on these data, we proposed that large organic anions in the CSF are actively transported into CPE cells by apical OATP1A2 (OATP1A5 in mice), then subsequently effluxed into the blood by basolateral multidrug resistance associated proteins (MRPs). As OATP1A2 transports a wide range of xenobiotics and endogenous compounds, the presence of this transporter at the BCSFB apical membrane may imply a novel route for removing neurohormones, drugs, and toxins from the CSF.

Previous studies report that P-gp and Bcrp are expressed apically or subapically at the blood-CSF barrier, implying a paradoxical function to mediate blood-to-CSF transport of xenobiotics. To probe P-gp and BCRP function at the BCSFB, I utilized the approach described in Chapter 2 alongside selective inhibitors and knockout models to functionally evaluate the activity, mechanisms, and potential interplay of P-gp and Bcrp BCSFB transport. Using qRT-PCR I identified the relative mRNA expression of P-gp and Bcrp isoforms at the murine BCSFB. Through quantitative fluorescence microscopy in isolated CP tissues of wild-type and Bcrp$^{-/-}$ mice, I demonstrated BODIPY FL-prazosin was actively transported by Bcrp, indicating

functional activity of apical Bcrp efflux. Furthermore, I detected an additional Bcrp-independent, elacridar-sensitive apical efflux mechanism at the BCSFB, suggested, but not confirmed, to be P-gp. As Bcrp and P-gp at the BCSFB apical (CSF-facing) membrane may contribute to the entry of endogenous compounds and nutrients into the CNS and may alter the disposition of drugs within the CNS, this study highlights the need for further research on characterizing the role of these transporters towards endobiotic and xenobiotic transport at the BCSFB.

This dissertation research has contributed greatly to our understanding of the molecular mechanisms mediating drug transport at the blood-CSF barrier. Notably, I revealed a functional role of OATP1A5 in clearing large organic anions at the BCSFB apical membrane from the CSF in mice and suggested a similar role for OATP1A2 at the human BCSFB. In addition, I have provided supporting evidence towards Bcrp and P-gp functional efflux activity at the BCSFB apical membrane in mice. Taken together, this research established an uptake transport mechanism of large organic anions at the BCSFB and provides novel mechanistic insights into several poorly defined transport pathways at the BCSFB. Knowledge gained from this dissertation research contributes to a mechanistic understanding of several major BCSFB drug transporters in regulating CSF drug concentrations and suggests potential roles of these transporters in modulating CNS disposition of drugs and endogenous substances. This knowledge can benefit our understanding of the relationship between CSF and unbound brain concentrations for transported drug substrates, which can subsequently improve the predictions of CNS drug disposition, efficacy, and toxicity in humans.

TABLE OF CONTENTS

LIST OF FIGURES

LIST OF TABLES

ACKNOWLEDGEMENTS

This journey would not have been possible without all the wonderful people that have supported me and that have worked alongside me during the PhD program.

Firstly, I would like to thank my advisor, Joanne Wang, for her guidance and support as my advisor throughout the PhD. Under Joanne's direction, I learned how to develop a keen eye to assess scientific data and how to clearly visualize and communicate my findings. I am grateful for my time working in your lab. Thank you for believing in me and supporting me as I piloted my project forward.

Thank you to my thesis committee, Drs. Kelly, Ho, Unadkat, and Xu for their insightful comments, career advice, encouragement, and technical expertise for the more challenging experiments in my work.

Thank you to all the members of the Wang lab that I overlapped with. I am very lucky to have worked with such an amazing, talented, friendly, and supportive group of scientists. Even though my project was very different from everyone else's, everyone in the lab was willing to provide crucial guidance and advice on how to push my research forward. I would like to especially thank Antonio, Leticia, and Tim. My project was not easy. There were many times that I felt lost, but I'm glad that I never felt alone. I am thankful to have gone through this journey with you all by my side, and our lab hangouts are some of my fondest memories of grad school.

Thank you to my parents, my 姥姥, and the rest of my family for their encouragement and pushing me to take new learning opportunities. I never would have made it this far without the foundation that you all have given me.

Most of all, thank you to Vanessa. Thank you for being by my side through this entire journey. Even though I spent so much time working in the lab these past 5-6 years in Seattle, that is not how I remember my time here. I remember finding new restaurants to try, camping and hiking in the summertime, and weathering a global pandemic with you by my side. I don't think I could have finished grad school without you.

To everyone else that I have met, worked with, and become friends with, thank you all for being a part of my life.

Chapter 1. INTRODUCTION

(Part of this chapter was published in:
Sun, A. and Wang, J."Choroid Plexus and Drug Removal Mechanisms" *The AAPS Journal* (2021) **23,** 61.)

1.1 INTRODUCTION TO THE CP-CSF SYSTEM AND ITS ROLE IN DRUG CLEARANCE

The mammalian central nervous system (CNS) is separated from the blood circulation by two major permeability barriers: the blood-brain barrier (BBB) and the blood-cerebrospinal fluid barrier (BCSFB). The BBB is formed by the endothelial cells of the brain capillaries, whereas the BCSFB is formed by the choroid plexuses (CP) located in the brain ventricles. While these barriers restrict the free entry of circulating substances into brain, they do not provide complete protection of the CNS from exposure to environmental substances, drugs, and other potentially harmful compounds. Lipophilic compounds can cross these barriers by passive diffusion whereas hydrophilic substances may enter the brain through transporter-mediated processes. Furthermore, metabolic wastes and neurotoxic species can be generated within the brain by physiological and pathophysiological processes. Thus, timely and efficient removal of xenobiotics and metabolites from the brain is crucial for maintaining the homeostasis and normal function of the brain.

The CP-CSF system utilizes several different mechanisms to maintain healthy brain homeostasis. The CP produces CSF that bathes and cushions the brain. As the CSF flows through the ventricular system and gets reabsorbed into the general circulation, drugs, metabolites, and macromolecules are cleared from the brain. The CPE cells can also actively remove solutes from the CSF by transporting them across the BCSFB into the blood circulation. This process is conducted through specific uptake and efflux transporters expressed by the CPE cells. While beyond the scope of this introduction, the CPE cells also express several intracellular detoxifying

and conjugating enzymes, which enzymatically inactivate reactive or toxic substances. This chapter provides a current review of CSF bulk flow and BCSFB transporter-mediated clearance processes within the CP-CSF system. Following a brief overview of the anatomical features of the CP-CSF system, the functional characteristics and major contributors to the major clearance pathways are summarized. Recent developments in CSF flow dynamics and the impact of CP transporter on CSF drug concentrations are highlighted. The relevance of the CP drug removal mechanisms to the interplay of drug concentrations between the CSF and the brain interstitial fluid is also discussed.

1.2 ANATOMY AND FUNCTIONS OF THE CP-CSF SYSTEM

The brain ventricular system is highly conserved across mammalian species and consists of a set of interconnected cavities (lateral, third and fourth ventricles) filled with the CSF (1,2). The fourth ventricle is continuous with the central canal of the spinal cord, allowing the CSF to flow down the canal and circulate to the subarachnoid space (**Figure 1.1**). The CP is a secretory tissue located in each brain ventricle that continuously secretes CSF into the ventricles. The CP tissues from the lateral, third and fourth ventricles share similar ultrastructure, consisting of an outer layer of cuboidal epithelial cells surrounding a core of capillaries and connective tissue (**Figure 1.1**). Unlike the endothelial cells forming the BBB, the CP capillaries are fenestrated with leaky inter-endothelial junctions. This facilitates the rapid exchange of water and solutes between the general circulation and interstitial fluids in the subepithelial space. The CPE cells are joined by tight junctions that restrict the free exchange of solutes and macromolecules between the blood and CSF (i.e. the blood–CSF barrier). The CPE cells are polarized with their apical membrane domain facing the CSF and the basolateral membrane facing the blood circulation (**Figure 1.1**). The apical

domains of the CPE cells have a brush border lining (microvilli) that effectively enlarges the surface area by 10-30 fold (3).

A primary function of the CP is to manufacture and secrete CSF. This process is accomplished by inorganic ion and water transport across the CP epithelium. A network of ion pumps, ion transporters and channels expressed at the basolateral and apical membranes of the CPE cells mediate the net flux of Na^+, Cl^-, and HCO_3^- across the CP epithelium from the blood side to the CSF side. This creates an osmotic pressure gradient which then drives the flow of plasma water across the CP membranes into the ventricles (4). On the other hand, there is a net flux of K^+ from the CSF to the blood. Overall, the CSF is 5 mOsM hyperosmolar compared to the plasma, with a 5mV transepithelial electrical potential difference across the CPE epithelium (4–6).

The CP–CSF system carries out several physiological functions crucial for the hemostasis and normal functions of the brain. The CSF provides buoyancy to the brain, which reduces the effective brain weight by about 70% in humans and protects the brain from the adversity of gravity and mechanical injury (2). The CP is also an entry site for micronutrients and hormones (e.g. vitamin C, folate), which are further carried by CSF to nourish internal brain cells. The CP-CSF system is essential for clearing waste products and xenobiotics from the brain, which is the focus of this review. The CP-CSF system employs three co-existing and intertwined pathways to clear metabolic wastes, protein debris, drugs, and environmental substances from the CNS. These clearance mechanisms, i.e. clearance by bulk CSF flow, transport and metabolism in CPE cells, will be discussed in detail. In addition, emerging studies suggest that CP serves a gateway for immune cell entry into the CNS and also plays an active role in the regulation of neural stem cells (1,2). CP-associated macrophages are understood to monitor ventricular CSF in healthy conditions, while memory T cells monitor the subarachnoid and leptomeningeal CSF (7–9).

During neuroinflammation, CPE cells respond by recruiting and trafficking leukocytes into the CNS (10).

1.3 CLEARANCE VIA CSF FLOW

1.3.1 *CSF composition and flow dynamic*

In humans, about 500–600 mL of CSF is produced each day. The majority of the CSF is produced by the CPs, with the remainder of CSF derived from drainage from brain interstitial fluid and passage across the blood arachnoid barrier (11–13). The CSF is not an ultrafiltrate of the plasma (14,15) and is slightly hypertonic compared to the plasma (4). Compared to the plasma, the CSF has lower protein and cell density, with slightly altered ion and solute concentrations. The Na^+, $HCO3^-$, Cl^- and Mg^{2+} ion concentrations are slightly higher in the CSF while K^+ and Ca^{2+} concentrations are lower (11). The protein concentration in the CSF is two to three orders of magnitude lower than that in blood, ranging from 15-45mg/dl in young adults (16,17). Around 20% of the total CSF protein originates from the brain, with the remainder derived from the plasma (18). The CSF also contains a small circulating cell population, estimated to be 5 cells per mL (19). This population includes leukocytes associated with immune surveillance.

Historically, the net circulation of CSF is thought to be unidirectional. Following production, the CSF flows from the lateral ventricles through the interventricular foramina into the third ventricle. The CSF flows outward through the cerebral aqueduct to the fourth ventricle, where it then travels through the median aperture into the cisterna magna and the greater cranial subarachnoid space. From there, the CSF can also flow caudally into the spinal subarachnoid space (19). The CSF is cleared through reabsorption at the arachnoid villi or by drainage along the cranial nerve sheaths into the lymphatics (13,19). The flow of CSF is pulsatile, corresponding with the cardiac cycle (20). While the net movement of CSF is directional from the ventricles to

subarachnoid spaces, the second-to-second pulsatile movement enables mixing of contents between the different CSF compartments (13,21,22).

The average flow rate of CSF is estimated to be 0.37 mL/min in humans, based on ventriculo-cisternal perfusion measures (23–25). The CSF flow rate is also age dependent. Older populations have been shown to have impaired CSF production and flow (26–29). Additionally, CSF production is further reduced in patients with neurodegenerative disorders (30–32). Neurodegenerative diseases such as Alzheimer's, Parkinson's, and multiple sclerosis are characterized by misfolded proteins or protein aggregates that may be harmful (or pathogenic). Given the significance of CSF bulk flow in clearing such wastes from the CNS, there is substantial interest in studying the role of CSF production and flow in pathogenesis of these diseases.

Recent evidence has also pointed to a relationship between sleep cycles and CSF production and flow patterns. A study utilizing magnetic resonance imaging to visualize CSF flow found that CSF production followed the circadian cycle, with increased production during nighttime (20). In addition, a study by Alperin et al. suggested that a supine position increased the oscillatory CSF volume relative to the upright position (33). This contributed to the hypothesis that sleep contributes to healthy brain function by increasing CSF-mediated clearance of waste products out of the CNS. A study published in 2019 explored CSF flow characteristics in humans during sleep (34). The authors were able to observe unique patterns of CSF pulsatile flow during non-rapid eye movement (REM) sleep. While CSF typically flows directionally out of the ventricles in an awake state, an opposing pulsating flow of CSF into the ventricles was observed in subjects experiencing non-REM, slow-wave sleep (34). This reversal of CSF flow during slow-wave sleep is thought to facilitate the mixing of subarachnoid and ventricular fluids, which may

facilitate communication between fluid compartments and the overall clearance of waste products (35).

1.3.2 *Cerebrospinal fluid and brain interstitial fluid exchange and the glymphatic system hypothesis*

The cells of the brain parenchyma are surrounded by the interstitial fluid (ISF), which is essential for cell-cell communication and maintaining healthy brain homeostasis. Unlike other organs, the brain lacks a true lymphatic system to assist in the removal of interstitial metabolic waste products (36,37). Instead, the CSF maintains an analogous role for the CNS, responsible for the clearance of metabolic wastes and cellular debris from the brain (13). The brain ISF, containing debris and waste products from brain cells, exchanges with the CSF. The CSF renews the ISF and removes waste products by continuously flowing out of the brain. While this concept is widely appreciated, how fluid and solute exchange between the CSF and the ISF occurs has not been fully understood.

It was previously assumed that CSF and brain ISF freely exchanged with one another and were in rapid equilibrium. This led to the notion that the BCSFB could act as a drug delivery pathway to the CNS and brain parenchyma (38). However, failures in drug development based on this rationale led to this notion falling out of favor. Subsequent research began to unveil that the exchange between CSF and brain ISF was much more nuanced than previously assumed. In some studies, diffusion appeared to dominate, whereby molecular size of the solute and distance from the CSF system dictated the clearance rate from the brain ISF (39–41). However, other studies found that compounds, regardless of molecular size, disappeared from the brain ISF at similar rates, suggesting a bulk flow (i.e. advection) of ISF into the CSF (36,42–44).

In 2013, Iliff et al. published a seminal paper on the 'glymphatic system', a term coined to describe brain CSF-ISF exchange routes along the perivascular spaces (45). The authors demonstrated that cisternal CSF injection of fluorescent tracers into mice led to tracer accumulation alongside cerebral surface arteries. At later time points, tracers accumulated along parenchymal venules and cerebral veins. Furthermore, knockout of Aquaporin-4 significantly reduced the movement of the tracers used. Based on these observations, a brain-wide glymphatic system was proposed for fluid movement in the brain, which includes the para-arterial influx of subarachnoid CSF into the brain interstitium, followed by the clearance of ISF along large draining veins. Aquaporin-4, a water channel protein expressed at the astrocytic end feet, is thought to provide the driving force for the continuous movement of fluid through the glymphatic system. This system is thought to play a critical role in the clearance of interstitial solutes and macromolecules including $A\beta_{1-40}$ from the brain.

Since the work of Iliff et al., the idea and significance of the glymphatic pathway has been a subject of great interest and debate. Xie et al. demonstrated that mice showed increased glymphatic exchange between CSF and brain ISF when asleep through fluorescent tracer infusions (46). They additionally demonstrated that Aβ, the main component of amyloid plaques characteristic of Alzheimer's disease, was cleared from the brain faster in sleeping mice (46). A study by Smith et al. demonstrated that loss of Aquaporin-4 did not change transport of fluorescent tracers from the subarachnoid space to the brain (47). However, a later study by Mestre et al. demonstrated that loss of Aquaporin-4 did indeed decrease tracer transport across four independently generated knockout lines (48). Some groups contend that diffusion between the CSF and brain ISF is still the predominant mechanism of solute exchange (13,41,47,49,50). There is still no consensus on the relative contribution of glymphatic flow to total CSF/brain ISF exchange

(13,41). Regardless, debates surrounding the glymphatic hypothesis have renewed discussions and interests in the relationship between brain ISF and CSF, which is also relevant to drug distribution kinetics in the brain and the prediction of CNS pharmacokinetics.

1.4 `TRANSPORTER MEDIATED CLEARANCE

Membrane transporters can have a large influence on the disposition of drugs. These drug transporters have been extensively studied in the small intestine, liver, and kidney, where they contribute to the systemic absorption and clearance of their drug substrates (51). In peripheral tissues, transporters can determine local tissue concentrations, impacting drug efficacy or tissue-specific toxicity (52). The BCSFB expresses xenobiotic transporters responsible for the elimination of harmful compounds from the CSF. The apical (CSF-facing) membranes of the CP epithelial cells have microvillous structures, increasing the absorptive surface area and thus enabling efficient extraction of xenobiotics from the ventricular CSF. Clearance across the BCSFB typically occurs in a stepwise manner. First, uptake transporters on the apical membrane transport a substrate from the CSF into the CPE cells. Efflux transporters on the basolateral (blood-facing) membrane then remove the substrate out of the cell and into the blood, where they can be further delivered to the liver or the kidney for systemic elimination.

There are two superfamilies of transporters, the ATP-binding cassette transporters (ABC) and the solute carrier transporters (SLC) (53). The ABC transporters utilize ATP hydrolysis to actively efflux substrate out of cells. There are about 48 ABC transporter members in humans. The SLC transporters are a more diverse superfamily of transporters, consisting of over 400 members. Some SLC transporters utilize electrochemical or ion gradients to actively transport substrates across the membrane while others operate as facilitative transporters (54). Previous gene profiling studies have indicated the presence of several polyspecific xenobiotic ABC and SLC transporters at the

choroid plexus (55–57). We previously performed Slc transporter gene profiling in the mouse brain and our results showed that Slc transporter expression profiles at the BCSFB are substantially different from that at the BBB and other brain areas (55,56). Recently, absolute protein expression levels of xenobiotic transporters have been determined using quantitative targeted proteomic methods in several different species (58–60).

Current methods to study BCSFB transport function *in vitro* or *ex vivo* include transport assays using conditionally immortalized CPE cells, primary culture of CPE cells, and freshly isolated CP tissue (61). While cell-based systems are straightforward for drug transport analyses using standard uptake or transwell assays, immortalized CP cell lines and primary CP cells have been demonstrated to have lower expression of xenobiotic transporters and weakened tight junction formation (62). Freshly isolated CP tissues from preclinical species maintain the tissue physiology, barrier integrity and transporter expression reflected *in vivo;* and transport studies in isolated CP tissues have contributed to much of our understanding of the functional transport systems at the BCSFB. However, human CP tissues are difficult to obtain and cannot typically be studied using this approach. Further, the anatomy of the isolated tissue only allows for the study of CSF-to-blood drug transport in vitro. Recently, a human pluripotent stem-cell derived organoid model has been developed for CP (63). The organoids developed tight junctions and produced CSF-like fluid in a self-contained compartment. They also appear to express xenobiotic transporters previously observed at the CP (63). This newly established CP organoid system represents a novel and promising *in vitro* approach to characterize human CP function and aid in the study of drug transport at the BCSFB.

In this section, we highlight the ABC and SLC drug transporters whose functional roles at the choroid plexus epithelial cells that form the BCSFB have been unequivocally established with

transporter knockout mice studies. These include the SLC uptake transporters organic anion transporter 3 (OAT3), peptide transporter 2 (PEPT2), and plasma membrane monoamine transporter (PMAT), and the ABC efflux transporters multi-drug resistance-associated proteins (MRPs) 1 and 4. These transporters compose the pathways of clearance for organic anions, small peptides, and organic cations (**Figure 1.2**). We next highlight other ABC and SLC xenobiotic transporters have been indicated to be expressed at the BCSFB, although their functional roles in drug transport at the BCSFB are less characterized. These include Bcrp, P-gp, and Oatps(57,58,64). For a general review of transporter expression and localization at the BCSFB, see the review by Morris et al. 2017 (65).

1.4.1 *Functionally Characterized Uptake Transporters*

1.4.1.1 <u>OAT3 (SLC22A8)</u>

OAT3 is a tertiary active uptake transporter that operates through dicarboxylate exchange, typically utilizing alpha-ketoglutarate as a counterion (66). Outside of the BCSFB, OAT3 is expressed in the kidney, brain capillary endothelium, and retina (67). OAT3, alongside OAT1, is basolaterally expressed in the kidney proximal tubules and plays a major role in mediating tubular secretion of small organic anion compounds from blood to urine. Drug substrates include antineoplastic drugs, antiviral drugs, antibiotics, and diuretics (Table 1.1). Oat3 knockout studies indicate reduced clearance of methotrexate and penicillin G due to diminished renal secretion (68,69). The International Transport Consortium and the Food and Drug Administration recognize OAT3, alongside OAT1, as determinants of clinical drug interactions (53).

Active removal of organic anions from the CSF has been observed in humans since the 1960s (70–73). Compounds like penicillin G and methotrexate were observed to have much lower CSF levels compared to blood when systemically administered, limiting the utility of these

compounds for the treatment of meningitis and brain cancer. Penicillin G and methotrexate clearance from the CSF were both observed to be sensitive to probenecid inhibition (71,74). Soon after the discovery of the organic anion transporter family, Oat3 was found to be expressed at the apical membrane of the CPE cells and confirmed to be functionally active through knockout studies, responsible for apical uptake of substrates from the CSF (75,76). Radiolabel uptake studies using para-aminohippurate, a prototype Oat substrate, showed marked reduction in Oat3 knockout CP tissue compared to wild-type controls. Transport was shown to be sodium dependent and sensitive to probenecid inhibition, consistent with Oat function. Confocal imaging studies indicated significant accumulation of fluorescein in wild-type CP, while accumulation in the Oat3 knockout CP was significantly reduced (76,77). In wild type CP, fluorescein primarily accumulated in the blood capillaries adjacent to the CP, suggesting a coupled efflux system exists at the basolateral membrane, leading to a CSF-to-blood directional clearance of small organic anions. As discussed below, members of the MRP families are most likely to mediate the efflux step of organic anions at the basolateral membrane.

1.4.1.2 PEPT2 (SLC15A2)

PEPT2 is a member of the proton-coupled oligopeptide transporter family (SLC15) first identified in 1995 (78). PEPT2 is a secondary active uptake transporter driven by the proton gradient through proton co-transport (79). PEPT2 primarily transports di- and tri- peptides alongside peptidomimetic drugs. Drug substrates include amoxicillin and cephalosporin antibiotics (Table 1.1). PepT2 is primarily expressed at the kidney and the CP, but transcripts have also been observed in the lungs, mammary glands, and spleen (79). PepT2 is the predominant peptide transporter at the kidney, responsible for tubular reabsorption of filtered di- and tripeptide substrates. Knockout of PepT2 results in 2-3-fold reductions in systemic exposure of its substrates

due to increased renal clearance. This has been observed for GlySar, cefadroxil, and carnosine in pharmacokinetic studies utilizing PepT2 KO mice (80–83).

PepT2 is localized on the apical membrane of CPE cells, responsible for uptake of substrates from the CSF (84,85). In CP tissues isolated from PepT2 knockout mice, uptake of GlySar, a probe substrate of Pept2, was reduced by 90%, demonstrating that PepT2 is the primary di- and tri-peptide uptake transporter at the BCSFB (86). While coupled uptake and efflux has been observed for small organic anions at the BCSFB, there does not appear to be a coupled basolateral efflux system for small peptide drugs. A study characterizing transport properties of PepT2 in rat CP epithelial tissue and primary culture cells observed unsaturable cellular efflux of cefadroxil, indicating that basolateral efflux may occur by passive diffusion (87). Functional characterization of PepT2 has also been studied through *in vivo* pharmacokinetic studies. In Pept2 knockout mice, CSF: blood ratio of cefadroxil increased by 6 fold as compared to wild type animals (82). More recently, using *in vivo* intracerebral microdialysis, it was shown that PEPT2 ablation significantly increased the brain ISF and CSF levels of cefadroxil after IV infusion (88). Together, these studies demonstrated that PEPT2 at the CP contributes to BCSFB-mediated drug clearance from the CSF and limits brain exposure to cefadroxil and possibly other di- and tripeptide drugs.

1.4.1.3 <u>PMAT (SLC29A4)</u>

PMAT is a newer polyspecific organic cation transporter first cloned and characterized by our laboratory (89). Initially suspected of transporting nucleosides, PMAT was found to transport a wide range of organic cation compounds. Its substrate profile includes monoamine neurotransmitters, neurotoxins, and cationic drugs, with substrate overlap with the organic cation transporters (OCT) in the SLC22 family (90) (Table 1.1). PMAT also strongly interacts with HIV

protease inhibitors; lopinavir acts as a potent and selective PMAT inhibitor (91). Transport by PMAT is electrogenic, utilizing the membrane potential gradient as its driving force (89,90,92,93). PMAT mRNA is highly expressed in the brain, although lower levels of mRNA transcripts are also found in the other tissues (89,94,95). Within the brain, PMAT is broadly distributed with highest expression found the CP, cerebral cortex, hippocampus, and cerebellum (94). PMAT is believed to play a role in regulation of monoamine neurotransmission, while also contributing to tissue specific disposition of organic cation drugs and toxins (90).

Work conducted in our laboratory has established the expression and function of PMAT at the blood-CSF barrier. PMAT is expressed and localized on the apical membrane of CPE cells, responsible for uptake of substrates from the CSF into CPE cells (96). Prior to the discovery of PMAT, organic cation transporter 2 (OCT2) was thought to be a mediator of organic cation uptake at the BCSFB. In particular, Sweet et al. showed that mRNA expression of Oct2 by RT-PCR and demonstrated an apical localization when GFP-tagged rat Oct2 was transfected into rat CP (97). However, protein expression and activity of endogenous Oct2 was never demonstrated in the rat CP. Our laboratory and others were unable to confirm Oct2 expression at the rodent BCSFB (57,58,96). Using quantitative real time PCR, we compared polyspecific organic cation transporter expression at both the human and mouse CP tissues (96). Our results showed that PMAT was expressed at much higher levels than any other transporter tested; other organic cation transporters, including OCT1/2/3 and MATE1/2 were found to be minimally expressed. Protein expression of PMAT in human tissues was further confirmed by western blot and immunostaining (96). To further establish the role of PMAT at the BCSFB, we developed a Pmat knockout mouse model. Using this model, we observed significant decreases in organic cation and monoamine uptake in isolated CP from Pmat knockouts. Inhibitors of the Octs and neurotransmitter transporters had no

effect on CP uptake of organic cations. These results clearly demonstrated that PMAT, rather than the OCTs, is responsible for the organic cation uptake in the CP (96). By removing its substrates from the CSF, PMAT could play an important role in protecting the brain from cationic neurotoxins and other potentially toxic organic cations.

Currently, it is unknown how organic cations are effluxed out of the CPE cells at the basolateral membrane. MATE1/2, the proton-organic cation exchangers responsible for the final organic cation excretion step in renal tubular cells, are minimally expressed in CPE cells and thus may not play a significant role in organic cation efflux at the BCSFB. Miller et al. previously suggested that basolateral efflux of organic cations may occur through a vesicular transport mechanism independent of a carrier-mediated pathway (98).

1.4.2 *Functionally Characterized Efflux Transporters*

1.4.2.1 MRP1 (ABCC1)

The MRP subfamily transporters act as primary active ATP-dependent efflux transporters of endogenous substrates and xenobiotics. The first member of the MRP subfamily, MRP1, was first cloned and identified in 1992 (99). Initially found to efflux chemotherapeutics in cancer cells, MRP1 was later found to be ubiquitously expressed in the body with a wide substrate profile and capable of transporting both hydrophobic and anionic molecules. Endogenous substrates include glutathione or other anionic conjugates, while xenobiotic substrates include antineoplastic, antibiotic, and antiviral drugs (100) (Table 1.1).

MRP1 has been primarily studied in the context of multidrug resistance in cancer. MRP1 overexpression in cancer tissues is associated with reduced overall survival and relapse propensity in cancer patients (101). Although MRP1 is ubiquitously expressed in the body, it does not appear to play a significant role in systemic drug disposition. However, tissue-specific protective effects

have been observed with MRP1. MRP1 expressed in the heart has a cardioprotective role during chemotherapy, where polymorphisms in MRP1 expression have been linked to drug-induced cardiac dysfunction and toxicity (101–104).

Mrp1 is expressed and localized to the basolateral membrane of CPE cells, consistent with a role in CPE-to-blood transport of drugs out of the CSF and preventing drug entry into the CSF from general circulation (64,105). Mrp1 activity was initially demonstrated by Rao et al., who showed that ^{99m}Tc-sestamibi transport across rat CP was sensitive to inhibition by MK-571, an inhibitor of MRPs (64). The role of Mrp1 at the BCSFB was further evaluated in an *in vivo* study in Mrp1 deficient mice by Wijnholds, et al (106). In Mrp1 KO mice, a 10-fold increase in CSF accumulation of etoposide, a chemotherapeutic agent, was observed after intravenous administration of the drug (106). In contrast, there is no change in total brain and plasma drug levels. These data suggest that Mrp1 at the BCSFB plays an important role in determining drug levels in the CSF, either by limiting drug entry from the blood and/or by promoting drug efflux from the CSF.

1.4.2.2 MRP4 (ABCC4)

MRP4, first identified and cloned in 1997, also has a wide tissue distribution, though not as ubiquitous as MRP1 (107). Outside of the CP, MRP4 is notably expressed in the liver, kidney, and blood-brain barrier (108,109). In the liver, MRP4 is located at the sinusoidal membrane and mediates efflux of compounds from the hepatocytes into the blood, which represents an important protective function under cholestasis (110). In the kidney, MRP4 is apically localized in proximal tubule epithelial cells, where it contributes to the active tubular secretion of a range of small anionic drugs (108). Substrates of MRP4 include nucleoside analogues, diuretics, antivirals, antibiotics, and antineoplastic drugs (108) (Table 1.1).

Similar to Mrp1, Mrp4 is expressed and localized to the basolateral membrane of CPE cells, contributing to CPE-to-blood efflux of drugs out of the CSF (111). Mrp4 has been shown to limit accumulation of topotecan into the CSF (111). Mrp deficient mice demonstrated 10 fold higher concentrations of topotecan in the CSF compared to wild-type controls. (111). However, since Mrp4 is normally expressed at both the BCSFB and the BBB, the relative contribution of Mrp4 at the two barriers to brain drug levels could not be determined. Mrp4 has also been shown to contribute to active removal of compounds from the CSF in *ex vivo* tissue studies (112). Confocal imaging of fluorescein-cyclic AMP (fluo-cAMP), a fluorescent MRP4 probe, in isolated rat CP showed rapid accumulation of fluo-cAMP in subepithelial blood vessel areas, indicating a rapid transcellular flux of the fluorescent probe from the CSF side to the blood side. Transport of fluo-cAMP was insensitive to Mrp1 inhibition but was reduced by Mrp4 selective inhibitors, indicating the involvement of Mrp4 (112). Mrp4 activity and expression has also been demonstrated using immortalized CP epithelial cell lines (62). Recently, Mrp4 expression at the mouse CP was shown to be sex-dependent with male mice displaying a significant reduction in Mrp4 expression (113). Consistent with the expression data, vascular accumulation of fluo-cAMP was markedly reduced in CP tissues isolated from male mice (113). These studies strongly suggested a significant role of Mrp4 in promoting drug efflux at the basolateral membrane at the BCSFB. As many Mrp4 substrates are organic anions also transported by the apical Oat3, it is likely that these transporters form a transepithelial transport pathway to actively remove anionic drugs and metabolites from the CSF (**Figure 1.2**).

1.4.3 *Under characterized Uptake and Efflux Transporters*

The uptake and efflux transporters described in this section are poorly characterized with respect to drug transport at the BCSFB. These transporters may have narrow substrate profiles,

have limited or conflicting information on their expression and localization, or have limited functional characterization using experimental systems that may not reflect the *in vivo* transport. Therefore, the pharmacokinetic significance of these transporters at the blood-CSF barrier remains unknown.

1.4.3.1 OATP (SLCO)

The Organic anion-transporting polypeptide (OATP) family consists of over 300 total family members, with 11 family members currently identified in humans (114). OATPs typically operate as uptake transporters and transport a wide range of amphipathic organic anion endobiotics and xenobiotics. OATPs are expressed in many different tissues of the body, but these transporters best known for their role in drug disposition in the liver. The liver-specific isoforms OATP1B1 and OATP1B3, are expressed on the sinusoidal membrane of hepatocytes, where the transporters play an important role in the uptake of statin drugs, repaglinide, and other amphipathic anionic compounds (115). Liver OATPs can thus represent a significant drug-drug interaction liability. For example, coadministration of statin drugs with the OATP inhibitor cyclosporine can result in systemic AUC increases between 2-fold and 20-fold (115).

Several Oatp isoforms are purported to be expressed at the choroid plexus. The transporter Oatp1c1 is understood to play an important role in brain thyroid hormone homeostasis and is highly expressed at the rodent BCSFB at the mRNA level(116,117). The transporter primarily transports the thyroid hormones thyroxine (T4) and reverse T3, but also transports more typical Oatp substrates such as taurocholate, estradiol 17-β-D-glucuronide, and some statins (118). Immunofluorescence studies of Oatp1c1 suggest the transporter is localized to both membranes of the BCSFB, with a bias towards the basolateral membrane (119). Oatp3a1 is a prostaglandin transporter expressed on both membranes of the BCSFB (120). There have been 3 splice variants

identified for Oatp3a1. The Oatp3a1_v1 variant is expressed on the basolateral membrane of the BCSFB, while the Oatp3a1_v2 and Oatp3a1_v3 variants are expressed on the apical membrane of the BCSFB (120,121). Oatp3a1. The transporter does not transport classical Oatp substrates taurocholate or estrone-3-sulfate, though it may have some low affinity uptake of DHEAS (120,121). Oatp1a4 and Oatp1a5 are purported to be expressed at the basolateral and apical membranes of the rodent choroid plexus, respectively (122,123). These two transporters have a wider substrate pool, transporting the endogenous Oatp substrates taurocholate, DHEAS, estrone-3-sulfate, and estradiol 17-β-D-glucuronide and some drug substrates such as fexofenadine and statins (124–127). To our knowledge, Oatp1a4 functional activity has not been characterized at the rodent BCSFB. Oatp1a5 has been previously suggested to mediate organic anion uptake at the BCSFB (112,123). However, the functional contribution of Oatp1a5 towards organic anion uptake at the BCSFB has not been studied either using a specific substrate, or by using a specific inhibitor or knockout model. In the human choroid plexus, the functional role of OATP1A is unclear. The OATP1A2 isoform is the only OATP1A ortholog in humans. While SLCO1A2/OATP1A2 is expressed at the mRNA level (117), protein expression and localization of OATP1A2 has not been demonstrated at the human choroid plexus. Furthermore, species differences between rodent and human OATP1A isoforms have been shown (128), and it is therefore unclear the extent of substrate and function overlap across the species.

1.4.3.2 <u>P-gp (MDR1) and BCRP (ABCG2)</u>

The two transporters - breast cancer resistance protein (BCRP) and P-glycoprotein (P-gp) - are primary active ATP-dependent efflux transporters with a wide and considerably overlapping substrate pools. The two transporters have been extensively studied for their proposed role in multidrug resistance, whereby patient with cancer would develop resistance to structurally related

antineoplastic compounds (129). The expression of P-gp, BCRP, MRP1, and other ABC efflux transporters at tumor sites were believed to limit chemotherapeutic entry and contribute to the multidrug resistance phenotype (129). However, attempts overcome multidrug resistance by targeted inhibition of P-gp and other ABC transporters has been challenging. Currently, BCRP and P-gp are understood to transport not only chemotherapeutic agents, but also a range of non-chemotherapeutic drugs (130,131). The two transporters can have a significant role in the pharmacokinetics of their substrates. Furthermore, there is an emerging appreciation for the role of P-gp and BCRP in the transport of physiological substrates. P-gp can transport a variety of steroids, glucocorticoids, cytokines, and other important endogenous compounds (132). BCRP transports uric acid, and some genetic polymorphisms of BCRP are associated with higher uric acid sevels in the serum and the onset of gout (131). Other physiological compounds such as riboflavin, vitamin K, and folic acid are substrates of BCRP (133); however, the role of BCRP towards the transport of these nutrients has not been fully clarified.

P-gp is notably expressed in the intestine, liver, kidney, placenta, and the microvessel endothelial cells forming the blood-brain barrier (130). In humans, BCRP is expressed in many different tissues, including the small intestine, liver, kidney, the placenta, the mammary glands, and the microvessel endothelial cells forming the blood-brain barrier (131,134). At the blood brain barrier, BCRP and P-gp are both expressed at the luminal membrane, where they limit the entry of their substrates into the brain. For example, after infusion of the BCRP substrate dantrolene in wild-type and KO mice, the brain to plasma concentration ratio of dantrolene increased 3.3-fold in Bcrp knockout rats compared to wild-types, with no change in Mdr1a (P-gp) KO mice (135). For the P-gp substrate WEB 2086, brain to plasma concentration ratio increased 8-fold in Mdr1a KO, with no change in Bcrp KO mice (135). In some cases, compounds may be a substrate of both

BCRP and P-gp, and the two transporters can potentially synergistically limit CNS penetration of the shared substrate, whereby the inhibition or loss of function of both transporters can result in disproportionate increases of brain drug concentrations. Polli et al. conducted a study infusing the tyrosine kinase inhibitor lapanitib into wild-type, Bcrp KO, Mdr1a/b (P-gp) dual KO, and Bcrp/Mdr1a/b triple KO mice. Lapatinib had no change in brain-to-plasma ratio in Bcrp KO and a 3-to-4-fold increase in brain-to-plasma ratio in Mdr1a/1b (P-gp) dual KO mice compared to wild-types. However, in the triple KO mice, brain-to-plasma ratios were 40-fold higher compared to wild-types (136).

At the BCSFB, studies on Bcrp and P-gp expression, localization, and activity are limited and sometimes conflicting. Bcrp protein expression has been shown in the choroid plexus of rats, pigs, and a single human subject using a quantitative proteomics approach (58,60). Bcrp protein was under the limit of quantification in dog choroid plexus using a similar approach (59). P-gp protein was expressed in in all four species in the same studies (58–60). Using immunohistochemistry and immunofluorescence approaches, Bcrp has been localized to the apical membrane in mice (137,138), the basolateral membrane in neonatal rats (139), and undetectable in adult rats and humans in other studies (139–142). By immunohistochemistry and immunofluorescence, P-gp has been localized apically or subapically in rat, pig, and neonatal human CP (64,142,143). No detection of P-gp was found in a separate immunofluorescence study in rat CP (141). Functional studies of P-gp and Bcrp at the BCSFB are similarly conflicting and may utilize experimental systems that may not reflect *in vivo* transport. Transport of calcein-AM, a P-gp probe, was sensitive to valspodar, a P-gp inhibitor, in several rat and human cultured cell lines (62,144). The P-gp substrate ^{99m}Tc-sestamibi was transported in rat CPE primary cells and sensitive to elacridar (64). However, two P-gp substrates, rhodamine123 and verapamil, were not

transported in porcine primary cells (143). Evidence of Bcrp function at the BCSFB is even more limited; a single study demonstrated transport of BODIPY Fl Prazosin, a BCRP fluorescent probe, was sensitive to the BCRP specific inhibitor Ko143 in cultured human papilloma cells (144).

While transport at both the BCSFB and the BBB can mediate drug concentrations in the CNS, transport processes at the BCSFB remain under characterized and most pharmacokinetic models of the CNS do not consider active transport by the BCSFB. Additional study of these under characterized BCSFB transporters outlined in this section could clarify their role in CSF clearance, improving our predictions of CSF and ISF drug concentrations and informing future CNS drug development.

1.5 Relationship between CSF and brain ISF and pharmacokinetic significance

The relationship between CSF and brain ISF has been the subject of great interest, particularly with respect to the effective drug concentration in the brain. Based on the free drug hypothesis, the free or unbound drug concentration is assumed to be responsible for its pharmacological effect. The unbound brain ISF drug concentrations thus can reflect the pharmacologically active drug concentrations and are used as a measure to model the pharmacokinetic and pharmacodynamic relationship of CNS-acting drugs (145,146). Knowledge of the unbound brain ISF drug concentrations can be used to predict efficacy and toxicity of CNS drugs during drug development, which can better inform the design of the first-in-human doses. However, the brain ISF site cannot typically be sampled directly in humans, due to its inaccessibility and the invasiveness in sampling techniques. CSF collection remains the only

conventional, clinically applicable approach to obtain information on free drug concentrations in individual human brain.

It is important to note that the CSF should not be considered a uniform compartment and that the processes of blood, CSF, and brain ISF exchange are compartmentalized and may differ between the different regions of the CSF compartment. Although there is no physical divide between ventricular and subarachnoid CSF, the slow turnover rate of CSF enables uneven drug distribution within the CSF (147). Consequently, it is important to consider that different CSF sampling sites can yield different CSF drug concentrations, and the CSF-ISF relationship can vary based on the specific region of CSF sampled (i.e. ventricular, cisterna magna, lumbar) (147,148). Drugs present in ventricular CSF can diffuse through the leaky ependyma into the brain ISF, efflux or undergo metabolism by the BCSFB, or otherwise distribute to the subarachnoid space through the cisterna magna via bulk flow (**Figure 1.3**). Drug present in subarachnoid CSF can alternatively enter the brain ISF by glymphatic exchange or by diffusion through the pia mater. Reverse flow of CSF back into the cisterna magna and ventricles can occur during sleep. Drug in the subarachnoid CSF is primarily cleared by bulk CSF flow through arachnoid granulations or lymphatic drainage to venous blood. Additionally, there is some evidence of transporter mediated clearance at the blood-arachnoid barrier, which may contribute to the subarachnoid CSF clearance of organic anions (149).

The presence of transporters at both the BBB and BCSFB can muddle the relationship between unbound CSF and brain ISF concentrations of transported substrates. In a study conducted by Kido et al., substrates of BCRP demonstrated unbound CSF concentrations notably higher than unbound brain concentrations in CSF in dogs(150). However, this does not suggest that CSF should be discarded as a surrogate brain measure for transported substrates. Physiologically based

pharmacokinetic models can potentially utilize measures of CSF, while taking advantage of integrating transport and CSF flow processes to predict drug pharmacokinetic behaviors within the brain. Currently, most models of the CNS do not consider active transport by the BCSFB, and transport processes at the BCSFB remain understudied. Several transporters shown to be expressed at the BCSFB have yet to be functionally characterized. Missing information about drug transport and other ADME processes can significantly impact the accuracy of predictive models of the CNS(151). Additional study of transporters at the BCSFB is required to clarify their role in CSF clearance, improving our understanding of the CSF and brain ISF relationship and thus improving our capacity to predict CNS safety and efficacy for transported drugs.

1.6 KNOWLEDGE GAPS ON THE CHARACTERIZATION OF OATP, P-GP, AND BCRP TRANSPORT MECHANISMS AT THE BLOOD-CSF BARRIER

While this chapter highlights the functional characterization of some transporters, such as OAT3, PMAT, PEPT2, MRP1/4, at the blood-CSF barrier, the role of other major uptake and efflux drug transporters, OATP, P-gp, and BCRP, remain to be elucidated. Notably, the collective role of OATP, P-gp, and BCRP transporters at blood-CSF barrier in regulating drug uptake, retention and clearance is not clear. Transport processes at the blood-CSF barrier cannot directly be studied in humans, and other approaches to study blood-CSF barrier transport processes may be poorly validated or may not be physiologically representative. Specifically, primary cells and immortalized cell lines of the choroid plexus have been shown to have altered transporter expression and reduced tight junction formation compared to freshly isolated tissue (62). Our laboratory has reported an OATP-like transport function at the BCSFB apical membrane based on confocal image tracing of substrates in isolated choroid plexus tissues (117). While the previous imaging study was largely qualitative in nature, the development and utilization of a quantitative

fluorescence microscopy approach may enable more precise characterization of transport mechanisms at the blood-CSF barrier. Furthermore, a quantitative fluorescence microscopy approach can be used with targeted transporter knockout models to assess the localization and functional role of OATP, P-gp, and Bcrp transporters towards regulating CSF drug concentrations via the blood-CSF barrier. The hypothesis and specific aims for this dissertation research is presented in the next section.

1.7 HYPOTHESIS AND SPECIFIC AIMS

The overall goal of my research project is to characterize the expression, localization, and activity of Organic anion polypeptides (OATPs), breast cancer resistance protein (BCRP), and P-glycoprotein (P-gp) transporters at the BCSFB. The overarching hypothesis is as follows:

The OATP1A, Bcrp, and P-gp transporters are functionally active at the apical membrane of the BCSFB and may functionally regulate xenobiotic and endobiotic transport into and out of the CSF.

The specific aims intended to test this hypothesis are as follows:

Specific Aim 1: Establish a quantitative confocal microscopy approach to evaluate BCSFB large organic anion and cation transport.

In this aim I will develop and validate a quantitative confocal microscopy approach capable of characterizing compartment specific, real-time accumulation of substrates, perpetrator drug interactions, and rate-determining steps in transepithelial transport at the BCSFB. This approach will be applied to characterize the molecular mechanisms of CSF-to-blood transport of organic anion and lipophilic compounds hypothesized to be mediated by OATPs, BCRP, and P-gp.

Specific Aim 2: Identify and characterize the specific OATP isoform(s) contributing to apical uptake of organic anions at the BCSFB.

In this aim I will determine the specific contribution of individual OATP isoforms towards the apical uptake of anions at the BCSFB. Using the approach developed in **Specific Aim 1**, I will characterize individual OATP isoform contribution, focusing on the Oatp1a5

isoform, in murine BCSFB using pharmacological inhibition and an Slco1a/1b transporter KO model. Then I will explore functional similarities and differences between mouse Oatp1a5 and human OATP1A2 using transporter-overexpressing cell lines and evaluate the expression and localization of OATP1A2 in human choroid plexus tissue samples by immunofluorescence staining. This study will help characterize the role of OATP1A transporters in both mouse and human OATP, which may identify a novel transport pathway of xenobiotic and endobiotic organic anions from the CSF.

Specific Aim 3: Evaluate the expression, localization, and activity of BCRP and P-gp at the BCSFB

While the roles of BCRP and P-gp are well established at the BBB, there are conflicting findings of BCRP and P-gp localization and function at the BCSFB. Using the quantitative confocal approach developed in **Specific Aim 1** and a series of selective pharmacological inhibitors and transporter knockout models, I aim to probe and distinguish the functional activity of BCRP and P-gp at the murine BCSFB. As CSF drug concentrations are frequently used as a surrogate measure of CNS drug exposure, elucidating the functional role of these efflux transporters is critical for understanding the interplay of BBB and BCSFB transporters and their impact on CNS pharmacokinetics and pharmacodynamics.

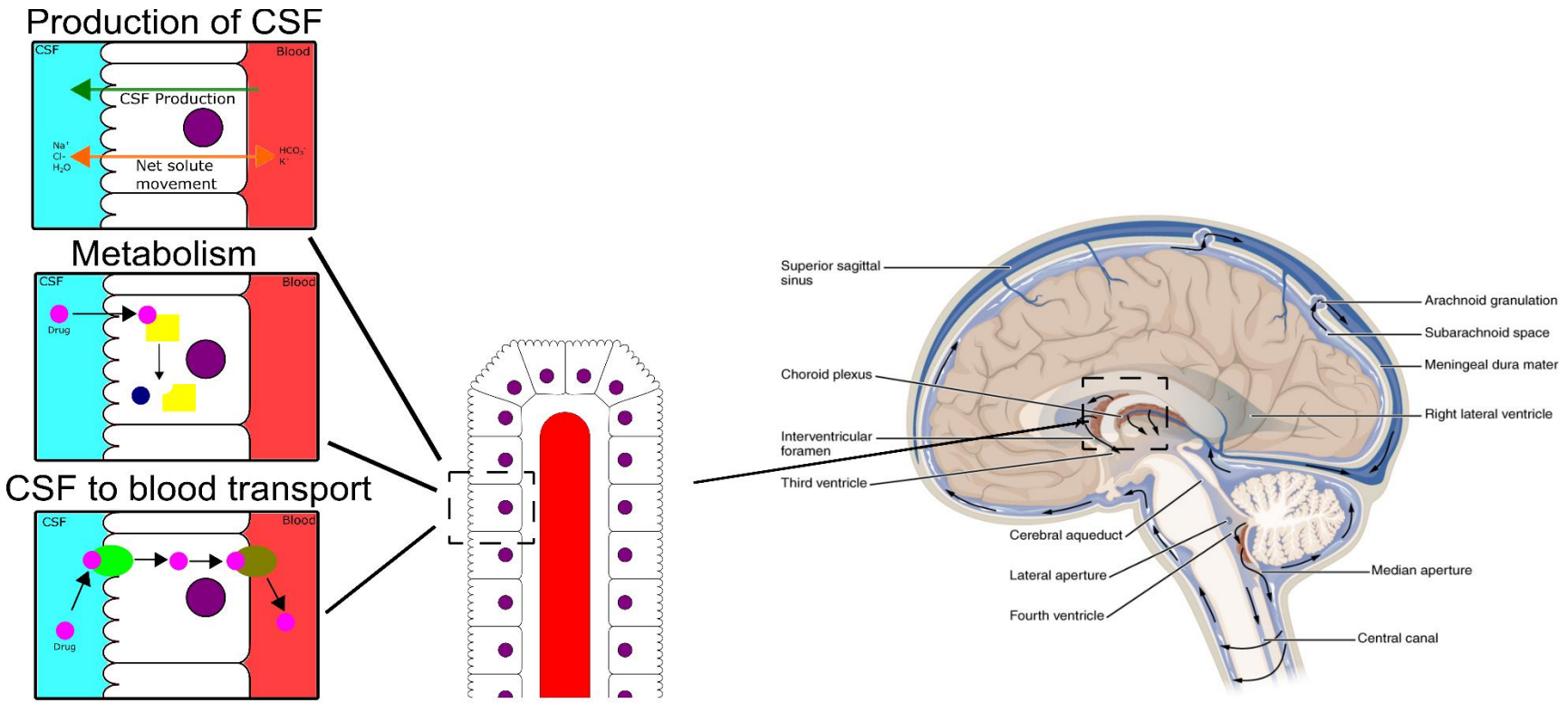

Figure 1.1. Schematic representation of the location, structure, and clearance pathways of the CP-CSF system.

The blood-CSF barrier is formed by choroid plexus epithelia cells. These cells contribute to drug clearance by production of CSF that drives bulk flow movement out of the CSF, biotransformation by intracellular drug metabolizing enzymes, and active transport removal by coordinated uptake and efflux out of the CSF. Portions of the figure are adapted from OpenStax Anatomy and Physiology under Creative Commons CC-BY-4.0 License (152).

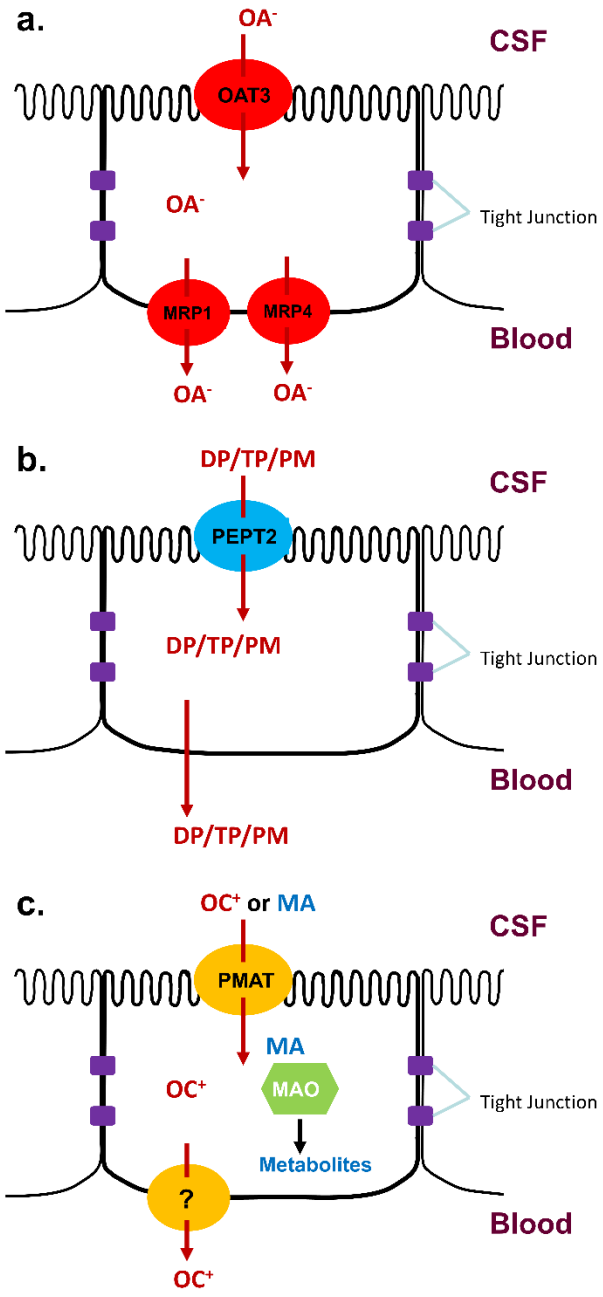

Figure 1.2. Cellular models for transport at the blood-CSF barrier.

Models of (a) organic anion, (b) oligopeptides and peptidomimetic, and (c) monoamine and organic cation transport at the blood-CSF barrier. OA^-, organic anion; DP, dipeptide; TP, tripeptide; PM, peptidomimetic; OC^+, organic cation; MA, monoamine; MAO, monoamine oxidase.

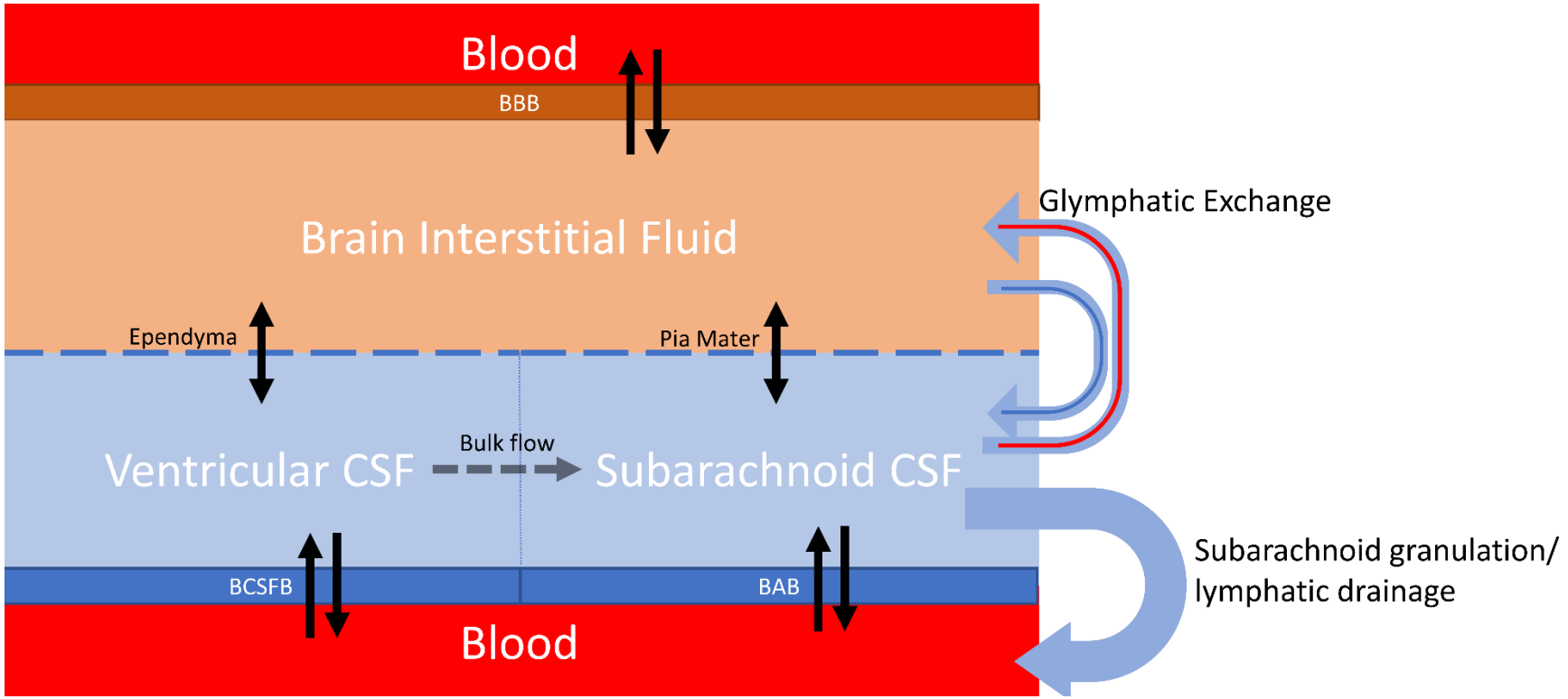

Figure 1.3. Compartmental diagram of CNS exchange pathways

Simple schematic diagram showing exchange pathways between cerebral blood, brain interstitial fluid, ventricular CSF, and subarachnoid CSF. BBB, blood-brain barrier; BCSFB, blood-CSF barrier. BAB, blood-arachnoid barrier.

Table 1.1. Localization and Selected Drug Substrates of Drug Transporters at the Blood-CSF Barrier

Transporter	BCSFB Localization	Drug Class	Example Drug Substrates	Km (uM)
OAT3	Apical (75)	Antineoplastic	Methotrexate	10.9 (153)
			Topotecan	56.5 (154)
		Antiviral	Zidovudine	145.1 (155)
		Antibiotic	Benzylpenicillin	52.1 (156)
			Cefaclor	Transported (157)
		Diuretic	Hydrochlorothiazide	134 (158)
			Furosemide	21.5 (159)
PMAT	Apical (96)	Antihyperglycemic	Metformin	1320 (92)
		Beta blocker	Atenolol	907 (160)
PEPT2	Apical (84)	Antibiotic	Cefadroxil	150.8 (161)
			Cefaclor	70.2 (162)
			Amoxicillin	1040 (162)
MRP1	Basolateral (64)	Antineoplastic	Daunorubicin	Transported (163)
			Vincristine	Transported (163)
			Methotrexate	2150 (164)
		Statin	Atorvastatin	Transported (165)
		Antiviral	Ritonavir	Transported (166)
		Antibiotic	Cefadroxil	3900 (167)
MRP4	Basolateral (111)	Antineoplastic	Methotrexate	220 (168)
			Topotecan	1.66 (169)
			6-mercaptopurine	Transported (170)
		Antiviral	Adefovir	1000+ (171)
		Antibiotic	Ceftizoxime	18 (172)
			Cefazolin	80 (172)
		Diuretic	Furosemide	Transported (173)

Chapter 2. EVALUATION OF BLOOD-CSF BARRIER TRANSPORT BY QUANTITATIVE REAL TIME FLUORESCENCE MICROSCOPY

Part of this chapter was published in:
Sun, A. and Wang, J.“ Evaluation of Blood-CSF Barrier Transport by Quantitative Real Time Fluorescence Microscopy” *Pharmaceutical Research* (2022) **29,** 1469-1480.

2.1 ABSTRACT

Purpose

Transporters at the blood-cerebrospinal fluid (CSF) barrier (BCSFB) play active roles in removing drugs and toxins from the CSF. The goal of this study is to develop a fluorescence microscopy approach to quantitatively study the transepithelial transport processes at the murine BCSFB in real time.

Methods

Choroid plexus (CP) tissues were isolated from mouse lateral ventricles and incubated with anionic (fluorescein-methotrexate, 8-fluorescein-cAMP) or cationic (IDT307) fluorescent probes. The CSF-to-blood transport was imaged and quantified using compartmental segmentation and digital image analysis. Real time images were captured and analyzed to obtain kinetic information and identify the rate-limiting step. The effect of transporter inhibitors was also evaluated.

Results

The transport processes of fluorescent probes can be captured and analyzed digitally. The intra- and inter- animal variability were 20.4% and 25.7%, respectively. Real time analysis showed distinct transport kinetics and rate-limiting step for anionic and cationic probes. A CP efflux index was proposed to distinguish between transepithelial flux and intracellular

accumulation. Rifampin and MK571 decreased the overall transepithelial transport of anionic probes by more than 90%, indicating a possible involvement of organic anion transporting polypeptides (Oatps) and multidrug resistance-associated proteins (Mrps).

Conclusions

A CP isolation method was described, and a quantitative fluorescence imaging approach was developed to evaluate CSF-to-blood transport in mouse CP. The method is consistent, reproducible, and capable of tracking real time transepithelial transport with temporal and spatial resolution. The approach can be used to evaluate transport mechanisms, assess tissue drug accumulation, and assay potential drug-drug interactions at the BCSFB.

2.2 INTRODUCTION

The choroid plexuses (CPs) that form the blood-cerebrospinal fluid barrier (BCSFB) are located in each of the four ventricles of the brain. The CP consists of a monolayer of polarized epithelial cells surrounding a core of blood capillaries (1,174). Unlike the endothelial cells forming the blood-brain barrier in other brain regions, the CP blood capillaries are fenestrated and lack tight junctions. Thus, the barrier function lies with the choroid plexus epithelial (CPE) cells joined by tight junctions (16,175). Coined as the "kidney of the brain", the CP plays a vital role in brain clearance of waste products and xenobiotics (13,174). A main function of the CP is to secrete CSF, which serves as a sink and a clearance pathway for removing solutes (e.g. drugs, metabolites) and macromolecules (e.g. β-amyloid) from the brain (29,174,176). The CPE cells also express polyspecific transporters and enzymes to actively remove xenobiotics and endobiotics from the CSF. The CSF-to-blood transport clearance at the BCSFB is initiated by drug uptake from the CSF into the CPE cells at the apical membrane followed by efflux into the subepithelial region at

the basolateral membrane (174). The compound can then diffuse across the stromal space and the fenestrated capillaries into the blood for systemic clearance (1). Drug transporters at the BCSFB can serve as a determinant of CSF drug concentrations, thus impacting drug efficacy and toxicity in the central nervous system (71,74,88). However, transporter functions at the BCSFB have not been well studied at the tissue level, and the overall significance of BCSFB transporters in brain drug disposition remains to be elucidated.

Several *ex vivo* and *in vitro* approaches have been used to study drug transport processes at the BCSFB. For instance, primary culture of CPE cells from rodents were used to demonstrate the functional activity of PepT2 at the BCSFB (84,87). A human choroid plexus papilloma (HIBCPP) cell line has been used to study drug efflux transporter function at human BCSFB (144). Immortalized CP cell lines and primary CP cells can both be cultured as a monolayer on a transwell filter, enabling study of transepithelial basolateral-to-apical or apical-to-basolateral directional transport. However, immortalized CP cell lines or primary CP cell culture can exhibit altered expression of xenobiotic transporters and weakened tight junction formation (62), and thus may not faithfully recapitulate the *in vivo* transport capability of BCSFB drug transporters. Another approach commonly used in CP transport research is to conduct radiotracer uptake studies using freshly isolated CP tissues from animal species. These isolated CP maintain the tissue physiology, barrier integrity, and transporter expression reflected *in vivo*. In addition, CP tissue can be obtained from mouse knockout models to determine the specific contribution of a single transporter at the BCSFB. This method has been successfully applied to characterize the transport function of several apical (CSF-facing) membrane transporters including Pept2, Oat3 and Pmat (77,96,177). However, radiotracer uptake in isolated CP tissues measures apical uptake in CPE cells, as only this side of the membrane is accessible to the outside buffer. As such, results from CP uptake

studies reflect total tissue accumulation but provide little information on whether the substrate is further effluxed into the blood side by basolateral transporters. This information is important as inefficient transport at the basolateral membrane can lead to drug accumulation within CPE cells, which could result in CPE cell toxicity and compromise CSF production and BCSFB barrier integrity.

Fluorescent substrate-based imaging methods have been used to probe transporter function at the cell, tissue, and organ levels (178–181). Confocal fluorescence microscopy is uniquely suited to study transepithelial transport processes at the BCSFB owing to the simple anatomy of the CP tissue. CP tissues isolated from small laboratory animals such as mice are semi-transparent, and the cobblestone-shaped CPE cells are readily distinguishable from the underlining subepithelial space. Previously, Miller and coworkers have pioneered the use of confocal microscopy to study the transport of fluorescent organic anion probes in CP tissues isolated from dogfish sharks and rats(182,183). This method has also been applied to CP tissues from knockout mice to probe the transport function of Oat3 (76). Using confocal imaging and fluorescent probes, we recently observed distinct transcellular transport patterns for organic anions and cations in isolated mouse CP tissues (117). We showed that the cationic probe IDT307 is transported into CPE cells by the apical plasma membrane monoamine transporter (PMAT) and highly accumulates within CPE cells. In contrast, the anionic probe fluorescein-methotrexate (FL-MTX), a substrate of OATPs and MRPs, was rapidly transported across the CPE cells into the subepithelial space with little intracellular accumulation. However, previous fluorescence imaging studies in CP were largely descriptive and there was generally a lack of quantitative methods for analyzing imaging data, especially those acquired in real time. Furthermore, few studies have

applied quantitative analysis to deconvolute the kinetics of the transport processes occurring at the apical and basolateral membranes of the BCSFB.

In this study, we developed a quantitative confocal microscopy approach to study the CSF-to-blood transport processes at the BCSFB using freshly isolated murine CP tissues. We described techniques of harvesting lateral ventricle CP tissues and a method to verify tissue viability and integrity. We then described a method of digital image analysis for quantifying fluorescent probe transport data at the BCSFB. The consistency and reproducibility of this approach was validated using fluorescein-methotrexate (FL-MTX), a large organic anion probe. The imaging approach was then applied to measure the transepithelial transport of additional fluorescent organic anion or organic cation molecules with rich temporal and spatial resolution. A novel parameter, the choroid plexus efflux index (CPEI), was proposed to distinguish between subepithelial and CPE cell accumulation. Lastly, the potential interactions of FL-MTX and 8-fluorescein- cyclic-AMP (fluo-cAMP) with organic anion transporting polypeptide (OATP)- and multidrug resistance associated protein (MRP)- inhibitors were evaluated.

2.3 Materials and Methods

2.3.1 *Chemicals and Materials*

Fluorescein-methotrexate (FL-MTX, MW: 925 Da) was purchased from Biotium (San Francisco, CA). 8-Fluorescein-cyclic-AMP (fluo-cAMP, MW: 815.7 Da) was purchased from Axxora (Farmingdale, NY). IDT307 (MW: 340.2 Da) was purchased from Sigma Aldrich (St. Louis, MO). Unless otherwise specified, all other chemicals and reagents were obtained from

Sigma-Aldrich (St. Louis, MO). All chemicals were 95% purity or higher and were obtained from commercial sources.

2.3.2 *Preparation of Mouse Choroid Plexus*

Animal experiments were carried out in accordance with the Guide for the Care and Use of Laboratory Animals as adopted and promulgated by the U.S. National Institutes of Health and in accordance with animal protocols approved by the Institutional Animal Care and Use Committee at the University of Washington. Animals were housed in the specific pathogen free facility at the University of Washington.

Adult (10-14 week old) male C57BL/6J mice were euthanized by CO_2 inhalation, followed by decapitation. Mouse brain was isolated and maintained in ice cold artificial CSF (aCSF: 119 mM NaCl, 26.2 mM $NaHCO_3$, 2.5 mM KCl, 1 mM NaH2PO4, 1.3 mM MgCl2, 2.5 mM CaCl2, 10 mM glucose, previously gassed with 95% O2/5% CO2) for tissue isolation. Lateral ventricle CP was isolated from mouse brain under a dissecting microscope. Briefly, an incision was made along midline of the sagittal plane between the hemispheres of the brain using surgical scissors or superfine forceps. The lateral ventricle can be identified as a cavity alongside the inner wall of the brain hemisphere revealed by the incision. The lateral ventricle was exposed using one set of superfine forceps, revealing the CP which presents as a floating, faintly vascularized, semi-transparent tissue. The CP was removed using another set of superfine forceps. The tissue was transferred into pre-gassed, ice-cold aCSF immediately after removal, and the process was repeated for the other hemisphere.

2.3.3 *Viability Test in Isolated CP*

Trypan blue exclusion test was performed to verify CP tissue viability and integrity. Isolated CP tissue was incubated with 0.2% trypan blue in aCSF buffer for 5 minutes at room temperature. The tissue was then transferred to a 35mm sterile confocal dish (VWR, Radnor, PA) and placed onto a Zeiss LSM 710 confocal microscope. Brightfield images of damaged and undamaged tissue regions were captured using a OnePlus 7 Pro smartphone camera mounted onto the ocular lens of a Zeiss LSM 710 confocal microscope.

2.3.4 *Transport Studies in Isolated CP*

Intact CP tissues were used for imaging studies within 2 hours of isolation. Transport studies using freshly isolated mouse CP were performed using a modified approach previously described (96). Briefly, lateral ventricle CP tissues were cut into two pieces. Tissue was then transferred into 35mm sterile confocal dishes (VWR, Radnor, PA) containing aCSF buffer at room temperature. Tissue was maintained in room temperature aCSF for 5 minutes to acclimate before initiating uptake.

Single time-point transport studies were initiated by adding 2 µM of fluorescent compound with or without inhibitor (100 µM) into aCSF. Incubations were carried out for 20 minutes in sealed Ziploc bags containing 95% O_2, 5% CO_2. To terminate uptake, tissue was washed 3 times with ice cold aCSF and kept on ice until image acquisition. Each CP tissue under investigation was inspected under low-intensity brightfield imaging for apparent tissue damage and cell membrane rupture. 1-4 undamaged observation areas containing both CPE cells and adjacent subepithelial region were selected, and the fluorescent signals were recorded. To record real-time transport of fluorescent substrate, a specific observation area containing intact CP epithelial cells

and adjacent subepithelial region was selected and immobilized in pre-gassed aCSF. Transport was initiated by adding 2 µM of fluorescent compound, and fluorescent signals were recorded every minute for 20 minutes.

2.3.5 *Confocal Image Acquisition and Analysis*

Image acquisition was performed using a Zeiss LSM 710 confocal microscope fitted with a Zeiss 40x, NA 1.3 oil immersion objective (total magnification: 400x), and digital image collection was performed using Zeiss Zen 2009 Microscope Software. Brightfield imaging was used to identify observation areas containing CPE cells with adjacent blood capillaries. Samples were illuminated using a 488 nm fixed wavelength argon laser equipped with a 488 nm dichroic and a 492-630 nm emission filter. Low laser intensity (less than 8% of maximum) was used to minimize sample photobleaching. Laser gain and offset was set such that autofluorescence of tissue was minimally detectable (data not shown), with the pinhole set to 36.8 µm. Confocal images were captured as 15 second scans at 1024x1024 resolution, 16 frames line-averaged, with a pixel dwell of 0.79 µsec. Replicate studies were performed using the same objective lens, identical laser power, and identical detector settings. A trans-PMT detector was used to capture accompanying differential image contrast (DIC) imaging.

Digital image analysis was performed using FIJI ImageJ (1.53c) (184). CPE cell and subepithelial regions of interests were identified in the acquired confocal images, supported by accompanying DIC images. CPE cell and subepithelial regions were defined and manually segmented by free hand drawing over the identified regions of interest. To segment the CPE cell region for quantification, a free hand outline was drawn over the CSF facing membrane of the CPE cell, and an exclusionary outline was drawn around the subepithelial region. Mean fluorescence,

measured by average pixel intensity, was measured in the manually segmented CPE cell and subepithelial regions, averaged from three free hand segmentations. CPE cell and subepithelial region fluorescence were corrected for background fluorescence, obtained from the surrounding bathing media in single-time point experiments and from the mean fluorescence prior to fluorescent probe addition for time-dependent transport experiments.

2.3.6 *Calculation of Choroid Plexus Efflux Index (CPEI)*

CPEI was calculated according to the following formula:

Equation 2.1: $$CPEI(\%) = \frac{\sum pixel\ intensity_{se}}{\sum pixel\ intensity_{cells+se}}$$

where Σpixel intensity$_{se}$ is the sum average pixel intensity in the subepithelial region from three segmentations, and Σpixel intensity$_{cells+se}$ is the combined sum average pixel intensity in the subepithelial and intracellular CPE cell regions from three segmentations.

2.3.7 *Intra- animal variability*

Average pixel intensity in the primary accumulation site (e.g. subepithelial region for FL-MTX, CPE cell for IDT307) was used to calculate inter- and intra-animal variability parameters. The inter- and intra-animal variabilities of FL-MTX transport were calculated using a root mean squares approach based on the following analysis of variance (ANOVA) equations:

Equation 2.2: $$Intra - animal\ variability = \frac{\sqrt{MS_{intra}}}{mean_{all}}\ x\ 100\%$$

Equation 2.3: $$Inter - animal\ variability = \frac{\sqrt{(MS_{inter} - MS_{intra})/n}}{mean_{all}}\ x\ 100\%$$

where MS_{intra} and MS_{inter} are the mean squares within a group and between a group, respectively. $Mean_{all}$ is the arithmetic mean of all the measured accumulations and n is the total number of

observation areas. Initial uptake rate was calculated by the linear slope of primary site accumulation over time during the initial linear phase of uptake, defined as the first three minutes of captured uptake for FL-MTX and fluo-cAMP and between five to ten minutes for IDT307. If a plateau in the time course was achieved, the time to maximal accumulation was determined by the first time point that subepithelial accumulation exceeding 90% of the maximal accumulation over the 20-minute time course interval.

2.3.8 *Statistical Analysis*

All imaging experiments were carried out with CP tissue isolated from at least 3 animals. Calculated intensity values were presented as mean ± SD. Statistical significance was determined by using a one-way ANOVA followed by Dunnett's test or by an unpaired Student's t-test. P value less than 0.05 indicated a statistically significant difference.

2.4 RESULTS

2.4.1 *Experimental Workflow and Tissue Integrity*

Figure 2.1 illustrates the overall scheme of the experimental workflow. Briefly, mouse brain was harvested and maintained in ice-cold aCSF. A midline incision was made along the sagittal plane to expose the lateral ventricle. The CP tissue was removed under a dissecting microscope, maintained in ice-cold pre-gassed aCSF, and checked for tissue integrity. For transport imaging studies, intact CP tissue was transferred to a sterile confocal dish containing aCSF buffer at room temperature and incubated for 5 minutes to allow tissue acclimation. To initiate the transport study, a fluorescent substrate was added to the aCSF buffer at a final desired concentration. Images were then captured under a confocal microscope for real-time recording.

For single time point studies, images were captured after incubation for a specified time period. A detailed description of the experimental procedure is provided in the Materials and Methods section.

Prior to transport studies, CP was checked for normal tissue morphology and integrity under a microscopy. Only undamaged CP tissues were used for imaging studies. The viability and integrity of the CP tissue was also confirmed using the trypan blue exclusion method. As shown in **Figure 2.2**, when incubated with trypan blue, healthy, intact CP showed no staining, indicating that both cell vitality and barrier integrity of the BCSFB are maintained. In contrast, damaged CP showed strong staining of trypan blue and leakage of the dye into the inner tissue area. Previously, we and others have shown that isolated CP tissues maintain their vitality and transport activity for up to 2-3 hours after isolation (96,112,117). All imaging studies were performed within 2 hours after tissue isolation.

2.4.2 *Imaging and Quantification of FL-MTX and IDT307 Transport in Mouse CP*

Figure 2.3 depicts the anatomy of the CP. A monolayer of CPE cells lines the outer surface of the CP and separates the CSF from the capillaries residing in the interior subepithelial space. The CPE cells are polarized, with the apical membrane facing the CSF and the basolateral membrane facing the internal subepithelial space. The CPE cells are joined by tight junctions, limiting paracellular transport. Under DIC microscopy, freshly isolated murine CP in aCSF buffer showed typical morphology (**Figure 2.3**). Notably, the aCSF only interfaces with the tight junction-lined CPE cells at the apical membrane, and the interior vascular region is rendered inaccessible from the outside solution. To examine the CSF-to-blood transport processes at the BCSFB, CP was incubated in aCSF in a confocal dish, and FL-MTX or IDT307 was added to the aCSF solution. After a 20 minute incubation, the tissue was rinsed and imaged by confocal

microscopy. Consistent with our previous observation (117), FL-MTX, an organic anion, primarily accumulated in the subepithelial space, indicating a transepithelial flux from the CSF into the blood (**Figure 2.3**). IDT307, a fluorescent analog of the prototype organic cation 1-methyl-4-phenylpyridinium (MPP+), primarily accumulated in the CPE cells, indicating uptake from the CSF and retention within the CPE cells (**Figure 2.3**).

Quantification of FL-MTX and IDT307 accumulation in CPE cell and subepithelial regions was then performed by digital image analysis using FIJI (184). Manual segmentation of CPE cell and subepithelial regions for FL-MTX accumulation was performed as described in the Materials and Methods (**Figure 2.4**). Mean fluorescence intensity was quantified in the segmented CPE cell and adjacent subepithelial regions. As shown in **Figure 2.4**, FL-MTX accumulation in the subepithelial region was about 6.6-fold greater than that in CPE cells. Similarly, segmentation of IDT307 was performed, and fluorescence intensity measurements were obtained (**Figure 2.4**). IDT307 preferentially accumulated in the CPE cells, exhibiting a 3.3-fold higher accumulation over the subepithelial space.

2.4.3 *Variability and Reproducibility*

One major advantage of the confocal imaging approach is the ability to visualize real time transport of a fluorescent probe in a single CP tissue. However, only a single, fixed observation area can be observed for a time-dependent imaging experiment. To determine the representativeness of a single observation area, the intra- and inter-animal variabilities in fluorescent substrate accumulation were examined. Uptake of 2 μM FL-MTX was performed in immobilized CP tissue obtained from five animals. After 20 minutes, images were obtained from 3-7 different observation areas in each CP, and the subepithelial region accumulation was

calculated for each observation area. The intra- and inter-animal variabilities of subepithelial accumulation are shown in Table 2.1. The intra-animal variability ranged from 9.5% to 31.3% in each animal, with an overall intra-animal variability of 20.4%. The inter-animal variability was 25.7% across the 5 animals. These data suggest that the confocal imaging approach can be applied to study BCSFB transport in a quantitative manner, and when conducted appropriately, the transport data generated are consistent and reproducible. Additionally, agreement between observation areas suggests that real time recording obtained from a single observation area is representative of transport process occurring at the whole tissue.

2.4.4 *Real Time Analysis of Transport*

To further explore the applicability of this quantitative microscopy approach to study drug transport at the BCSFB, we recorded real-time transport of FL-MTX, fluo-cAMP, and IDT307 to obtain kinetic information of the transepithelial process. FL-MTX and fluo-cAMP are large organic anions known to be OATP substrates whereas IDT307 is an organic cation known to be a PMAT substrate (178,185,186). **Figure 2.5** depict time-courses of transport in different CP tissue compartments obtained from single animals. For the large organic anion substrates, transport is characterized by an initial linear phase, followed by a plateau. Both FL-MTX and fluo-cAMP primarily accumulated in the blood capillaries across the 20-minute time-course (**Figure 2.4**). Even at the earliest time points, most of the observed fluorescence intensity is located in the subepithelial space with minimal intracellular accumulation in CPE cells. This indicates the majority of substrate taken up by the CPE cells is rapidly effluxed into the subepithelial space, suggesting that basolateral efflux occurs at a rate much greater than apical uptake. Hence, apical uptake is the rate-limiting step for the transepithelial transport of FL-MTX and fluo-cAMP. In

contrast, the organic cation IDT307 was primarily retained within the CPE cells throughout the time course, indicating minimal basolateral efflux transport of IDT307 from the CPE cell into blood side (**Figure 2.5**).

Table 2.2 shows the average initial uptake rate and time to maximal accumulation obtained from 3-5 animals. Initial transport rate is similar between FL-MTX and fluo-cAMP, suggesting that the two organic anions exhibit similar uptake rate at the apical membrane. Fluo-cAMP exhibits a longer, though not statistically different, time to maximal accumulation than FL-MTX, possibly due to a longer linear phase. A maximal accumulation time was not calculated for IDT307, as the compound continued to accumulate in the CPE cells and did not reach a plateau at 20 minutes.

2.4.5 *The Choroid Plexus Efflux Index (CPEI)*

Based on the data shown, it is apparent that the organic anions and organic cation exhibit different patterns of compartmental accumulation. We therefore sought to develop a simple parameter to distinguish BCSFB transport patterns between these fluorescent probes. The choroid plexus efflux index (CPEI) (**Equation 2.1**) was thus developed. The CPEI represents the percentage of substrate taken up by the CPE cells that is further effluxed into the subepithelial region. A higher CPEI indicates a greater proportion of substrate entering the CPE cells accumulates in the blood capillaries and hence undergoes CSF-to-blood flux across the BCSFB. A lower CPEI indicates the substrate is taken up from the CSF but is retained within CPE cells. The 20-minute CSF-to-blood transport of FL-MTX, fluo-cAMP, and IDT307 were parameterized by CPEI (**Figure 1.1**). The CPEI remained stable after the initial uptake period for all three substrates. $CPEI_{20min}$ obtained from 3-5 different animals is described in Table 2.2. The CPEI parameter captures that 80-90% of FL-MTX and fluo-cAMP entering the CPE cells is effluxed

into the subepithelial space whereas only ~20% of IDT307 is further transported into the subepithelial region.

2.4.6 *Effects of Oatp and Mrp Inhibitors on BCSFB Organic Anion Transport*

The above data demonstrated the feasibility of using quantitative fluorescence microscopy to characterize the CSF-to-blood transport of large organic anions (FL-MTX, fluo-cAMP) at the BCSFB using isolated CP. These compounds are known substrates of OATPs and MRPs (112,185,187,188). Several Oatps and Mrps are expressed respectively at the apical and basolateral membranes of the CPE cells (57,58,65). To characterize the potential contribution of Oatps and Mrps for FL-MTX and fluo-cAMP transport at the BCSFB, imaging studies were performed in the presence of classical inhibitors of these transporters (**Figure 2.6**). Co-incubation with rifampin (100 µM), an OATP/Oatp inhibitor led to more than 90% reduction in subepithelial accumulation for both FL-MTX and fluo-cAMP. Co-incubation with MK571 (100 µM), a pan-MRP inhibitor, also resulted in greater than 90% inhibition in the subepithelial accumulation for both compounds. Though not statistically significant, an apparent increase in CPE cell accumulation was also observed for MK571.

2.5 DISCUSSION

The BCSFB is an important, but understudied blood-brain interface with respect to drug, toxin, and metabolic waste clearance. In this study, we described the application of confocal microscopy to study the transepithelial transport processes at the murine BCSFB quantitatively and in real time. Using fluorescence labeled organic anion and cation molecules, we showed that our method is consistent, reproducible, and capable of tracking real time transepithelial transport

at the BCSFB with temporal and spatial resolution. Kinetic information and the rate-limiting step can be obtained by analyzing time-dependent compartmental accumulation data. A novel parameter, CPEI, was proposed to distinguish between transepithelial flux and CPE cell accumulation. In addition, we showed that the approach can also be used to study inhibitor effects and probe the molecular mechanisms of transport at the BCSFB.

Fluorescence-based imaging approaches have been demonstrated to be especially useful to characterize transepithelial drug transport processes at barrier tissues. For instance, fluorescence techniques have been successfully applied to study drug interactions with Mrp2 in the liver, demonstrating interactions with hepatocyte-generated drug metabolites and HIV protease inhibitors (20,21). Previously, confocal microscopy has been used to study the transport of fluorescent organic anions and cations in CP tissues isolated from several animal species (182,183,189). Most of the studies were carried out over a decade ago, where limited quantitative image analyses were performed using early image analysis software such as NIH Image or Scion Image. In this study, we obtained high quality confocal images of BCSFB transport in mouse CP tissue, manually segmented CPE cell and subepithelial compartments, and performed digital image analysis using the FIJI ImageJ software (**Figure 2.3**). FIJI is a newer, free-to-use open-source distribution of ImageJ2, which is built upon earlier versions of digital image analysis software(184). FIJI is continuously updated, supports a variety of file types and image sizes, and is compatible with external image software like Imaris through user-developed plugins (184), making it a powerful and user-friendly tool for advanced digital image analysis.

Using FL-MTX, we showed that the transport data obtained from our approach is consistent, reproducible, and capable of obtaining transport kinetic information (**Figure 2.5**, Table 2.1, Table 2.2). In our study, the primary tissue accumulation site (CPE cells or subepithelial

space) was used as a measure to ascertain inter- and intra-animal uptake variability and evaluate transport kinetics. We assumed that variability in total tissue accumulation (sum of subepithelial and CPE cell accumulation) was reflected by the primary accumulation site. To corroborate this assumption, we compared initial uptake rate and time to maximal accumulation using subepithelial accumulation alone against using total accumulation, and we did not observe a statistical difference between the measures in any of the substrates tested (data not shown). However, if a compound showed similar accumulation in both compartments, total accumulation may be more representative of tissue uptake.

We proposed CPEI as a simple parameter to describe the transepithelial flux across the BCSFB (**Figure 2.5**, Table 2.2). Since CPEI does not capture the amount of substrate removed from the aCSF by the CPE cells, it cannot be used to infer the transport clearance rate at the BCSFB. Instead, CPEI is useful for characterizing basolateral efflux activity and distinguishing the primary site of accumulation within the CP tissue compartments. While both large organic anion and organic cations are transported into CPE cells, the high CPEI parameters for FL-MTX and fluo-cAMP indicate that the majority of these anionic compounds are then rapidly effluxed at the basolateral membrane into the subepithelial region after their uptake at the apical membrane. In contrast, CPEI is much lower for IDT307. Apical IDT307 uptake is mediated by PMAT, but the compound is minimally effluxed into the blood and preferentially accumulates within the CPE cells (117) (**Figure 2.7**). These data suggest small organic cations such as the neurotoxin MPP+ may accumulate in CPE cells, posing a higher risk for CP tissue toxicity. The CPEI may thus be a useful parameter to evaluate drug toxicity risks in the CP.

Using inhibitors of Oatps and Mrps, we further showed that our imaging approach can be used to study the transport mechanisms at the BCSFB. Several Oatp isoforms are known to be

expressed at both human and rodent BCSFB (56–58). While the specific roles of these Oatps in BCSFB drug transport remain to be clarified, we suspect that one or more Oatps is responsible for FL-MTX and fluo-cAMP uptake at the apical membrane since these compounds are known substrates of human OATPs. Co-incubation with rifampin, an OATP/Oatp inhibitor, abolished total tissue accumulation of both FL-MTX and fluo-cAMP, which is in line with our hypothesis. Both Mrp1 and Mrp4 are known to be expressed on the basolateral membrane of CPE cells (106,111) and likely mediate basolateral efflux of FL-MTX and fluo-cAMP observed in our study (**Figure 2.7**). Previously, Mrp4 mediated efflux of fluo-cAMP was reported in rat CP (112). Breen et al. (2004) also reported an increase in CPE cell accumulation of FL-MTX in the presence of MK571 in rat CP (190). In our study, MK571 increased CPE cell accumulation, though the increase was not found to be statistically significant (**Figure 2.6**). A potential explanation of this finding is that MK571 may also inhibit the apical uptake mechanism to some capacity, limiting CPE cell accumulation of FL-MTX and fluo-cAMP. MK571 was previously reported to inhibit human OATP1B1 and OATP1B3-mediated uptake at higher concentrations (191) but its interaction with murine Oatps have not been studied. Further studies utilizing CP from transporter knockout mice would be useful to definitively establish the specific roles of various Oatp and Mrp isoforms at the BCSFB.

While our study demonstrates several utilities of applying quantitative fluorescence microscopy to study drug transport processes at the rodent BCSFB, it also has significant limitations. Transporters have been shown to exhibit species differences in function (192). The majority of clinically used drugs are not fluorescent and cannot be directly examined by confocal microscopy. Fluorophore-conjugated drug molecules have been developed, but the observed transport mechanisms may not reflect the unconjugated form. Notably in our study we utilized

fluorescein-conjugated methotrexate (FL-MTX) to study OATP and MRP transport. FL-MTX and methotrexate are suggested to be transported by different mechanisms at the CP (190), and we cannot assume the same transport mechanisms observed in our study can reflect that of methotrexate at the BCSFB. Even for innately fluorescent drug molecules, absolute concentrations cannot be extrapolated from tissue fluorescent signals to quantitatively assess transport capacity. In addition, there are caveats when interpreting quantitative fluorescence data. Fluorescent signals can be altered by the nearby microenvironment and imaging conditions (193). Furthermore, the confocal laser scanning microscopy method utilized in this study produced 2-D images of single observation areas every minute to capture the time course of CP transport. Rapidly advancing imaging tools such as spinning disk confocal microscopy or multiphoton microscopy may permit 3-D imaging of whole tissue transport at high temporal resolution. Recently, two-photon microscopy has been successfully applied to examine calcium activity and immune cell response in *ex vivo* and *in vivo* murine choroid plexus (194). Another application has been demonstrated by Babbey et al., utilizing intravital microscopy to examine the effects of rifampin on fluorescein transport by the rat liver (195). Notwithstanding, we envision that the quantitative confocal microscopy technique described in this study provides an alternative approach to study transepithelial drug transport at the BCSFB, and the CPEI determined *ex vivo* may have predictive value for assessing drug accumulation and toxicity in CP tissues.

2.6 CONCLUSIONS

In conclusion, have developed and validated a novel method to probe CSF-to-blood drug transport processes in real time at the blood-CSF barrier, distinguishing between substrate accumulation in choroid plexus cells and the subepithelial space. We have demonstrated that this

quantitative confocal imaging approach is valuable for characterizing compartment specific accumulation of substrates, perpetrator drug interactions, and rate-determining steps in transepithelial transport at the BCSFB. We expect confocal fluorescence techniques to play a valuable role in future investigation of transport mechanisms at the BCSFB, an important but understudied blood-brain interface.

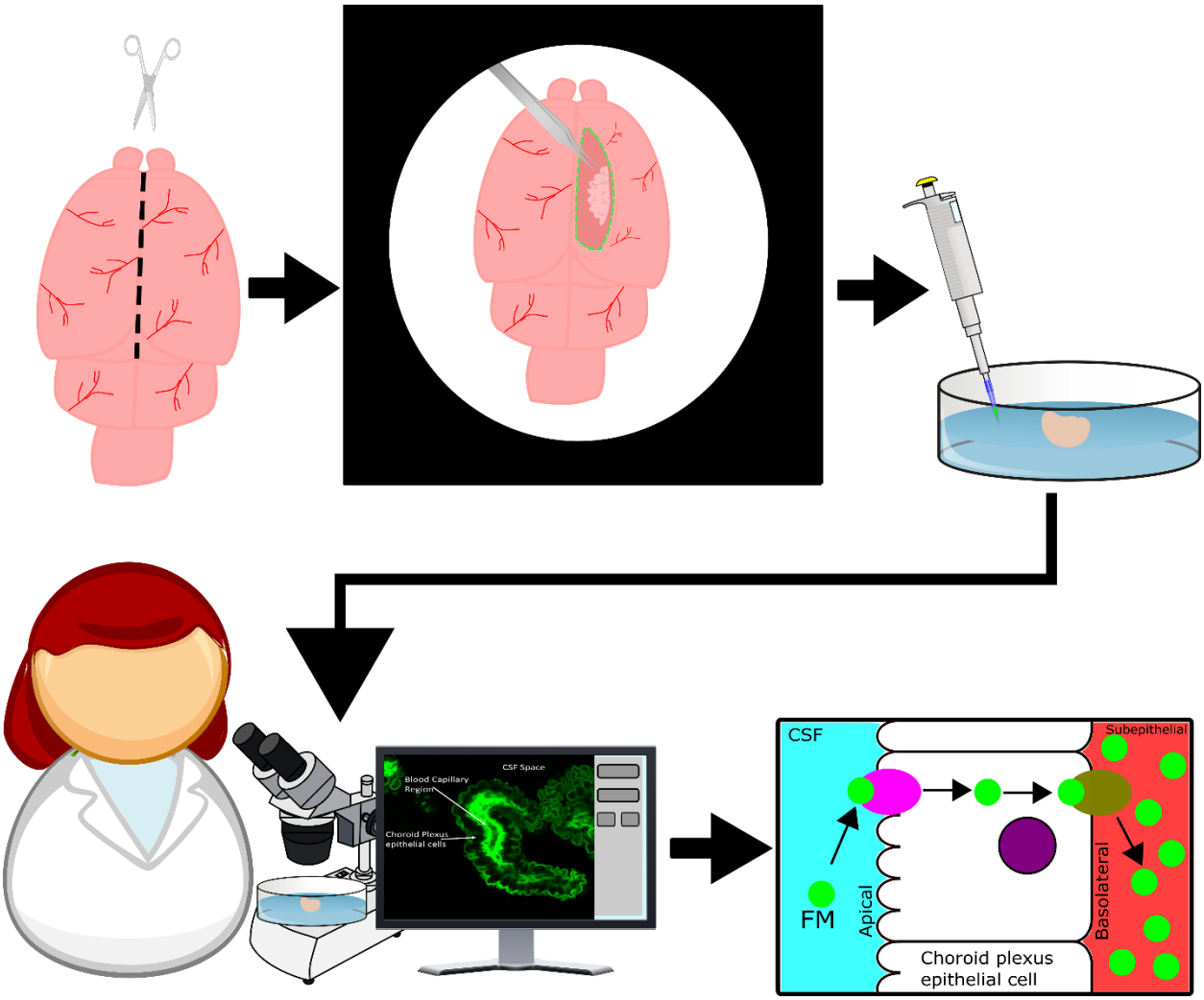

Figure 2.1. Schematic illustration of experimental workflow

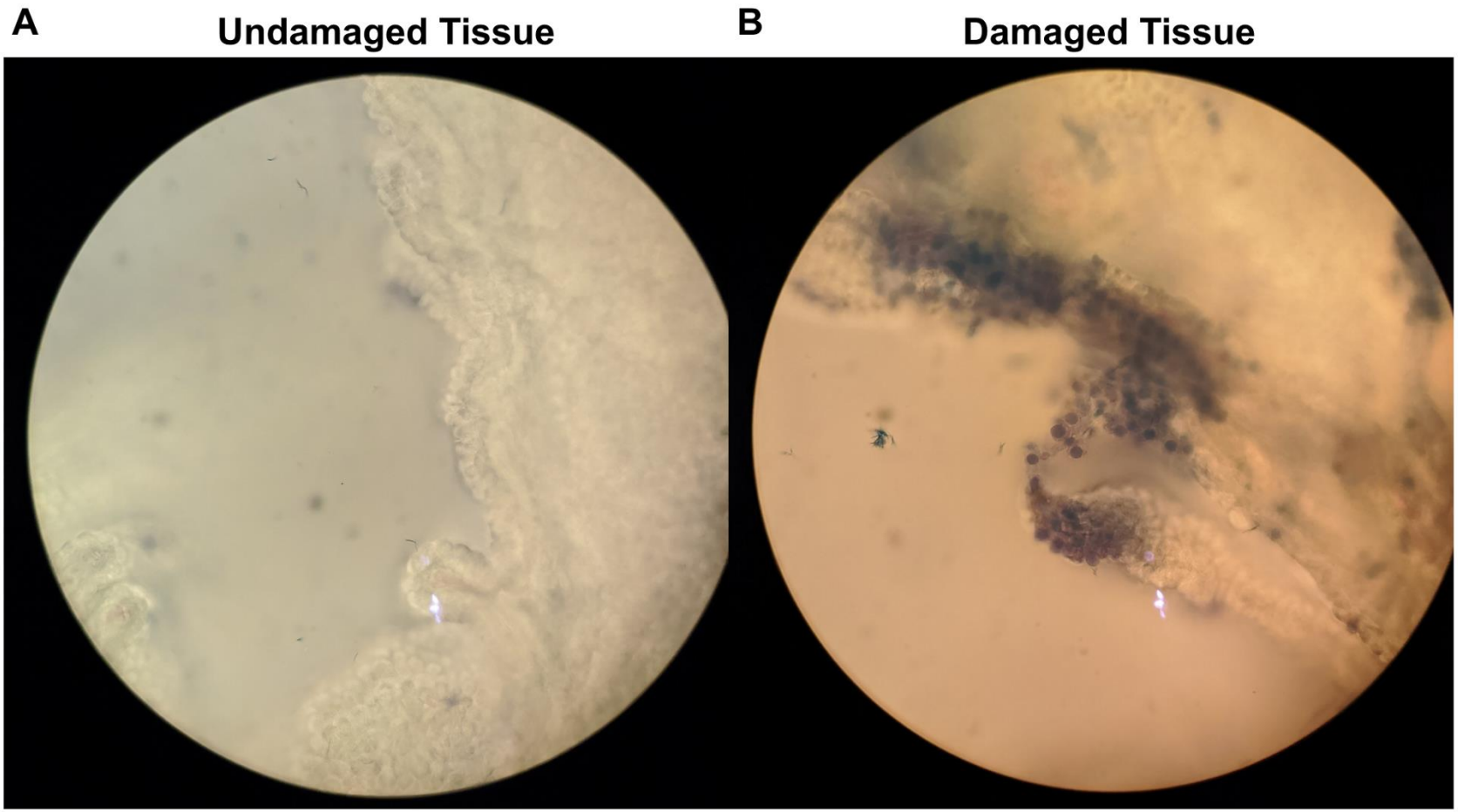

Figure 2.2. Representative images of intact and damaged CP tissues

Representative images of (A) intact and (B) damaged CP tissues after isolation from murine lateral ventricle and staining with trypan blue. CP, choroid plexus.

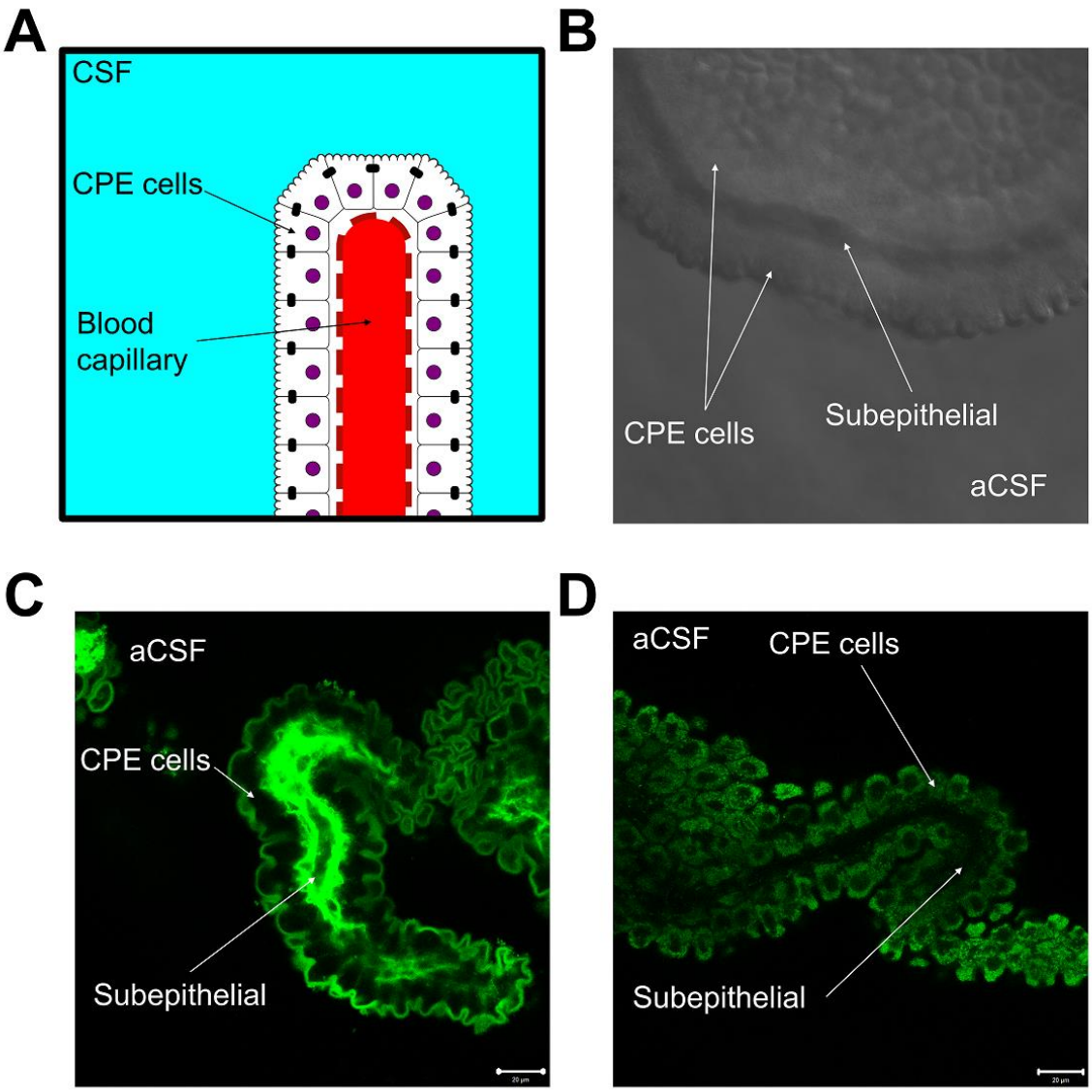

Figure 2.3. Illustrations and images of CP anatomy by schematic, DIC, and confocal imaging

(A) General schematic illustration of CP anatomy. (B) Representative differential image contrast image of mouse CP. (C) Confocal imaging of FL-MTX (2 μM) in mouse CP after 20 min incubation shows primarily subepithelial accumulation. (D). Confocal imaging of IDT307 (2 μM) in mouse CP after 20 minutes shows primarily CPE cell accumulation. CSF, cerebrospinal fluid; CP, choroid plexus; CPE cells, choroid plexus epithelial cells; aCSF, artificial CSF.

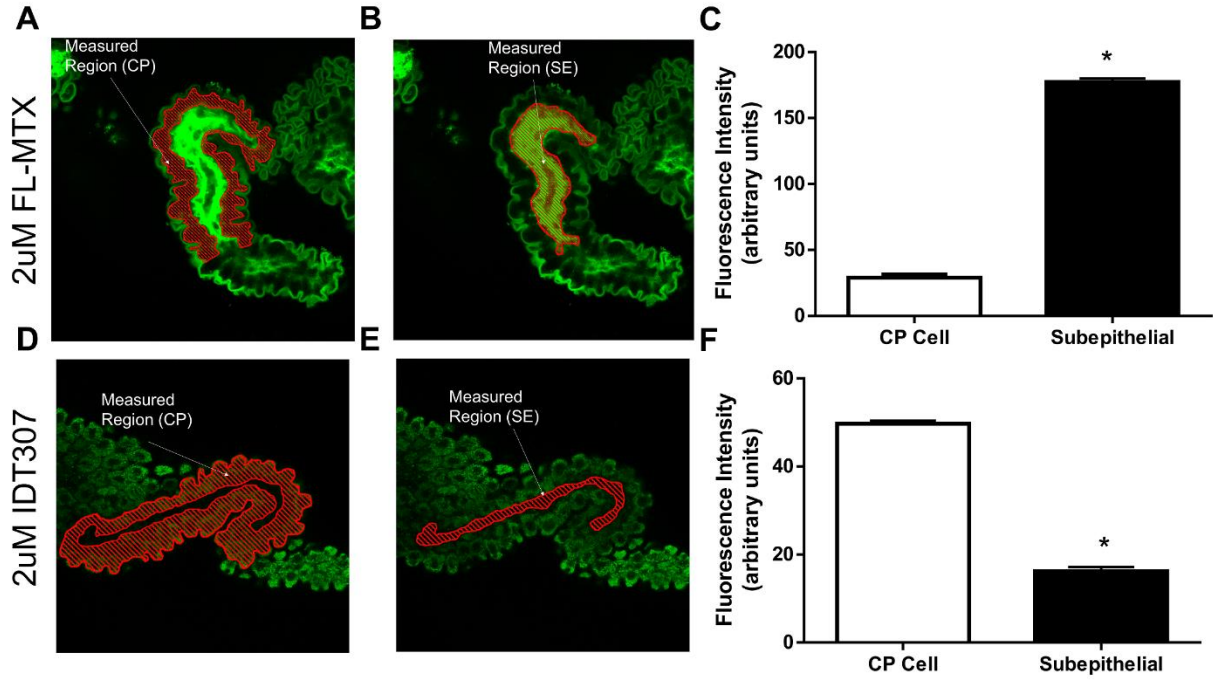

Figure 2.4. Segmentation and quantification of fluorescence intensity in different compartments of CP.

CPE cell and SE regions were manually segmented for quantification by free hand drawing over the identified regions of interest. Confocal image of FL-MTX or IDT307 in mouse CP segmented by CPE cell (A, D) and SE (B, E) regions with accompanying fluorescence quantification (C, F). Data are represented as the means ± S.D. from three independent image segmentations from a single CP. Statistical significance was determined by using an unpaired Student's t-test (*P<0.05). CP, choroid plexus; CPE, choroid plexus epithelial cell; SE, subepithelial.

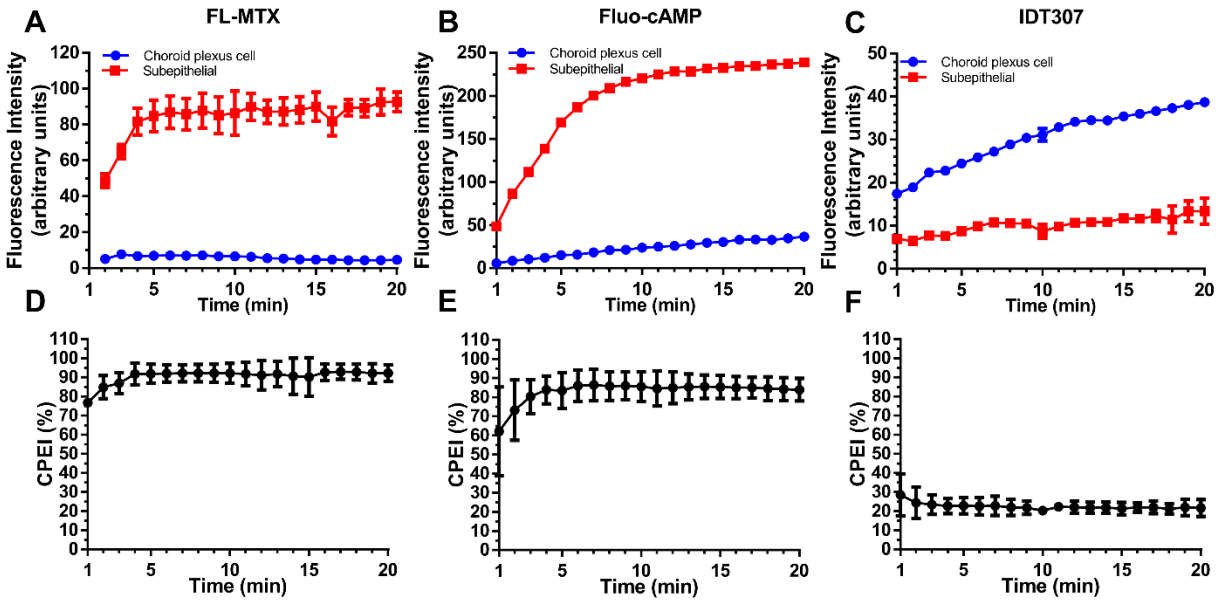

Figure 2.5. Time-dependent transport of FL-MTX, fluo-cAMP, and IDT307 in CP tissue, separated by tissue compartment

Time-dependent transport of (A) FL-MTX, (B) fluo-cAMP, and (C) IDT307 in CP tissue, separated by tissue compartment. CPEI over time for (D) FL-MTX, (E) fluo-cAMP, and (F) IDT307. The aCSF concentrations for all probes were 2 µM. Time courses were performed independently three times, and results from one representative experiment were shown. (A-C) Values are mean ± S.D. from 3 segmentations per time point. (D-F) Values are mean ± S.D. from 3-5 animals.

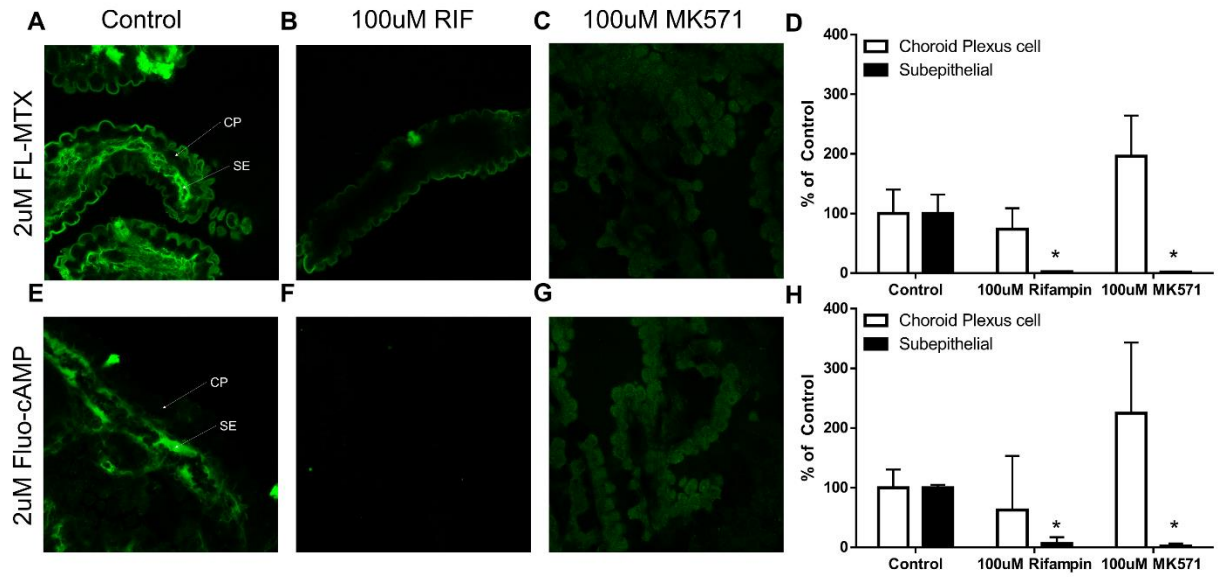

Figure 2.6. Inhibition of FL-MTX and fluo-cAMP with Rifampin and MK571

Representative images of 2 µM FL-MTX and fluo-cAMP accumulation after 20 minutes alone (A, E), with 100 µM rifampin (B, F), and with 100 µM MK571 (C, G). The accumulation of FL-MTX (G) and fluo-cAMP (H) in CPE cell and SE compartments after rifampin or MK571 treatment were compared with untreated tissue (control). Values are mean ± S.D. from 3 animals. Statistical significance was determined by using a one-way ANOVA followed by Dunnett's test (*P<0.05). CPE cells, choroid plexus epithelial cells; SE, subepithelial.

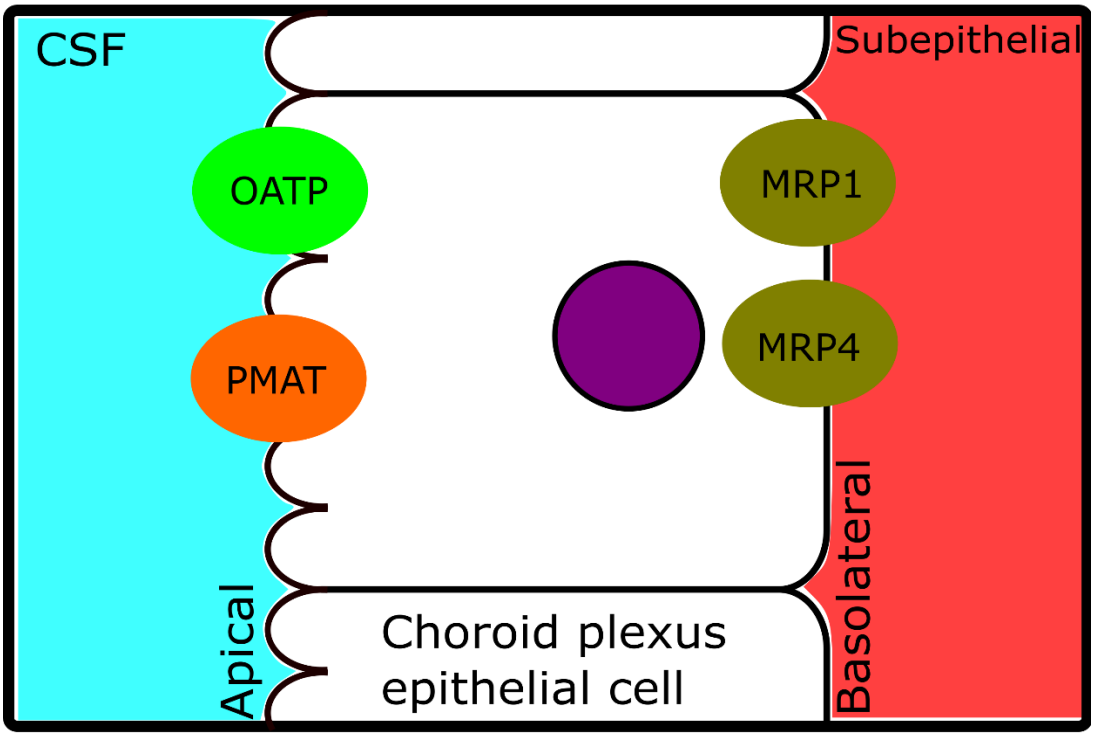

Figure 2.7. Purported large organic anion and organic cation transporter localization at the BCSFB

PMAT transports small organic cation molecules (i.e. IDT307), while OATPs and MRPs transport organic anion molecules (i.e. FL-MTX, fluo-cAMP).

Table 2.1. Assay variability of FL-MTX accumulation in subepithelial region

	Animal 1	Animal 2	Animal 3	Animal 4	Animal 5
Tissue Regions Observed (n=)	7	3	5	3	4
Variability per animal	25.1%	11.8%	9.5%	19.9%	31.3%
	Intra-animal variability		Inter-animal variability		
Overall Variability of assay	20.4%		25.7%		

Table 2.2. Initial rate, time to max accumulation, and CPEI% determined in mouse CP
Values are expressed as mean ± SD obtained from 3-5 animals. AU, arbitrary units

	FL-MTX	Fluo-cAMP	IDT307
Initial Transport Rate (AU/min)	18.07±1.79	20.27±11.37	1.38±1.51
Time to Max Accumulation (min)	6.00±1.87	11.33±6.11	N.D.
CPEI% at 20 min	92.19±4.36	82.18±6.80	22.05±4.53

Chapter 3. MOLECULAR MECHANISMS OF OATP/*SLCO*-MEDIATED ORGANIC ANION CLEARANCE AT THE BLOOD-CEREBROSPINAL FLUID BARRIER

3.1 ABSTRACT

The blood-cerebrospinal fluid barrier (BCSFB), formed by the choroid plexus epithelial (CPE) cells, plays an active role in removing drugs and metabolic wastes from the brain. Recent functional studies in isolated mouse choroid plexus (CP) tissues suggested the existence of organic anion transporting polypeptides (OATPs) at the apical membrane of BCSFB, which may clear large organic anions from the cerebrospinal fluid (CSF). However, the specific OATP isoform involved is unclear. Using quantitative fluorescence imaging, we showed that the fluorescent anions, sulforhodamine101 (SR101), fluorescein methotrexate (FL-MTX), and 8-fluorescein-cAMP (Fluo-cAMP), are actively transported from the CSF to the subepithelial space in CP tissues isolated from wild-type mice. In contrast, transepithelial transport of these compounds across the CPE cells was abolished in Oatp1a/1b$^{-/-}$ mice due to impaired apical uptake. Using transporter-expressing cell lines, SR101, FL-MTX and Fluo-cAMP were additionally shown to be transported by mouse OATP1A5 and its human counterpart OATP1A2. Kinetic analysis showed that estrone-3-sulfate and SR101 are transported by OATP1A2 and OATP1A5 with similar K_m values. Immunofluorescence staining further revealed the presence of OATP1A2 protein in human CP tissues. Together, our results suggest that large organic anions in the CSF are actively transported into CPE cells by apical OATP1A2 (OATP1A5 in mice), then subsequently effluxed into the blood

by basolateral multidrug resistance associated proteins (MRPs). As OATP1A2 transports a wide array of endogenous compounds and xenobiotics, the presence of this transporter at the BCSFB may suggest a novel route for removing neurohormones, drugs and toxins from the CSF.

3.2 Significance Statement

Drug transporters at the blood-cerebrospinal fluid (CSF) barrier play an important, but understudied, role in brain drug disposition. Quantitative fluorescence imaging and molecular analyses revealed a functional role of rodent OATP1A5 in clearing large organic anions from the CSF and suggest a similar role for OATP1A2 at the human blood-CSF barrier. Delineating the molecular mechanisms governing organic anionic clearance from the CSF may help improve the prediction of central nervous system (CNS) pharmacokinetics and inform the identification of drug candidates with favorable CNS pharmacokinetic properties.

3.3 Introduction

Neurological disorders are the primary cause of disability and the second leading cause of death worldwide (196). Consequently, there is a need to develop novel treatments and therapies targeting the central nervous system (CNS). However, CNS drugs face many hurdles in drug development, and the attrition rate for CNS drugs is very high (197). One challenge of CNS drug development is the difficulty in predicting CNS drug pharmacokinetics and exposure, which is linked to and drives efficacy and toxicity. The pharmacokinetic and pharmacodynamic relationship within the CNS is often driven by the unbound brain drug concentration, which is influenced by multiple transport and distribution mechanisms at the blood-brain barrier and the blood-cerebrospinal fluid barrier (BCSFB) (198,199).

The BCSFB is formed by the choroid plexuses (CP), which consist of polarized choroid plexus epithelial (CPE) cells that surround a core of blood capillaries (1,174). As the CP blood capillaries are fenestrated and lack tight junctions, the barrier function lies with the tight junction-linked CPE cells (16,175). The CPE cells express polyspecific transporters and enzymes that contribute to xenobiotic and endogenous compound clearance from the cerebrospinal fluid (CSF) (174). However, transporters at the human BCSFB are understudied with respect to function and activity. Functional studies are largely performed in preclinical species due to the lack of human *in vitro* systems, and characterization of transporter protein expression at the human BCSFB is limited. Thus, the overall significance of BCSFB transporters in brain drug disposition is still not fully understood.

The organic anion transporting polypeptide (OATP/*SLCO*) transporters are a superfamily of drug transporters involved in the uptake and disposition of a wide array of xenobiotics and endogenous substrates. Among the 11 human OATPs and 15 murine OATPs, members of the OATP1A/1B family are especially important in drug transport due to their broad substrate specificity (114). The pharmacokinetic relevance of OATPs has been well studied in the liver, where OATP1B1 and 1B3 play an important role in hepatic uptake and elimination of amphipathic drugs such as statins, repaglinide, and other compounds (115). Interestingly, while some human OATPs have direct rodent orthologs, this is not the case for OATP1A and OATP1B transporter isoforms. In mice, there are four members in the OATP1A family (OATP1A1, OATP1A4, OATP1A5, and OATP1A6) whereas humans only have one member (OATP1A2). In the liver-specific OATP1B family, mice only have one member (OATP1B2) while humans have two isoforms (OATP1B1 and OATP1B3) (114). In human and mice CPs, the mRNA expression of OATP1A2, OATP1A4, and OATP1A5 have been reported (117). The OATP1A4 protein has been

localized to the basolateral membrane (122); while OATP1A5 protein is localized apically (123). The human OATP1A2 protein localization has yet to be characterized and is currently unknown.

Our laboratory recently applied confocal microscopy and live-tissue imaging techniques to study the transcellular transport mechanisms for organic cations and organic anions at the BCSFB (117,200). Using live CP tissues isolated from the mouse brain, we observed that the CPE cells lack an intact transcellular transport system for organic cations but possess a highly functional CSF-to-blood transport system for large and amphipathic organic anions. Pharmacological inhibition studies suggested that the anion transport system likely consists of OATPs at the apical (CSF-facing) membrane and the multidrug resistance associated proteins 1/4 (MRP1/4) at the basolateral (blood-facing) membrane (117). Using quantitative analysis and real-time imaging, we further showed that apical uptake of fluorescent organic anions (e.g. fluorescein methotrexate (FL-MTX), fluorescein-cyclic AMP (Fluo-cAMP)), is the rate-limiting step in the overall CSF-to-blood transport process and highly sensitive to the OATP inhibitor rifampin (117,200). However, definitive data establishing the role of OATPs in CPE cell apical uptake is lacking, and the specific OATP isoform(s) involved in this rate-limiting clearance step remain unknown. Furthermore, the protein expression, localization, and functional relevance of OATP1A2 are unknown in the human CP.

In this study, we investigated the molecular mechanisms underlying transepithelial transport of large organic anions using fluorescent OATP probes sulforhodamine101 (SR101), FL-MTX, and fluo-cAMP in freshly isolated murine CP tissues. The specific activity of OATP1A/1B transporters was defined using a cluster KO mouse model. The transport of the fluorescent probes were further characterized and compared in human OATP1A2 and mouse OATP1A5

overexpressing cells. Lastly, the expression and localization of OATP1A2 was determined in human CP samples.

3.4 MATERIALS AND METHODS

3.4.1 *Materials*

[^{3}H]Estrone-3-Sulfate (49.19 Ci/mmol) was purchased from Perkin Elmer. Sulforhodamine101 was purchased from Sigma-Aldrich (St. Louis, MO). Fluorescein-methotrexate was purchased from Biotium (San Francisco, CA). 8-Fluorescein-cAMP was purchased from Axxora (Farmingdale, NY). Cell culture media and reagents were purchased from ThermoFisher Scientific (Waltham, MA). Cell culture plastic wares were purchased from Grenier Bio One (Monroe, NC) or ThermoFisher Scientific (Waltham, MA). Unless otherwise specified, all chemicals were purchased from Sigma-Aldrich (St. Louis, MO).

3.4.2 *Animals and Choroid Plexus Tissue Collection*

Animal experiments were carried out in accordance with the Guide for the Care and Use of Laboratory Animals as adopted and promulgated by the U.S. National Institutes of Health. All animal procedures were approved by the Institutional Animal Care and Use Committee at the University of Washington. Animals were housed in the specific pathogen free facility at the University of Washington and maintained under standard conditions, with food and water available ad libitum. FVB wild-type and *Slco1a/1b*$^{-/-}$ (referred to as Oatp1a/1b$^{-/-}$) mice were obtained from

Taconic Biosciences (Germantown, NY). Oatp1a/1b$^{-/-}$ mice have a gene cluster deletion removing *Slco1a1*, *Slco1a4*, *Slco1a5*, *Slco1a6*, and *Slco1b2* that encode for Oatp1a and Oatp1b protein products. Generation and physiological characteristics of this strain was described previously (201).

Adult (10–14 week old) male FVB wild-type and Oatp1a/1b$^{-/-}$ mice were euthanized by CO_2 inhalation, followed by decapitation. Mouse brain was isolated and maintained in ice cold artificial CSF (aCSF: 119 mM NaCl, 26.2 mM $NaHCO_3$, 2.5 mM KCl, 1 mM NaH_2PO_4, 1.3 mM $MgCl_2$, 2.5 mM $CaCl_2$, 10 mM glucose, previously gassed with 95% O_2/5% CO_2 for tissue isolation. Lateral ventricle CP was isolated from mouse brain under a dissecting microscope as previously described (200). The CP tissue was either snap frozen for mRNA analysis or transferred to pre-gassed, aCSF for transport imaging studies.

3.4.3 *Quantification of Transporter mRNA Expression by Real Time PCR*

Following CP isolation, tissues were then flash frozen in liquid nitrogen and stored in a -80°C freezer until further processing. Frozen tissue was then homogenized by bead disruptor, and total RNA was extracted by RNeasy Mini Kit (Qiagen, Hilden, Germany). Total RNA was then converted to cDNA by reverse transcription using the High-Capacity cDNA Reverse Transcription Kit (Applied Biosystems, Waltham, MA). Expression of transporters at the CP was quantified using TaqMan Real-Time PCR Master Mix (Applied Biosystems) as described previously (96,117). The relative mRNA levels of these transporters in CP were normalized to glyceraldehyde-3-phosphate dehydrogenase (*Gapdh*). The list of TaqMan Gene Expression

Assays can be found in

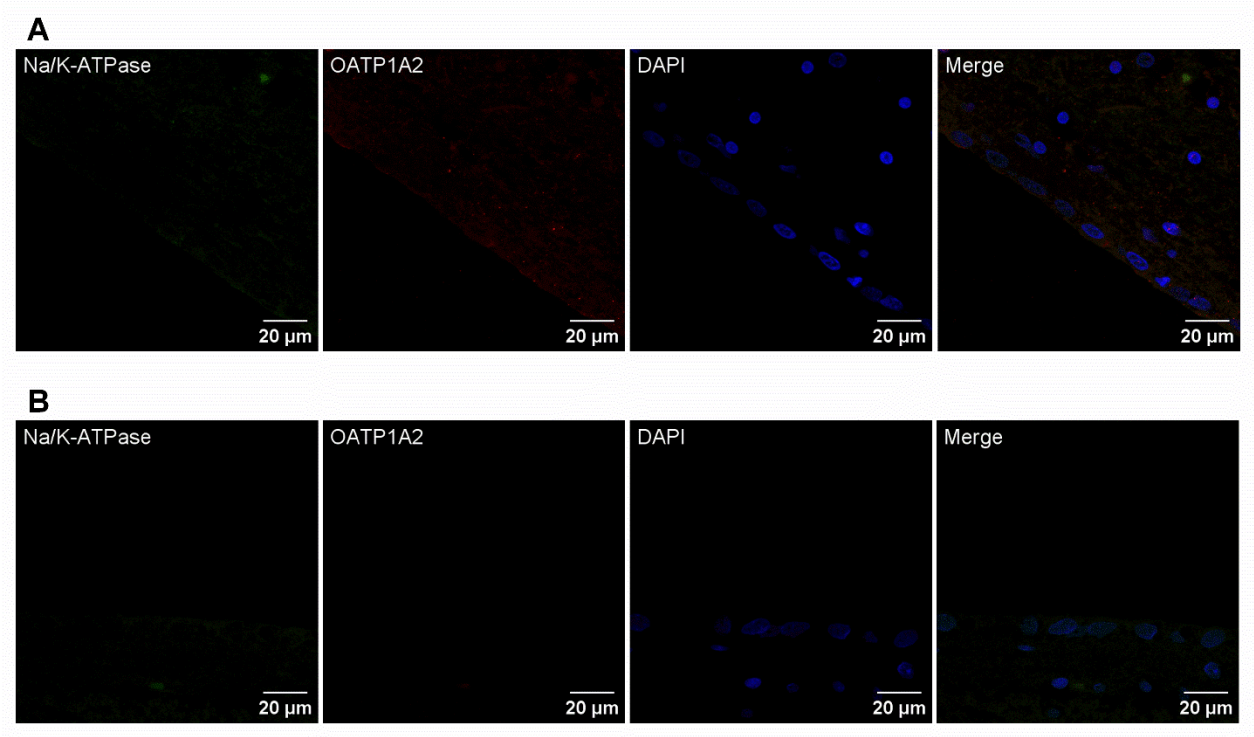

Figure 3.15. Immunofluorescence staining for Na^+/K^+-ATPase and OATP1A2 in human ventricular ependyma

(A) Immunofluorescence staining for Na^+/K^+-ATPase and OATP1A2 in human ventricular ependyma. Na^+/K^+-ATPase and OATP1A2 staining is markedly insubstantial in ventricular ependyma. (B) Control immunofluorescence stain without primary antibody treatment. Deidentified choroid plexus was sourced from a 60-year-old male.

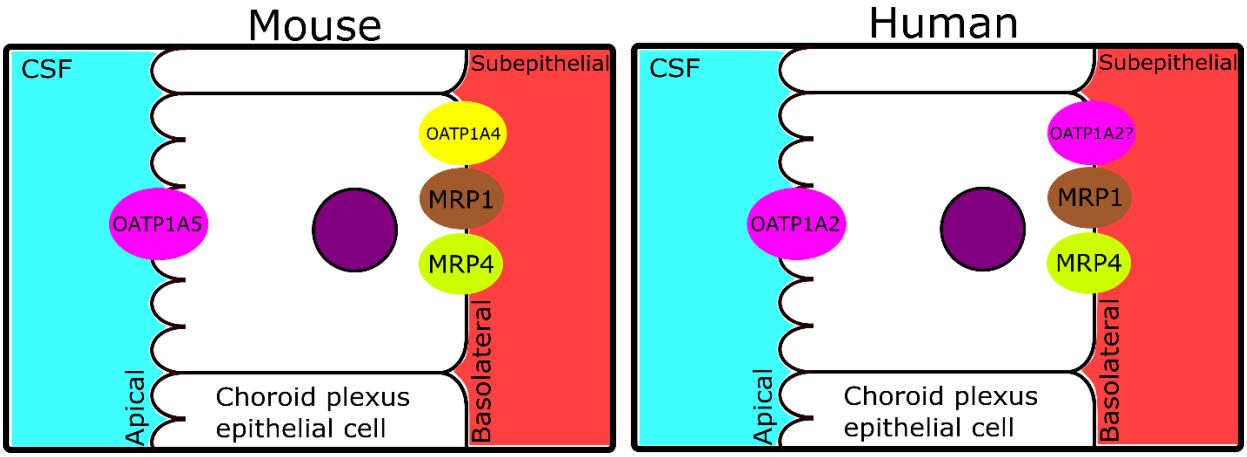

Figure 3.16. Proposed roles of OATP and MRP transporters in BCSFB clearance at the rodent and human BCSFB.

Proposed roles of OATP and MRP transporters in BCSFB clearance at the rodent and human BCSFB. Models are based on data compiled from previous studies (64,111,122,123) and the present study.

Table 3.1.

3.4.4 *Confocal Imaging and Transport Studies in Freshly Isolated CP Tissues from Wild-type and Oatp1a/1b$^{-/-}$ Mice.*

Transport studies using freshly isolated mouse CP were performed using an approach previously described (117,200). Briefly, lateral ventricle CP tissues were transferred immediately after isolation into 35 mm sterile confocal dishes (VWR, Radnor, PA) containing aCSF buffer at room temperature. Isolated CP tissues maintain vitality and transport activity for up to 2-3 hours after isolation, and all transport studies were performed within 2 hours after isolation (200). Single time-point transport studies were initiated by adding 2 μM of fluorescent compound with or without an inhibitor (100 μM) into aCSF. Incubations were carried out for 20 min in sealed Ziploc bags containing 95% O_2/5% CO_2. One to four undamaged observation areas containing both CPE cells and adjacent subepithelial region were selected, and the fluorescent signals were recorded. To record real-time transport of fluorescent substrate, a specific observation area containing intact CPE cells and adjacent subepithelial region was selected and immobilized in pregassed aCSF. Transport was initiated by adding 2 μM of fluorescent compound, and fluorescent signals were recorded every minute for 20 minutes. Additional observation areas containing CPE cells and adjacent subepithelial region were recorded after 20 minutes of uptake.

For live tissue uptake, image acquisition and analysis were performed using procedures previously described (200). Briefly, imaging was performed using a Zeiss LSM 710 confocal microscope fitted with a Zeiss 40x, NA 1.3 oil immersion objective (total magnification: 400x). Brightfield imaging was used to identify observation areas containing CPE cells with adjacent blood capillaries. Samples containing FL-MTX or fluo-cAMP were illuminated using a 488nm

fixed wavelength argon laser. Samples containing SR101 were illuminated using a 594 nm fixed wavelength helium-neon laser. Appropriate corresponding dichroic and emission filters were used to detect the emission of the fluorescent probes. Low laser intensity (less than 8% of maximum) was used to minimize sample photobleaching. Laser gain and offset was set such that autofluorescence of tissue was minimally detectable, with the pinhole set to 36.8 μm. Confocal images were captured as 15 sec scans at 1024 × 1024 resolution, 16 frames line-averaged, with a pixel dwell of 0.79 μsec. Replicate studies were performed using the same objective lens, identical laser power, and identical detector settings.

Digital image analysis was performed using Fiji ImageJ (1.53t) (184). CPE cell and subepithelial regions were defined and manually segmented as previously described (200). Mean fluorescence, measured by average pixel intensity, was measured in segmented CPE cell and subepithelial regions, averaged from three independent segmented regions. CPE cell and subepithelial region fluorescence were corrected for background fluorescence, obtained from the surrounding bathing media in single-time point experiments and from the mean fluorescence prior to fluorescent probe addition for time-dependent transport experiment.

For live tissue uptake, image acquisition and analysis were performed using procedures previously described (200). Briefly, imaging was performed using a Zeiss LSM 710 confocal microscope fitted with a Zeiss 40x, NA 1.3 oil immersion objective (total magnification: 400x). Brightfield imaging was used to identify observation areas containing CPE cells with adjacent blood capillaries. Samples containing FL-MTX or fluo-cAMP were illuminated using a 488nm fixed wavelength argon laser. Samples containing SR101 were illuminated using a 594 nm fixed wavelength helium-neon laser. Appropriate corresponding dichroic and emission filters were used

to detect the emission of the fluorescent probes. Low laser intensity (less than 8% of maximum) was used to minimize sample photobleaching. Laser gain and offset was set such that autofluorescence of tissue was minimally detectable, with the pinhole set to 36.8 μm. Confocal images were captured as 15 sec scans at 1024 × 1024 resolution, 16 frames line-averaged, with a pixel dwell of 0.79 μsec. Replicate studies were performed using the same objective lens, identical laser power, and identical detector settings.

Digital image analysis was performed using Fiji ImageJ (1.53t) (184). CPE cell and subepithelial regions were defined and manually segmented as previously described (200). Mean fluorescence, measured by average pixel intensity, was measured in segmented CPE cell and subepithelial regions, averaged from three independent segmented regions. CPE cell and subepithelial region fluorescence were corrected for background fluorescence, obtained from the surrounding bathing media in single-time point experiments and from the mean fluorescence prior to fluorescent probe addition for time-dependent transport experiment.

3.4.5 *Generation of OATP1A5 and OATP1A2 Stable Cell Lines and Cell Culture*

OATP1A5/*Slco1a5* expression vector (MMM1013-202762445) was obtained from Horizon Discovery (Waterbeach, United Kingdom) and subsequently stably transfected into Flp-In HEK293 cells using a modified approach previously described (94). Briefly, the expression vector was digested by KpnI and XhoI (New England Biolabs, Ipswich, MA) to obtain the *Slco1a5* cDNA of interest, which was subsequently subcloned into the KpnI/XhoI sites of the pcDNA5/FRT vector (Invitrogen, Waltham, MA). The insert of the OATP1A5 expression vector was sequenced and aligned with the NCBI GenBank sequence BC013594 to ensure fidelity. This newly generated OATP1A5 expression vector was then co-transfected with pOG44 expressing the

Flp-recombinase into the Flp-In HEK293 cell line using Lipofectamine 3000 (ThermoFisher Scientific). Transfected cells were selected by hygromycin B treatment (250 μg/mL), whereby the optimal hygromycin B concentration was determined by a kill-curve in Flp-In HEK293 cells (data not shown). HEK293 cells expressing the empty pcDNA5/FRT vector were previously generated in our laboratory (94). Transfected HEK293 cells stably expressing the human OATP1A2 and empty vector were generated using a lentiviral construct in the Hagenbuch laboratory as follows. Lenti ORF particles encoding OATP1A2 (Myc-DDK tagged) along with Lenti ORF control particles pLenti-C-Myc-DDK-P2A-Puro were purchased from OriGene (Rockville, MD). HEK293 cells were transduced following a protocol supplied by OriGene. Briefly, HEK293 cells were seeded at 50,000 cells/well on a 24-well plate. Twenty-four hours later, the cells were transduced with an MOI of 5 in the presence of polybrene (8 μg/ml). The next day the medium was changed to normal medium. On day four, the cells were split onto 6cm plates in a medium containing 2μg/ml puromycin. Once confluent, the cells were split onto 10cm plates, and single colonies were isolated by limited dilution. The clone with the highest uptake of estrone-3-sulfate was used for further characterization. OATP1A2 and empty vector cells were maintained in Dulbecco's modified Eagle's medium (11054-020) supplemented with 10% Fetal Bovine Serum, 2% GlutaMax, 100 U/mL penicillin, 100 μg/mL streptomycin, 2 μg/mL puromycin, and a final concentration of 25 mM D-glucose. Generated OATP1A5 and empty vector cells were maintained in Dulbecco's modified Eagle's medium (11995-065) supplemented with 10% fetal bovine serum, 100 U/mL penicillin, 100 μg/mL streptomycin, and 150 μg/mL hygromycin B. The surface of the flasks was coated with 0.01% poly-D-lysine in phosphate-buffered saline to promote HEK293 cell attachment. Cells were cultured and maintained in a 37°C incubator with 5% CO_2.

3.4.6 *Uptake and Inhibition Assays in HEK293 Cells*

Uptake and inhibition assays were conducted using a modified approach previously described (202). Briefly, cells were seeded on 96-well plates and grown to greater than 90% confluency. Cells were washed with 37°C Krebs-Ringer-HEPES buffer (125 mM NaCl, 4.8 mM KCl, 1.2 mM $MgCl_2$, 1.2 mM $CaCl_2$, 5.6mM Glucose, 25 mM HEPES, 1.2 mM KH_2PO_4). Experiments were initiated by the addition of 100 µL of Krebs-Ringer-HEPES buffer containing substrate compound with or without an inhibitor. Uptake was quenched by removing the substrate-containing buffer and washing the cells with ice-cold buffer. After washing 3 times, cells were lysed with 10% acetonitrile, and the resulting lysate was used to determine the total protein amount by the BCA method and to quantify intracellular substrate concentrations. Fluorescence measurements of SR101 were performed from a top-read position in a Synergy HTX plate reader (Biotek, Winooski, Vermont) using a 585/10nm excitation and 620/40nm emission filter set. FL-MTX and fluo-cAMP were similarly detected using a 485/20 excitation and 528/20 emission filter set. Fluorescence values were background subtracted by fluorescence readings in wells containing cells without added fluorescent substrate. Transporter specific uptake was determined by subtracting the uptake in empty vector-transfected cell controls from that of transporter-expressing cells. To quantify intracellular SR101 concentrations and confirm the linearity of the fluorescent signal, the intracellular fluorescent signal was converted to concentrations using standard curves prepared in cell lysate and spiked with known quantities of SR101. The fluorescent signal was linear ($R>0.999$) in all experiments (data not shown). [^{3}H]Estrone-3-sulfate radioactivity was measured by Tri-Carb Liquid Scintillation Counter (Perkin Elmer, Waltham, MA).

3.4.7 *Immunofluorescence Staining of Human Choroid Plexus*

Deidentified human CP tissue sections from normal brains were obtained from Northwest BioSpecimen (NWBioSpecimen, Seattle, WA). CP tissue were preserved as formalin-fixed, paraffin-embedded tissue blocks that were then cut into 4 μm sections and mounted on positively charged microscope glass slides. To prepare samples for immunofluorescence, slides were deparaffinized and rehydrated in xylene and a series of ethanol. Antigen retrieval was performed using 10 mM citrate buffer containing 0.05% Tween-20 (pH 6.0) for 15 min at 98°C. Afterwards, tissues were maintained in low flow, cold deionized water for 10 min to reform the antigenic sites. CP tissues were then treated with 0.1% Sudan Black B for 20 min to quench autofluorescence and subsequently treated with Image-iT FX Signal Enhancer (ThermoFisher Scientific, Waltham, MA) for 15 minutes.

After washing, the tissues were blocked for one hour using a solution of 10% normal donkey serum (NDS) with 22.52 mg/mL glycine in PBS-T and then incubated overnight at 4°C in 1% NDS in PBS-T containing 2 μg/mL anti-OATP1A2 antibody (ab221804, Abcam) and 10 μg/mL anti-Na^+/K^+-ATPase (ab7671, Abcam). Anti-OATP1A2 antibody specificity were confirmed in overexpressing OATP1A2 and empty vector HEK293 cells (**Figure 3.1**). Negative controls were maintained in blocking buffer. The following day, tissues were washed and then incubated with 2.5% NDS in PBS-T containing 10 μg/mL Alexa Fluor 488-conjugated donkey anti-mouse (A21202, Invitrogen) and 10 μg/mL Alexa Fluor 555-conjugated donkey anti-rabbit (A31572, Invitrogen) for 2 hours at room temperature. The tissues were then washed, mounted (ab104139, Abcam), and coverslipped for subsequent confocal imaging.

Imaging of immunofluorescence stains was captured similarly with the following modifications: the Zeiss LSM 710 was fitted with a Zeiss 63x, NA 1.4 oil immersion objective (total magnification: 630x). DAPI stains were illuminated using a 405 nm laser diode equipped with an appropriate emission filter. Alexa Fluor 488-conjugated antibodies were illuminated using a 488 nm fixed wavelength argon laser. Alexa 555-conjugated antibodies were illuminated using a 561 nm diode-pumped solid-state laser. Appropriate corresponding dichroic and emission filters were used to detect the fluorescence emission. Confocal images were captured as 19s scans at 512 x 512 resolution, 16 frames line averaged, with a pixel dwell of 1.27 μsec and a pinhole of 60 μm. Tissue images were z-stacked using an average intensity projection approach. Linear brightness adjustments were performed consistently across immunofluorescence images in accordance with the Office of Research Integrity.

3.4.8 *Statistical Analysis and Data fitting*

Uptake and inhibition studies were performed in triplicate and repeated three times independently. The data were fitted by nonlinear regression using GraphPad Prism 7.0 (Graph-Pad Software Inc., La Jolla, CA) to obtain graphs and kinetic parameters. The uptake kinetics data were fitted to the Michaelis-Menten equation. For the dose-dependent inhibition of transporter-mediated uptake of SR101, the IC_{50} was calculated using a 4-parameter equation. Statistical significance was determined using a one-way ANOVA followed by Dunnett's test or an unpaired Student's *t* test as specified in the figure legends. A *P* value less than 0.05 was considered statistically significant.

3.5 RESULTS

3.5.1 *mRNA Expression of OATP/Slco 1a and 1b Isoforms in FVB mouse CP*

We first determined the mRNA expression of the rodent *Slco* 1a and 1b isoforms, encoding OATP 1A and 1B proteins, in the CP of wild-type FVB mice using RT-qPCR (**Figure 3.2**). FVB CPs express mRNA for *Slco1a4* and *Slco1a5*, whereas expression of *Slco1a1*, *Slco1a6*, and *Slco1b2* mRNA were minimal or undetectable. While *Slco1a4* is expressed at higher levels than *Slco1a5*, the OATP1A4 protein was previously localized to the basolateral membrane of CPE cells, and hence may not contribute to apical uptake of large organic anions from the CSF (122). In addition, mRNA for *Abcc1* and *Abcc4* encoding basolateral efflux MRP transporters, along with the mRNAs for uptake transporters of the OATP family, *Slco1c1* and *Slco3a1*, were highly expressed at the CPs of FVB mice (**Figure 3.3**). These results are consistent with our previous findings in the C57BL/6 strain (117).

3.5.2 *Large Organic Anion Uptake from the CSF is Likely Mediated by OATP1A5 at the Mouse BCSFB*

Based on RT-qPCR results and available localization data, we hypothesized that OATP1A5 may contribute to the uptake of organic anions from the CSF into CPE cells. To assess the contribution of OATPs towards organic anion uptake, CP tissues were incubated with SR101 in the absence or presence of bromosulphophthalein (BSP), a pan-OATP inhibitor (**Figure 3.4**). SR101 was recently characterized as a fluorescent substrate for human OATP1A2 and OATP1C1 (203). Representative graphical, differential interference contrast, and confocal images of mouse CP depicting morphological structure and subepithelial accumulation of SR101 are shown in

Figure 3.5. Real-time analysis showed that in wild-type CP, SR101 rapidly and primarily accumulates in the subepithelial space, demonstrating rapid transepithelial flux across the CPE cells (**Figure 3.6**). In age-matched Oatp1a/1b$^{-/-}$ mice (**Figure 3.4**; **Figure 3.6**), subepithelial accumulation in the KO tissue is reduced by 65.9±27.8% compared to the wild-type (**Figure 3.6**). BSP reduced the subepithelial accumulation of SR101 by 92.1±10.6% in wild-type mice but had no apparent effect in KO mice (**Figure 3.6**). These results suggest that OATP-mediated apical uptake of SR101 is abolished at the BCSFB in the Oatp1a/1b$^{-/-}$ animals. We then tested the transport of two additional OATP fluorescent substrates, FL-MTX and fluo-cAMP. We observed an 81.8±44.3% reduction of FL-MTX accumulation and an 89.8±35.3% reduction of fluo-cAMP accumulation in the subepithelial compartment in KO CP (**Figure 3.7**). Taken together, the data demonstrated that members of the OATP1A and 1B family are responsible for apical uptake of large organic anions at the murine BCSFB. As OATP1B transporters are liver specific (204), and OATP1A5 is the only OATP1A member localized to the apical membrane in rodent CPE cells (204), OATP1A5 is likely the major mediator transporting large organic anions from CSF into CPE cells.

3.5.3 *SR101, FL-MTX, and fluo-cAMP are substrates of mouse OATP1A5 and human OATP1A2*

While we have demonstrated strong evidence towards OATP1A5 function at the BCSFB, the molecular and functional properties of mouse OATP1A5 are poorly understood. We thus sought to characterize the transport properties of the fluorescent substrates utilized in our *ex vivo* CP experiments towards the mouse OATP1A5. Furthermore, we were interested in clarifying the functional similarity of mouse OATP1A5 and OATP1A2, the OATP1A homolog in humans. To address these questions, we generated HEK293 cell lines stably expressing mouse OATP1A5 and

human OATP1A2. The uptake of FL-MTX, fluo-cAMP, SR101, and the classical OATP substrate estrone-3-sulfate was measured. Compared with the vector control, uptake of all four substrates increased in OATP1A5-expressing cells after a 20-minute incubation (**Figure 3.8**), confirming that the substrates transported *ex vivo* in CP tissues are indeed substrates of OATP1A5. All the substrates were also transported by OATP1A2, suggesting similar substrate selectivity between human OATP1A2 and mouse OATP1A5.

3.5.4 *Kinetic characterization and comparison of Estrone-3-sulfate and SR101 uptake by OATP1A5 and OATP1A2*

The transport kinetics of estrone-3-sulfate and SR101 by OATP1A2 and OATP1A5 was further investigated. To determine the initial linear range of uptake by OATP1A2 and OATP1A5, time-dependent uptake of the two substrates was examined. Both compounds demonstrated linear uptake in the early time points before reaching a plateau by 20 minutes (**Figure 3.9**). Transporter-mediated uptake was linear in the first two minutes for estrone-3-sulfate and the first 8-12 minutes for SR101 by OATP1A2 and OATP1A5. As a result, concentration-dependent kinetic studies were performed using a 2-minute incubation time for estrone-3-sulfate and a 4-minute incubation time for SR101. Transporter-mediated uptake of estrone-3-sulfate and SR101 displayed typical Michaelis-Menten kinetics for both OATP1A2 and OATP1A5 (**Figure 3.10**). The K_m and V_{max} were derived from nonlinear regression fitting and are summarized in Table 3.2. The K_m values for estrone-3-sulfate and SR101 were very similar between OATP1A5 and OATP1A2, indicating a similar affinity for the studied substrates. We then performed a dose-dependent inhibition assay of SR101 uptake by BSP in both OATP1A2 and OATP1A5 expressing cell lines (**Figure 3.11**). Assays were performed using a 4 min incubation time at substrate concentrations below the K_m.

Consistent with the *ex vivo* CP inhibition data presented above, BSP inhibited the OATP1A5-mediated uptake of SR101 with an IC_{50} of 1.61 ± 0.39 µM. The IC_{50} for OATP1A2 is 15.09 ± 5.83 µM, 9.4-fold higher than that of OATP1A5.

3.5.5 *Expression and Localization of OATP1A2 at the Human Blood-CSF Barrier*

The above data suggest that large organic anion uptake from the CSF is likely mediated by Oatp1a5 at the rodent BCSFB, contributing to a clearance route for large organic anions from CSF to blood in rodents. However, it is currently unknown if a similar clearance pathway is present at the human BCSFB. While OATP1A2 mRNA expression has been previously reported at the human BCSFB (117), its protein expression and localization is unknown. We therefore sought to determine the expression and localization of OATP1A2 protein at the human BCSFB through immunofluorescence staining of human CP sections using an OATP1A2 polyclonal antibody. As shown in **Figure 3.12**, OATP1A2 protein is indeed expressed in human CP. Colocalization was observed with Na^+/K^+-ATPase, an established apical membrane marker in CPE cells (205,206), suggesting OATP1A2 localizes to the apical membrane in human CP (**Figure 3.12**). Besides apical staining, OATP1A2 signal was also observed intracellularly and possibly at the basolateral membrane. Minimal fluorescence signal was observed in CP tissue controls prepared without the primary antibodies (**Figure 3.13**). Expression and localization of OATP1A2 was consistent in the two human CP samples examined (**Figure 3.12**; **Figure 3.14**). OATP1A2 signal was minimally observed in the ventricular ependyma (**Figure 3.15**), suggesting the expression of OATP1A2 is enriched in CP relative to the surrounding tissue.

The above data suggest that large organic anion uptake from the CSF is likely mediated by OATP1A5 at the rodent BCSFB, contributing to a clearance route for large organic anions from

CSF to blood in rodents. However, it is currently unknown if a similar clearance pathway is present at the human BCSFB. While OATP1A2 mRNA expression has been previously reported at the human BCSFB (117), its protein expression and localization is unknown. We therefore sought to determine the expression and localization of OATP1A2 protein at the human BCSFB through immunofluorescence staining of human CP sections using an OATP1A2 polyclonal antibody. As shown in **Figure 3.12**, OATP1A2 protein is indeed expressed in human CP. Colocalization was observed with Na^+/K^+-ATPase, an established apical membrane marker in CPE cells (205,206), suggesting OATP1A2 localizes to the apical membrane in human CP (**Figure 3.12**). Besides apical staining, OATP1A2 signal was also observed intracellularly and possibly at the basolateral membrane. Minimal fluorescence signal was observed in CP tissue controls prepared without the primary antibodies (**Figure 3.13**). Expression and localization of OATP1A2 was consistent in the two human CP samples examined (**Figure 3.12**, **Figure 3.14**). OATP1A2 signal was minimally observed in the ventricular ependyma (**Figure 3.15**), suggesting the expression of OATP1A2 is enriched in CP relative to the surrounding tissue.

3.6 DISCUSSION

Previous work from our laboratory indicated that OATP transporters at the apical membrane of CPE cells work cooperatively with basolateral MRPs to mediate CSF-to-blood clearance of large amphipathic anions in mice. Several OATP isoforms are expressed in rodent and human CP but the specific contribution of individual OATPs to this process is unclear. In this study, we clarified the role of OATP1A members towards organic anion uptake at the BCSFB using Oatp1a/1b$^{-/-}$ mice, investigated the functional overlap between mouse OATP1A5 and human

OATP1A2, and established the presence of the OATP1A2 protein at the human BCSFB. Findings from our study provided novel insights into the molecular mechanisms underlying BCSFB clearance of large amphipathic organic anions from the CSF.

Our laboratory recently demonstrated that the apical uptake of FL-MTX and fluo-cAMP at the BCSFB is the rate-limiting step in the transepithelial transport process and plays an important kinetic role in the transport of large organic anions from the CSF into the blood (117,200). Apical uptake was highly sensitive to the OATP-inhibitor rifampin (117,200). Consistent with our earlier study, we also detected OATP/*Slco* mRNA expression of *Slco1a4/5*, *Slco1c1*, and *Slco3a1* in mouse CP tissues (Hu et al 2022) (**Figure 3.2**, **Figure 3.3**). OATP1C1 is a thyroid hormone transporter and is expressed basolaterally at the BCSFB, where it contributes to entry of thyroid hormones into the brain (119,207). OATP3A1 is expressed on both membranes of the BCSFB, but primarily transports prostaglandins (120). Thus, we hypothesized that members of OATP1A subfamily are most likely to be involved in apical uptake of large fluorescent anions previously observed in live CP tissues. Indeed, transport of SR101, FL-MTX, and fluo-cAMP was abolished in CPs isolated from Oatp1a/1b$^{-/-}$ mice (**Figure 3.4**, **Figure 3.6**). Further, SR101 transport in CP tissue of KO mice was not affected by BSP, suggesting OATP1C1 does not play an appreciable role in apical uptake of SR101. As OATP1A4 is localized basolaterally in rodent CP (122), our data using the Oatp1a/1b$^{-/-}$ model and RT-qPCR (**Figure 3.2**, **Figure 3.6**, **Figure 3.7**), alongside the reported apical localization of OATP1A5 (123), suggest that the CPE cell uptake of large organic anions is predominantly mediated by OATP1A5 in rodents (**Figure 3.16**). Additional study of CP transport in an OATP1A5 single knockout model with matched wild-types could confirm the contribution of OATP1A5 at the mouse BCSFB apical membrane and validate the proposition of minimal OATP1A4 contribution at the apical membrane due to basolateral

localization. Efflux of large organic anions at the basolateral membrane of the CPE cell is mediated by MRP1/*Abcc*1 and MRP4/*Abcc*4, previously established in knockout models (Wijnholds *et al.*, 2000; Leggas *et al.*, 2004). The apical uptake is the rate-limiting step of large organic anion transport across the BCSFB in the tested compounds, indicating that the basolateral efflux clearance mediated by MRP1 and MRP4 is much greater than the apical uptake clearance likely mediated by OATP1A5. This is also consistent with the higher mRNA expression of *Abcc1* and *Abcc4* than *Slco1a5* in mouse CP (**Figure 3.2**, **Figure 3.3**). While OATP1A4 is also localized basolaterally (122), the functional activity of OATP1A4 at the BCSFB has not been clearly demonstrated. OATP1A4 may contribute to some low efficiency efflux from CPE cell to blood. In addition, OATP1A4 is also expressed at the blood-brain-barrier and has been implicated in blood-to-brain transport of statin drugs (208).

Outside of the mouse, studies have shown that the CP can actively uptake large organic anions in several other species. In rat CP, the fluorescent molecules FL-MTX, Texas Red, and fluo-cAMP were all transported across the tissue and accumulated in the subepithelial compartment (112,190,209). Similar trends were also observed for Texas Red and FL-MTX in dogfish shark CP (183,209). While mice have four members in the OATP1A subfamily, larger animals, including humans, only have one 1A member, OATP1A2. Regardless of this difference, the expression of OATP1A transporters at the BCSFB appears to be present across different animal species. OATP1A5 protein is very highly expressed in rat CP, and OATP1A2 protein is expressed in dog and pig CP (58–60). Our laboratory has extended these findings into the human CP. We recently found OATP1A2 mRNA expression at the human BCSFB (117), and the data presented in this study demonstrate that OATP1A2 protein is also expressed, appearing to localize to the apical membrane (**Figure 3.12**). In this study, we also directly compared the transport by the poorly

characterized mouse OATP1A5 and human OATP1A2 using overexpressing cells. We observed that FL-MTX, fluo-cAMP, SR101, and estrone-3-sulfate were all transported by both OATP1A5 and OATP1A2 (**Figure 3.8**). Further kinetic studies revealed similar K_m values for SR101 and estrone-3-sulfate between the human and mouse transporters (Table 3.2). The data suggest that mouse OATP1A5 and human OATP1A2 share functional similarity and could both mediate endobiotic and xenobiotic clearance at the BCSFB. Taken together, we thus postulate that, like rodents, apical OATP1A2 and basolateral MRP1/4 exist at the human BCSFB to mediate CSF-to-blood transport and clearance of large organic anions (**Figure 3.16**). OATP1A2 expression is also observed intracellularly and possibly basolaterally, though further immunostaining is needed to validate this observation (**Figure 3.12**; **Figure 3.16**).

A myriad of endobiotics and toxins are substrates of OATP1A2, and hence CSF concentrations of these compounds could be regulated by OATP1A2 at the BCSFB. For instance, dehydroepiandrosterone sulfate (DHEAS), a substrate of OATP1A2 (210), is an important neurosteroid and neutrophin, with multiple neurobiological effects in the brain. DHEAS acts as a modulator for $GABA_A$, NDMA, and other receptors in the brain (211). Additionally, the steroid hormone is associated with neurogenesis and neuronal survival (211). DHEAS is believed to be synthesized in the brain (212), and OATP1A2 at the BCSFB may contribute to its clearance out of the CNS. OATP1A2 also transports the thyroid hormones thyroxine (T4) and triiodothyronine (T3), suggesting this transporter may play a secondary role in regulating thyroid hormone levels in the CNS alongside the prototype thyroid hormone transporters OATP1C1 and monocarboxylate transporter 8 (207,213).

The BCSFB remains an important, but understudied blood-CNS interface for brain drug disposition. For some diseases, the CSF can be considered a directly relevant pharmacokinetic and pharmacodynamic compartment. This is the case for bacterial meningitis, where the bacteria replicate within the CSF after penetrating the CNS (214). Interestingly, ceftriaxone, a cephalosporin antibiotic used to treat some forms of bacterial meningitis, has poor CSF penetration and is an OATP substrate (215,216), which may allude to the contribution of OATP1A2 to its clearance from the CSF. OATP1A2 additionally transports a variety of other drugs that are therapeutically relevant in the CNS. Triptans, which have been identified as substrates in OATP1A2 transduced HEK293 cells, are used in the treatment of migraines and cluster headaches (217). In addition, OATP1A2 transports a range of antivirals and antineoplastics (213). The CNS can often be a sanctuary site for HIV or malignant cancer cells and OATP1A2 at the CP may reduce therapeutic drug concentrations at the CSF (218,219). Future studies may clarify the relevance of OATP1A2 towards the CNS disposition and pharmacokinetics of these drugs.

Understanding the role of OATP1A2 at the BCSFB may also be highly relevant for CNS-active drug candidates in development. The CSF is often the only clinically accessible CNS compartment to obtain information on the free drug concentrations in the human brain (199). However, numerous studies have suggested disconnects between CSF and unbound brain extracellular fluid drug concentrations, possibly due to transport processes at the BCSFB and blood-brain barrier. This has been observed for substrates of P-gp, which is expressed luminally at the blood-brain barrier and apically or subapically at the BCSFB. For instance, Nagaya *et al.* demonstrated in monkeys that poor substrates of P-gp had a $K_{p,uu}$ ratio between CSF and brain interstitial fluid close to unity, while good substrates may have CSF concentrations 3-fold or higher than brain interstitial fluid (148). Understanding mechanisms regulating CSF drug concentrations

may help to fill the gaps in predicting unbound brain drug concentrations using mechanism-based modeling approaches such as physiologically based pharmacokinetic (PBPK) modeling.

In summary, we have clarified the molecular mechanism of OATP1A transport in rodent BCSFB and demonstrated the expression and apical localization of OATP1A2 protein at the human BCSFB. Our study in mice and human CP suggests that at the BCSFB, organic anions in the CSF can be actively transported into CPE cells by apical OATP1A2 (OATP1A5 in rodents) followed by MRP1/4-mediated basolateral efflux into the blood. As this process can influence CSF drug concentrations and brain exposure to CNS active compounds, delineating the molecular mechanisms and the specific impact of OATP1A2 on anionic drug clearance from the CSF may help to improve the prediction of CNS pharmacokinetics and identification of drug candidates with favorable CNS pharmacokinetic properties.

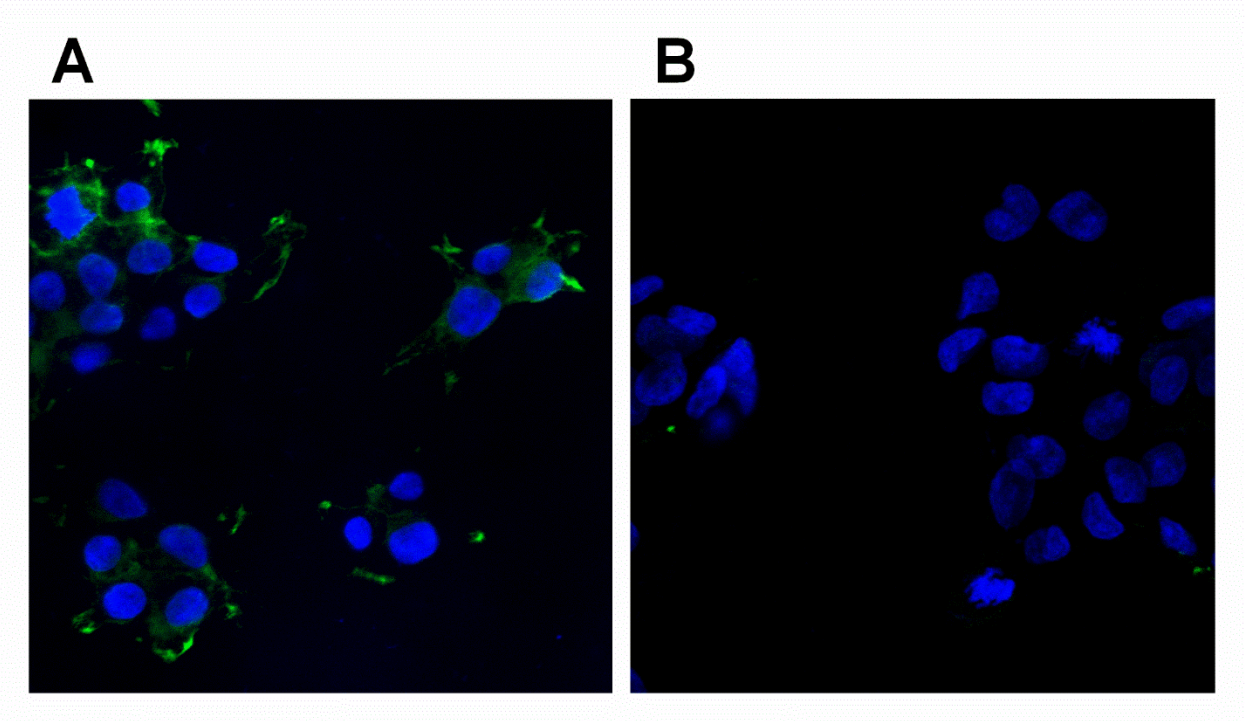

Figure 3.1. Anti-OATP1A2 ICC staining in OATP1A2 and empty vector overexpressing cells

Immunocytochemistry staining for OATP1A2 (green) and DAPI (blue) in (A) OATP1A2 overexpressing and (B) empty vector cells. Cells were treated with 2 µg/mL anti-OATP1A2 antibody, followed by 4 µg/mL Alexa Fluor™ 488 donkey anti-rabbit secondary antibody.

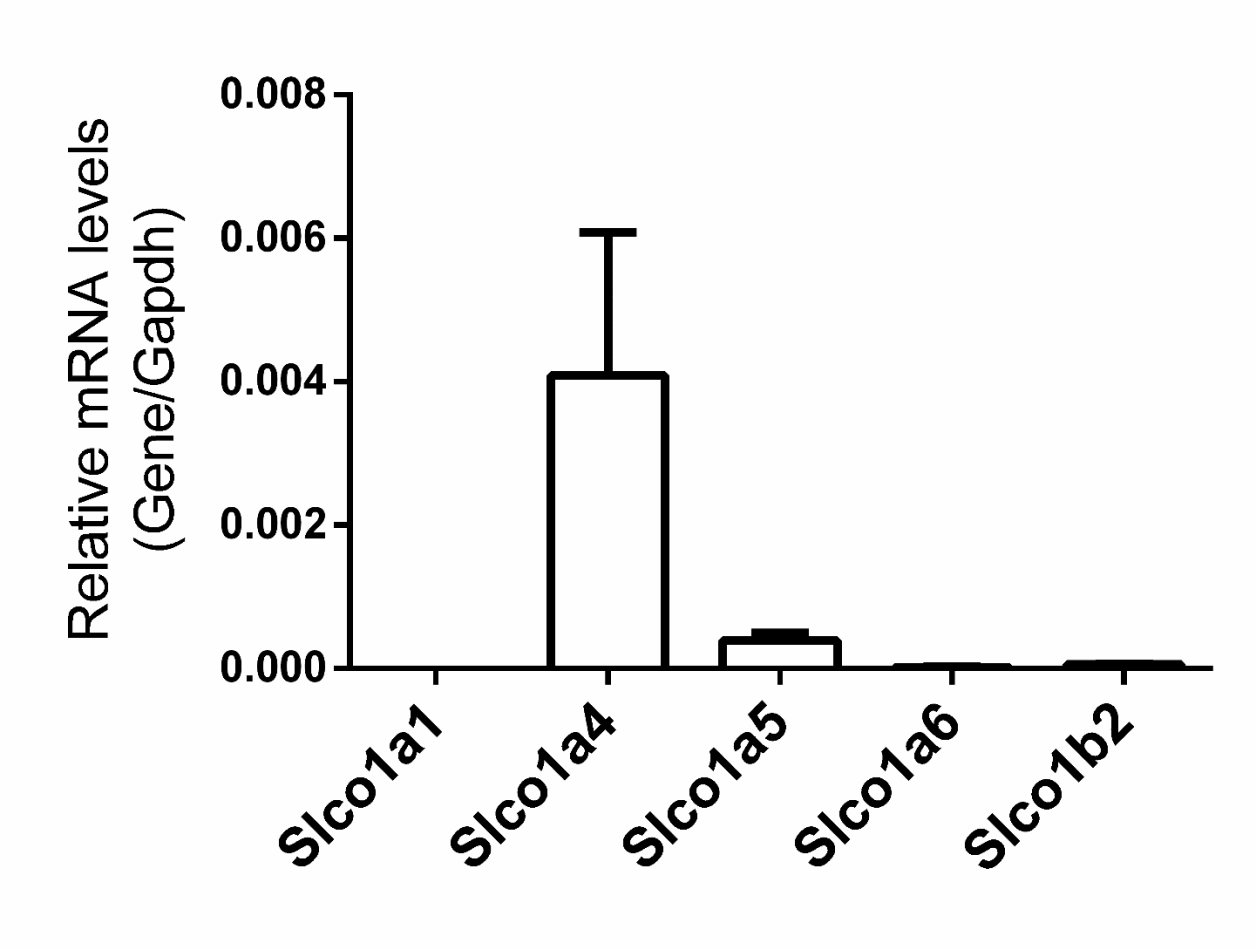

Figure 3.2. Relative mRNA expression of relevant OATP/Slco organic anion transporters

Relative mRNA expression of OATP/*Slco* 1a/1b organic anion transporters in FVB mouse lateral ventricle CP tissues (n=9, pooled groups of 3). Expression levels are normalized to the housekeeping gene *Gapdh*. Values are means ± SD across 3 pools of tissues, with each pool containing CP tissues from 3 mice.

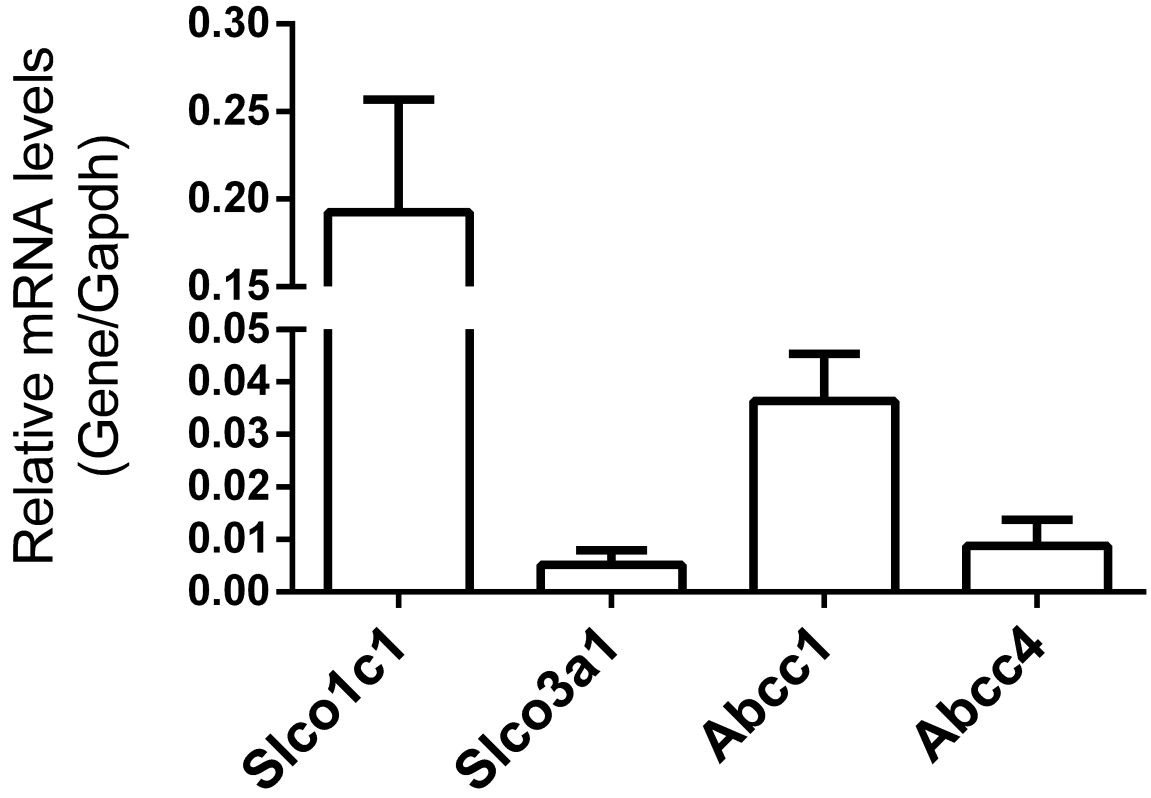

Figure 3.3. Expression of Relevant MRP/*Abcc* and other OATP/*Slco* transporters

Expression of Relevant Mrp/*Abcc* and Oatp/*Slco* transporters in FVB mouse lateral ventricle CP tissues. Expression levels are normalized to the housekeeping gene *Gapdh*. Values are means ± SD across 3 pools of tissues, with each pool containing CP tissues from 3 mice.

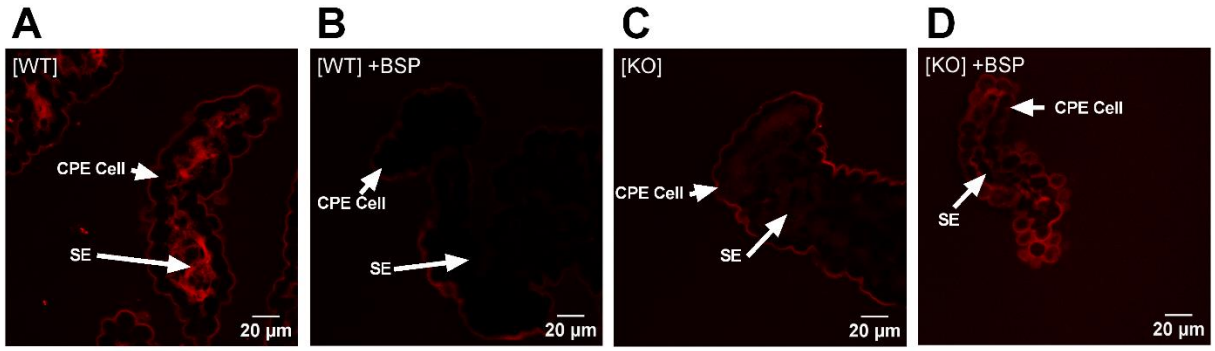

Figure 3.4. Representative confocal images of SR101 with or without BSP in CP obtained from wild-type and Oatp1a/1b$^{-/-}$ mice

Representative confocal images of SR101 (2 µM) with or without BSP (100 µM) in CP obtained from wild-type (A,B) and Oatp1a/1b$^{-/-}$ (C,D) mice after 20 min. The fluorescent signal is primarily observed in the subepithelial compartment, indicating transepithelial flux from the CSF, across the CPE cells, and into the subepithelial compartment.

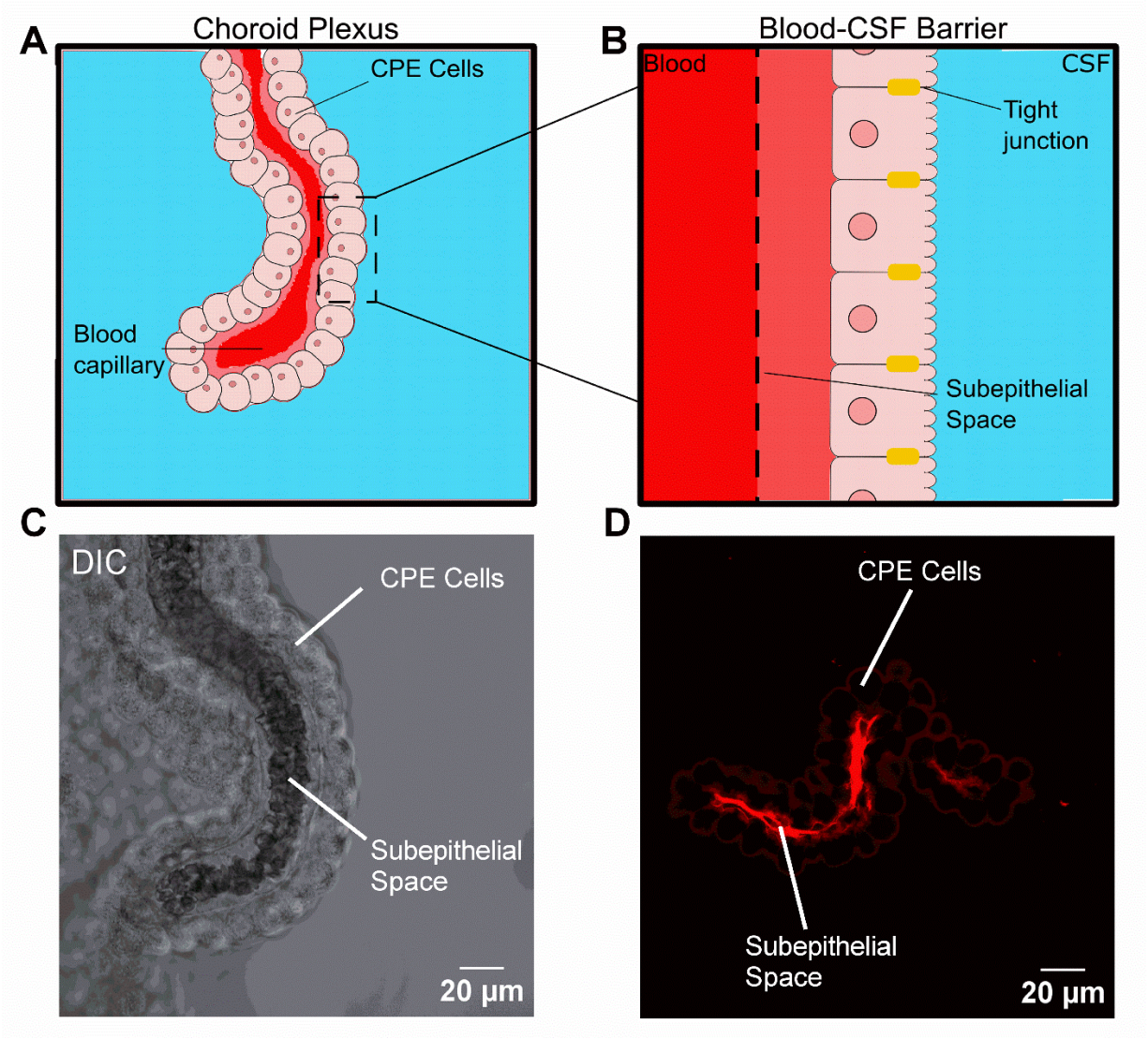

Figure 3.5. Diagrams, DIC image, and confocal image of choroid plexus

Schematic diagram showing (A) choroid plexus tissue composed of CPE cells surrounding the blood capillary. (B) Close-up schematic of the blood-CSF barrier. CPE cells are linked by tight junctions, separating the CSF from the subepithelial space in the blood compartment. (C) Representative differential interference contrast (DIC) image of the murine CP, showing CPE cells surrounding the red blood cell-containing subepithelial space. A trans-PMT detector was used to capture the DIC image. (D) Representative confocal image of CP after incubation with SR101 (2 µM), with indicated CPE cell and subepithelial regions.

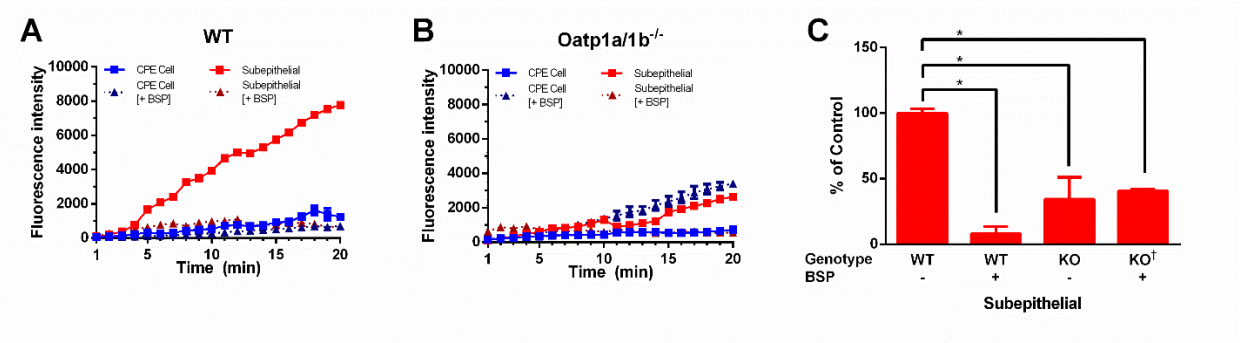

Figure 3.6. Quantification of SR101 accumulation in CPE cell and subepithelial compartments from CP obtained from wild-type and Oatp1a/1b$^{-/-}$ mice

Representative time courses of quantified SR101 accumulation in CPE cell and subepithelial compartments from CP obtained from (A) wild-type and (B) Oatp1a/1b$^{-/-}$ mice. (C) Changes in subepithelial accumulation between treatment groups. Data are normalized to SR101 subepithelial accumulation in wild-type tissues. Values are means ± SD across 3 biological replicates for all treatment groups unless otherwise noted. Statistical significance was determined using a one-way ANOVA followed by Dunnett's test (*P<0.05).

†Values for [KO] +BSP are means ± SD across 2 biological replicates

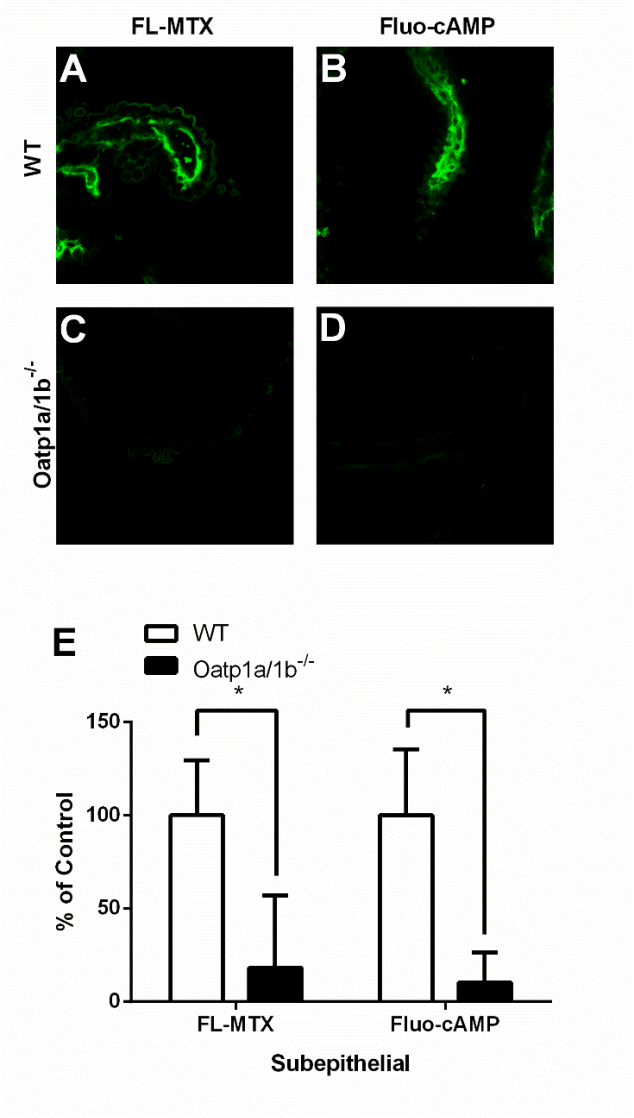

Figure 3.7. Accumulation of FL-MTX and fluo-cAMP in wild-type and Oatp1a/1b$^{-/-}$ CP tissue

Representative confocal images of (A) FL-MTX (2 µM) and (B) fluo-cAMP (2 µM) in wild-type and (C) FL-MTX (2 µM) and (D) fluo-cAMP (2 µM) in Oatp1a/1b$^{-/-}$ CP tissue. (E) Changes in subepithelial accumulation between treatment groups. Data are normalized to SR101 subepithelial accumulation in wild-type tissues. Values are means ± SD across 6 biological replicates for all treatment groups. Statistical significance was determined using an unpaired student's *t* test (*P<0.05).

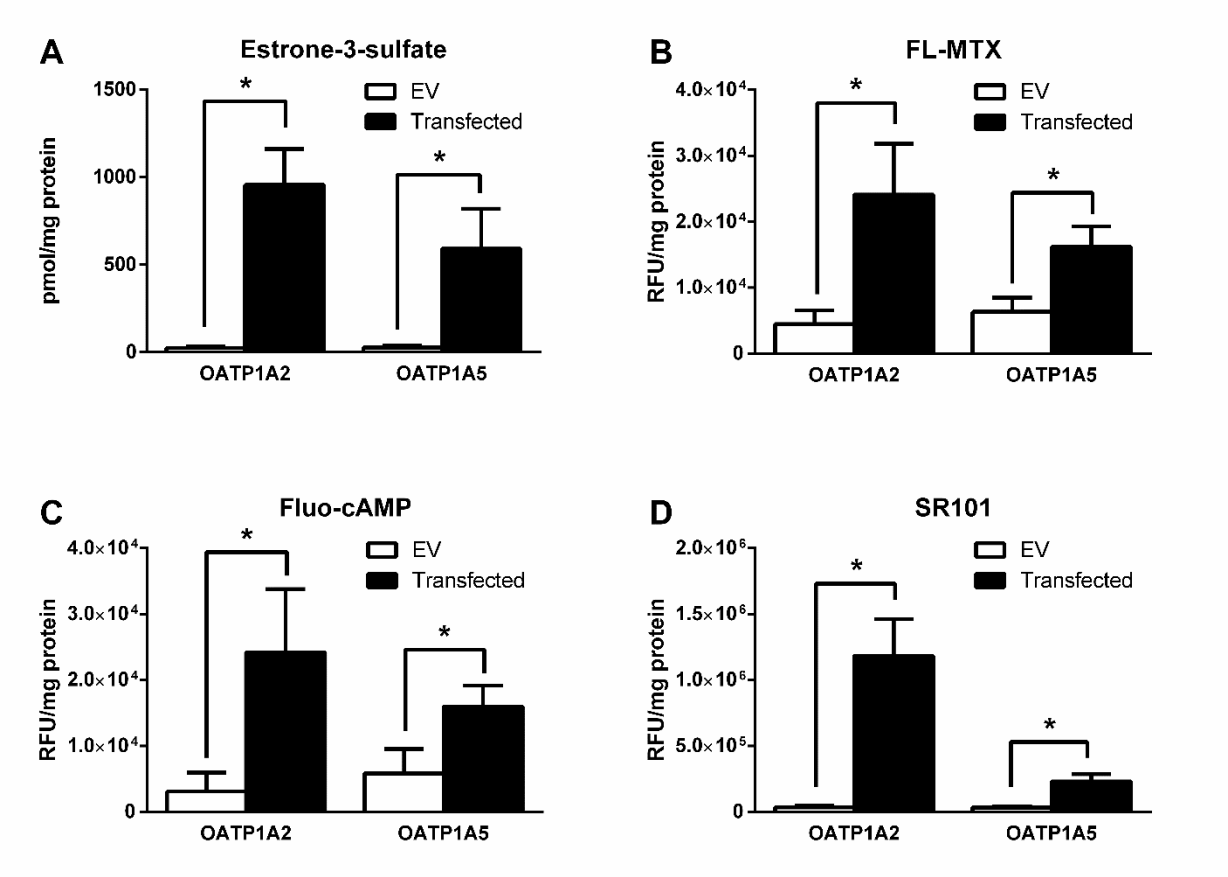

Figure 3.8. Uptake of estrone-3-sulfate, FL-MTX, fluo-cAMP, and SR101 by OATP1A2 and OATP1A5 overexpressing cell lines

Uptake of (A) estrone-3-sulfate, (B) FL-MTX, (C) fluo-cAMP, and (D) SR101 in OATP1A2 and OATP1A5 overexpressing cell lines. Uptake of 1 µM substrate was measured in both transporter-expressing and empty vector expressing HEK293 cells. Uptake was measured after 20 minutes of incubation at 37°C. Data are presented as the mean ± SD from three independent experiments. The uptake in transporter expressing cells was compared to empty vector (EV) expressing cells. Statistical significance was determined by using an unpaired student's *t* test (*P<0.05, **P<0.01).

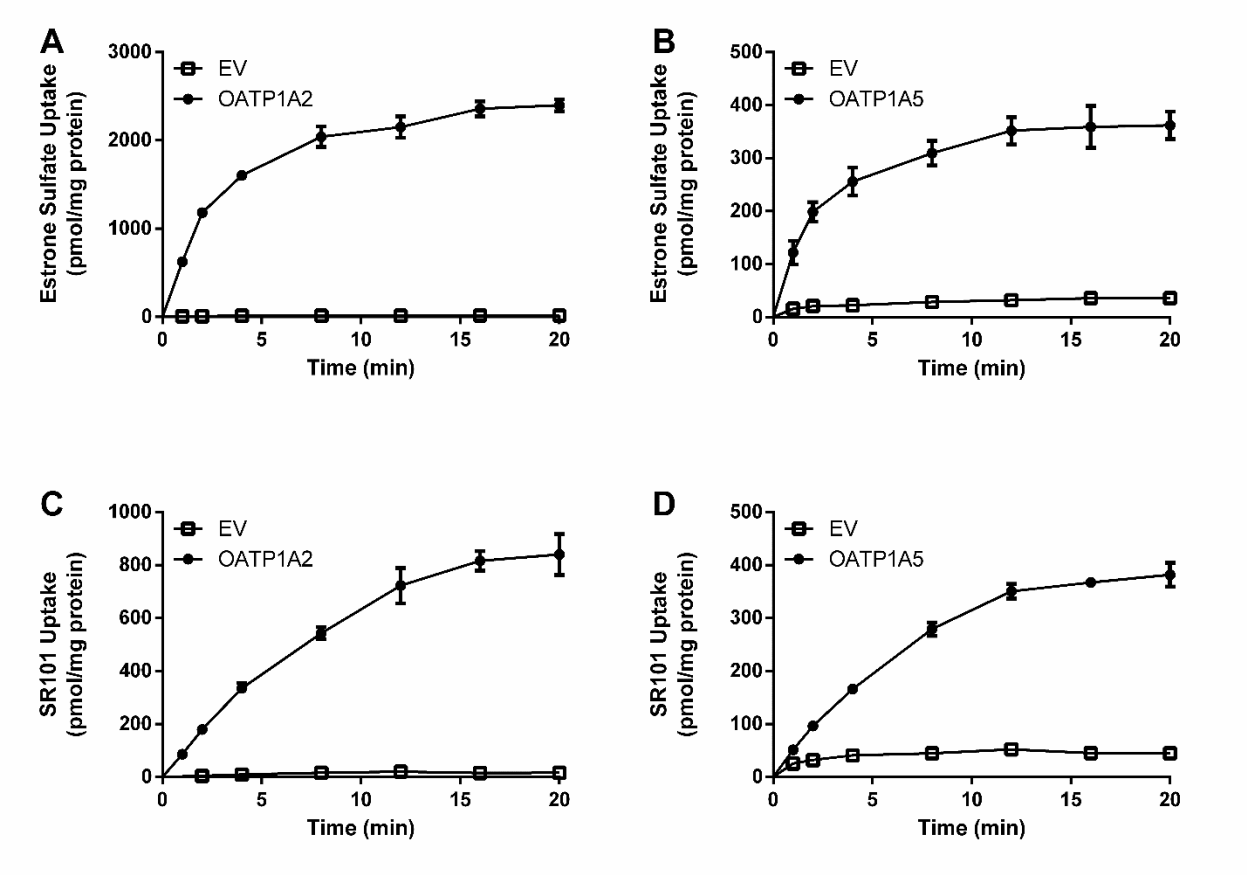

Figure 3.9. Time course of estrone-3-sulfate and SR101 uptake by OATP1A2 and OATP1A5

Time course of 1 µM estrone-3-sulfate (A,B) and SR101 (C,D) uptake by OATP1A2 and OATP1A5. Time courses were performed independently three times, and results from one representative experiment are shown. Data points represent the mean ± SD in triplicate.

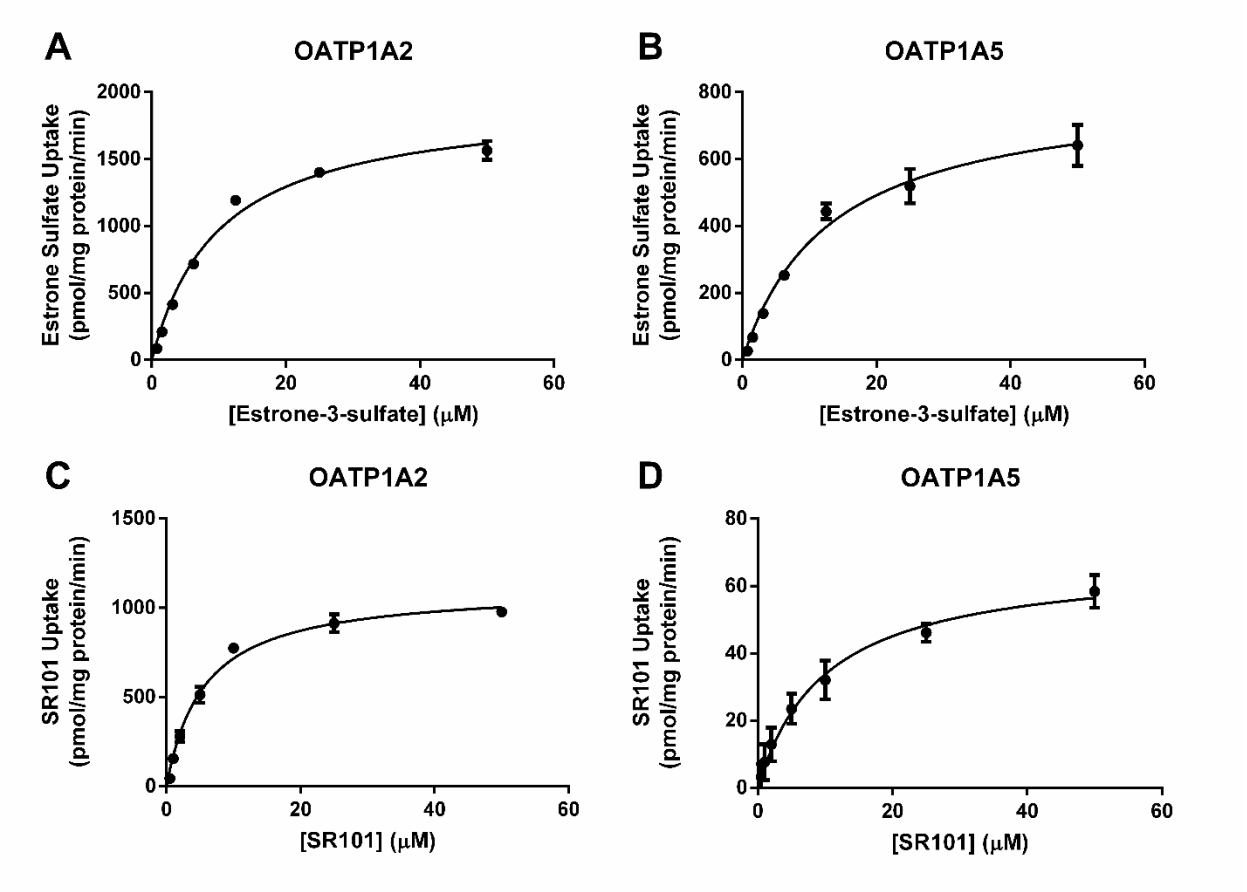

Figure 3.10. Concentration-dependent uptake of estrone-3-sulfate and SR101 by hOATP1A2 and mOatp1a5-

Concentration-dependent uptake of estrone-3-sulfate (A,B) and SR101 (C,D) by OATP1A2 and OATP1A5. Transporter-specific uptake was obtained by subtracting the activity in control cells from the activity in transporter-expressing cells after a 2-minute incubation for estrone-3-sulfate and a 4-minute incubation for SR101. The data were fitted to a standard Michaelis-Menten equation for both compounds. Concentration dependent uptake was performed independently three times, and results from one representative experiment are shown. Data points represent the means ± SD in triplicate.

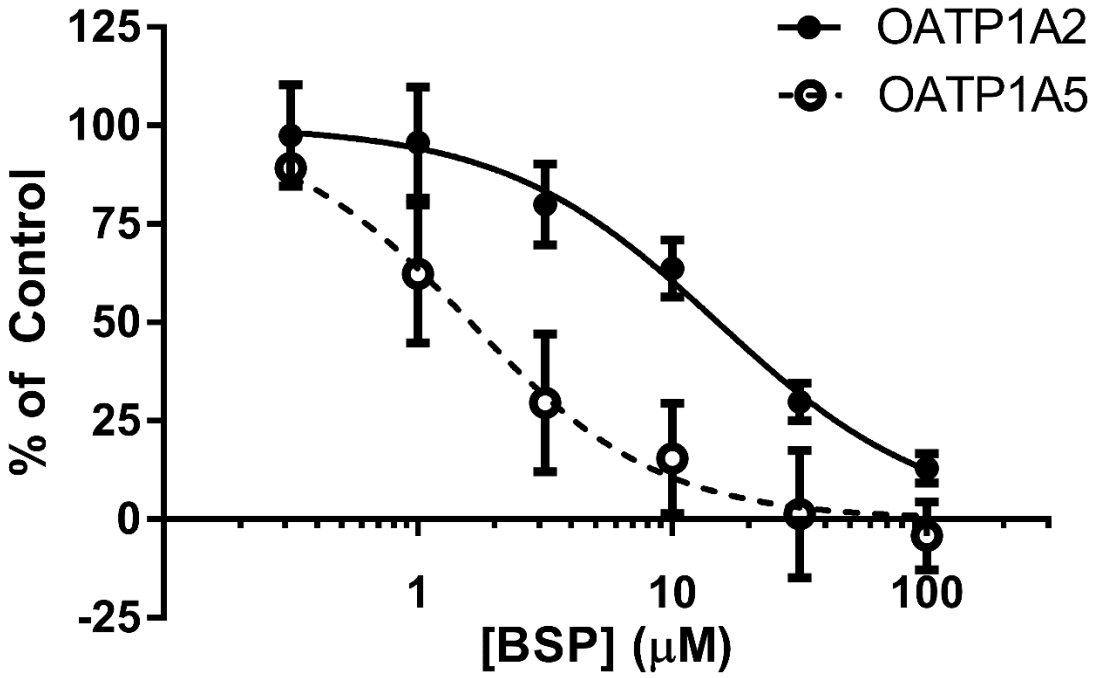

Figure 3.11. Dose-dependent inhibition of SR101 uptake in OATP1A2 and OATP1A5 cells by bromosulphalein (BSP).

Dose-dependent inhibition of SR101 uptake in OATP1A2 and OATP1A5 overexpressing cells by BSP. Uptake of 1 μM SR101 in the absence and presence of BSP was measured in empty vector, OATP1A2-, and OATP1A5- expressing HEK293 cells for 4 minutes. Transporter-specific uptake was obtained by subtracting the activity in empty vector cells from the activity in transporter-expressing cells. The results are expressed as a percentage of SR101 uptake in the absence of BSP and fitted to a 4-parameter inhibition model. Each data point represents the means ± SD from 3 independent experiments.

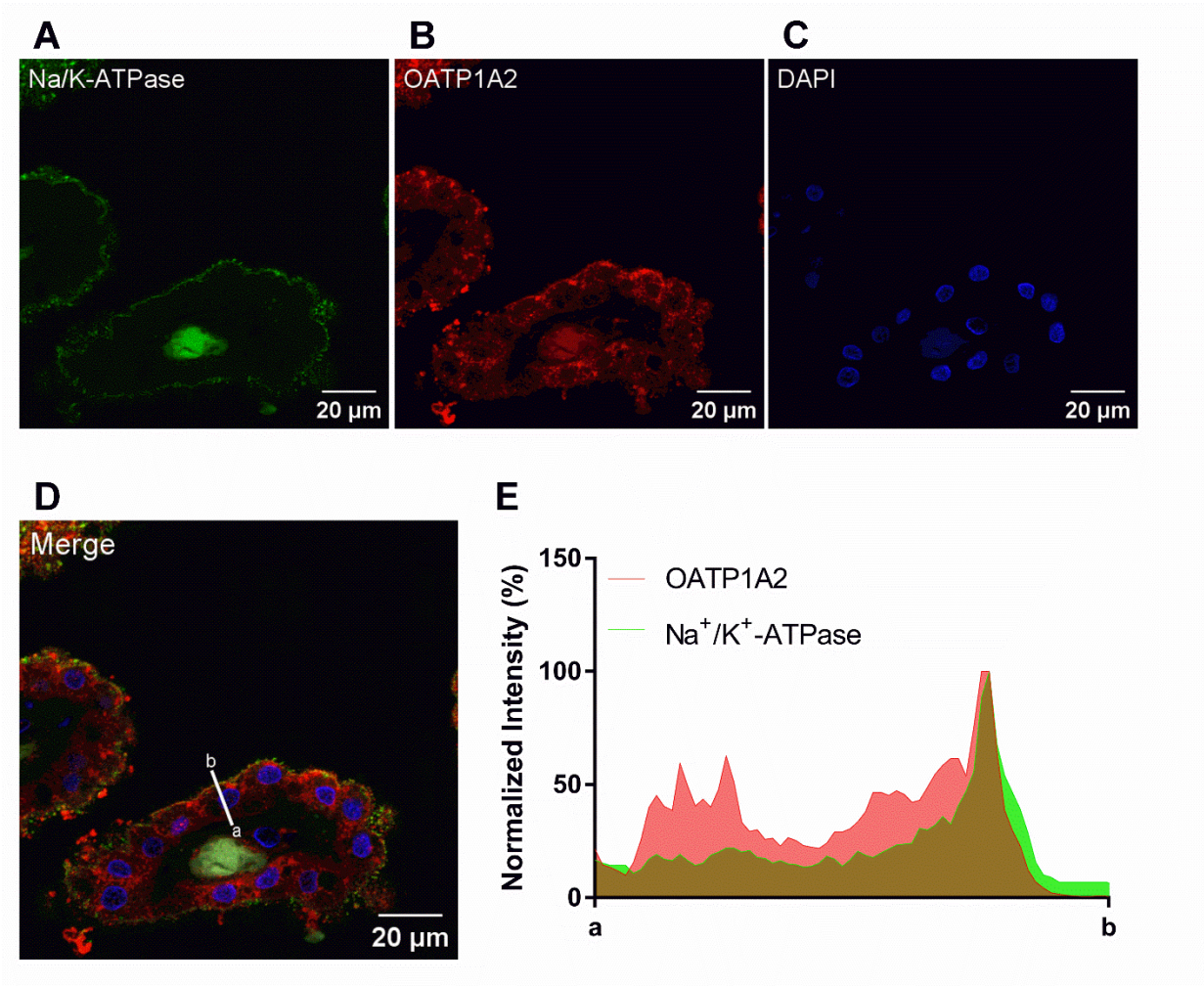

Figure 3.12. Immunofluorescence staining for Na^+/K^+-ATPase and OATP1A2 in human choroid plexus

Immunofluorescence staining for (A) Na^+/K^+-ATPase, (B) OATP1A2, and (C) DAPI in human CP. (D) Merged image showing colocalization of OATP1A2 with apical Na^+/K^+-ATPase. (E) Normalized intensity of OATP1A2 and Na^+/K^+-ATPase fluorescence across the human CPE cell. Deidentified CP was sourced from a 60-year-old male.

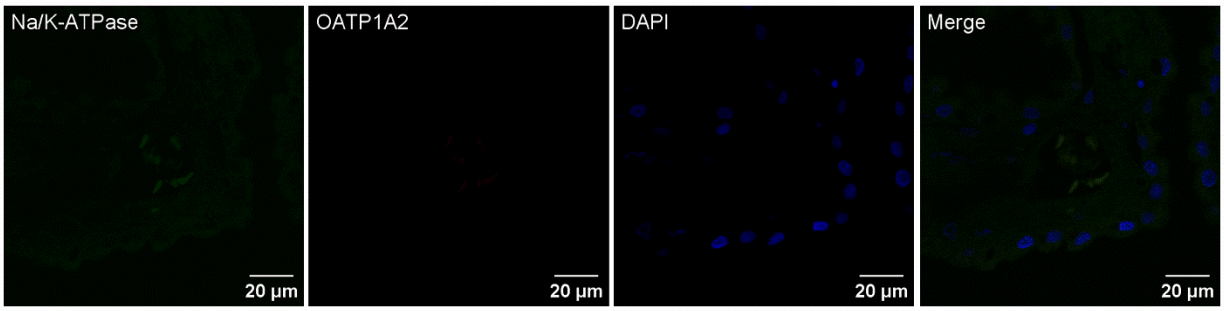

Figure 3.13. Control immunofluorescence staining in human choroid plexus without primary antibody treatment.

Control immunofluorescence stain without primary antibody treatment. Deidentified choroid plexus was sourced from a 60-year-old male.

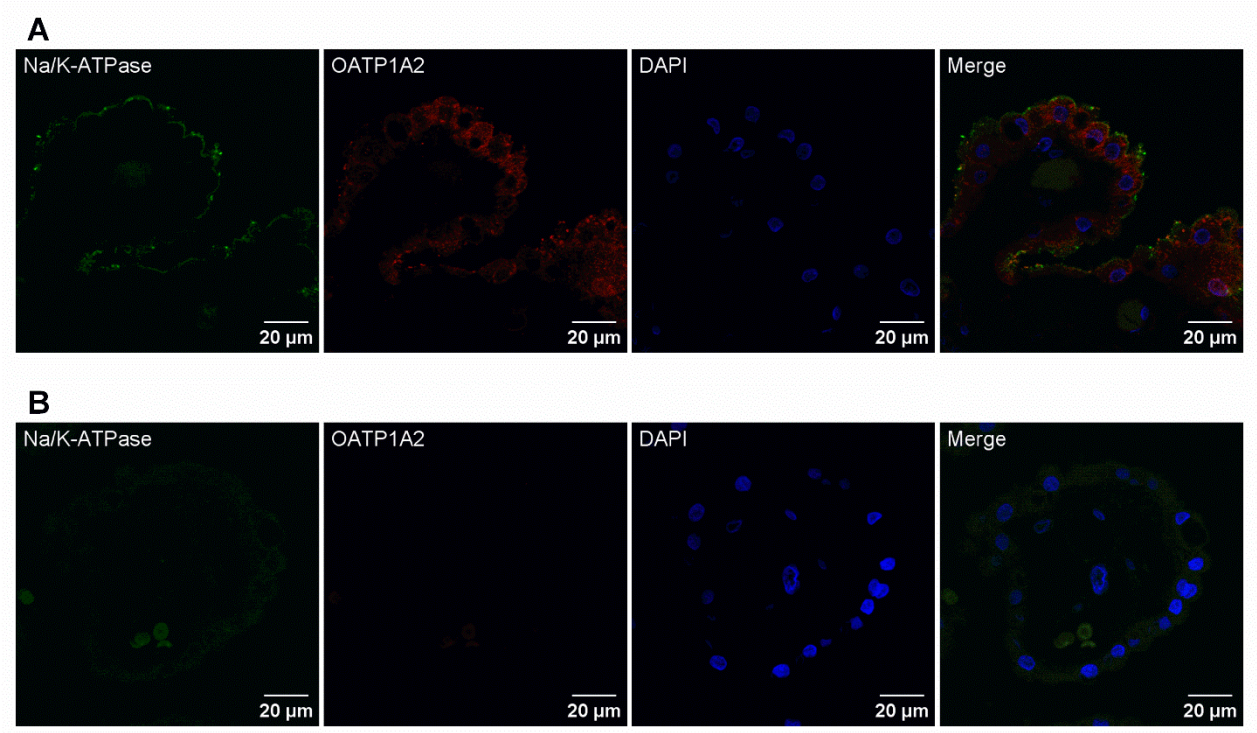

Figure 3.14. Immunofluorescence staining for Na^+/K^+-ATPase and OATP1A2 in second human choroid plexus

(A)Immunofluorescence staining for Na^+/K^+-ATPase and OATP1A2 in human choroid plexus. Nuclei are stained with DAPI (blue). (B) Control immunofluorescence stain without primary antibody treatment. Deidentified choroid plexus was sourced from a 61-year-old male.

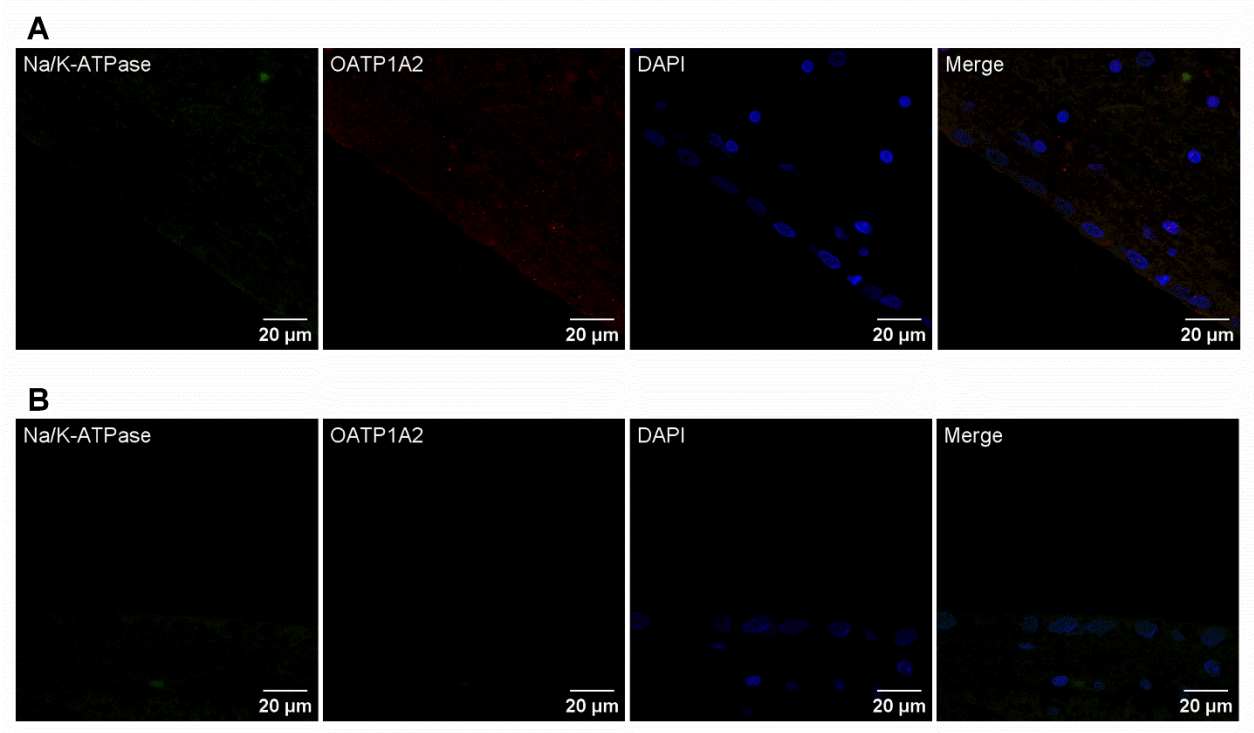

Figure 3.15. Immunofluorescence staining for Na^+/K^+-ATPase and OATP1A2 in human ventricular ependyma

(A) Immunofluorescence staining for Na^+/K^+-ATPase and OATP1A2 in human ventricular ependyma. Na^+/K^+-ATPase and OATP1A2 staining is markedly insubstantial in ventricular ependyma. (B) Control immunofluorescence stain without primary antibody treatment. Deidentified choroid plexus was sourced from a 60-year-old male.

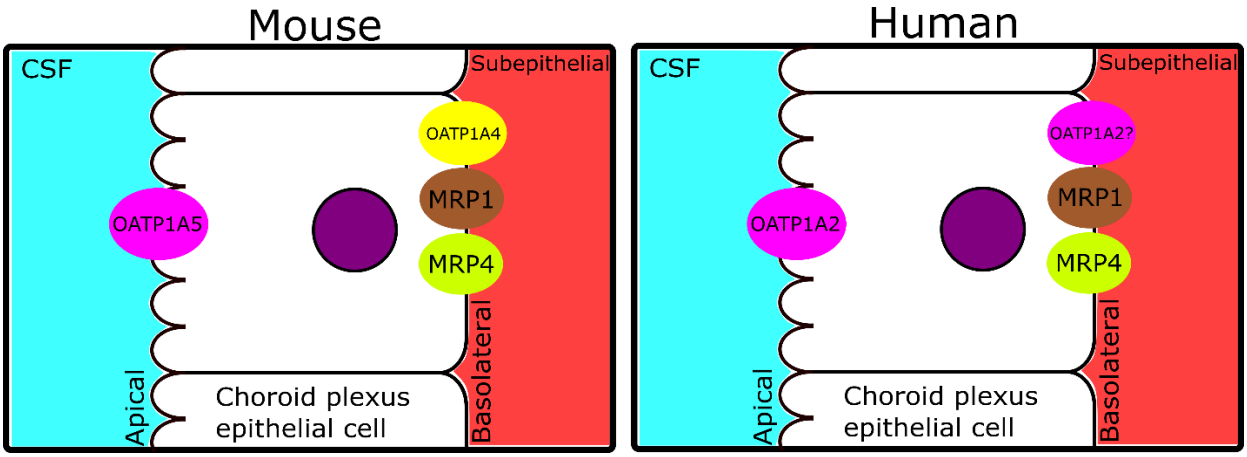

Figure 3.16. Proposed roles of OATP and MRP transporters in BCSFB clearance at the rodent and human BCSFB.

Proposed roles of OATP and MRP transporters in BCSFB clearance at the rodent and human BCSFB. Models are based on data compiled from previous studies (64,111,122,123) and the present study.

Table 3.1. TaqMan Gene Expression IDs used in RT-qPCR analysis

Gene	Protein	Assay ID
Slco1a1	OATP1A1	Mm01267415_m1
Slco1a4	OATP1A4	Mm01267407_m1
Slco1a5	OATP1A5	Mm00453720_m1
Slco1a6	OATP1A6	Mm01267368_m1
Slco1b2	OATP1B2	Mm00451510_m1
Slco1c1	OATP1C1	Mm00451845_m1
Slco3a1	OATP3A1	Mm00452449_m1
Abcc1	MRP1	Mm00456156_m1
Abcc4	MRP4	Mm01226381_m1
Gapdh	GAPDH	Mm99999915_m1

Table 3.2. Kinetic parameters of estrone-3-sulfate and SR101 uptake by hOATP1A2 and mOatp1a5

Values shown on the table are means (SD) of the K_m or V_{max} from three independent experiments. Units: K_m, µM; V_{max}, pmol/mg protein/min

	OATP1A2		OATP1A5	
	K_m	V_{max}	K_m	V_{max}
Estrone-3-sulfate	14.7±7.3	3050±1520	17.1±7.0	654±140
SR101	6.1±0.5	829.7±268.5	5.6±4.1	49.4±26.2

Chapter 4. FUNCTIONAL EVALUATION OF P-GP AND BCRP AT THE MURINE BLOOD-CEREBROSPINAL FLUID BARRIER

4.1 ABSTRACT

Purpose

The brain is protected by circulating metabolites and xenobiotics by two major barriers: blood-brain barrier (BBB) and the blood-cerebrospinal fluid (CSF) barrier. Previous studies report that P-gp and Bcrp are expressed apically or subapically at the blood-CSF barrier, implying a paradoxical function to mediate blood-to-CSF transport of xenobiotics. As evidence of P-gp and Bcrp activity at the blood-CSF barrier is limited, the goal of this study is to investigate functional activity of P-gp and Bcrp using a live tissue imaging approach.

Methods

The choroid plexuses (CP) that form the blood-CSF barrier were freshly isolated from mouse lateral ventricles and incubated with fluorescent probes calcein-AM and BODIPY FL-Prazosin. Using quantitative fluorescence microscopy, the functional contributions of Bcrp and P-gp were examined using inhibitors and mice with targeted deletion of the *Abcb1a/b* or *Abcg2* gene.

Results

Apical transport of calcein-AM at the blood-CSF barrier is sensitive to inhibition by elacridar and Ko143 but is unaffected by P-gp deletion. In CP tissues from the $Bcrp^{-/-}$ mice, CPE

cell accumulation of BODIPY FL-Prazosin was increased by 43% and can be further enhanced by elacridar. There was no change in P-gp mRNA expression in CP tissues from the Bcrp$^{-/-}$ mice.

Conclusions

This study demonstrated functional activity of Bcrp at the blood-CSF barrier apical membrane and also provided evidence supporting a Bcrp-independent, elacridar-sensitive apical efflux mechanism possibly mediated by P-gp. These findings contribute to the understanding of transport mechanisms that regulate CSF drug concentrations, which may benefit future predictions of CNS drug disposition, efficacy, and toxicity.

4.2 INTRODUCTION

There is a high, unmet need for future treatments of neurological disorders, which are the primary cause of disability and the second leading cause of death worldwide (196). The brain is the most physiologically complex organ in the human body, which can lead to many obstacles during central nervous system (CNS) drug development. Diseases of the brain and greater CNS, such as Alzheimer's disease, may have complex pathologies and several potential pharmacological targets. CNS pharmacokinetics are also complex and poorly understood, which in part contributes to the high attrition rate during the development of CNS drugs (197).

Drug transporters play an important role in mediating drug-drug interactions, drug disposition, and toxicity (53). At the blood-brain barrier (BBB), efflux transporters such as P-glycoprotein (P-gp) and breast cancer resistance protein (BCRP) are expressed on the luminal membrane, where they limit the entry of their substrates into the brain (65,220). The importance of P-gp and BCRP in restricting drug brain penetration has been well documented (220). The two transporters have an overlapping substrate pool, thus P-gp and BCRP can synergistically limit the

CNS penetration of shared substrates (220). P-gp and BCRP are also reportedly expressed in other blood-CNS barrier sites such as the blood-cerebrospinal fluid (CSF) barrier (64,65,137), implying a functional role beyond the BBB.

The blood-CSF barrier is formed by the choroid plexuses (CP), which are comprised of a layer of polarized, tight junction-linked choroid plexus epithelial (CPE) cells that surround a core of blood capillaries (1,174). The CPE cells express transporters and enzymes that contribute to xenobiotic and endobiotic clearance from the CSF (174). Several solute carrier transporters, including the peptide transporter 2 (PEPT2), organic anion transporter 3 (OAT3), and plasma membrane monoamine transporter (PMAT), are expressed at the apical (CSF-facing) membrane of the CPE cells and mediate drug uptake from the CSF into CPE cells (76,81,85,86,96). We recently showed that large organic anions are actively cleared from the CSF via the coordinated function of organic anion transporting polypeptides (OATPs) at the apical membrane and the multidrug resistance associated proteins (MRPs) at the basolateral membrane. By influencing drug concentrations in the CSF, transporters at the blood-CSF barrier may also play a role in regulating the effective drug concentrations in the CNS.

Interestingly, previous studies have suggested that BCRP and P-gp are expressed apically (CSF-facing) or subapically at the blood-CSF barrier. Using immunohistochemistry and immunofluorescence approaches, BCRP has been localized apically in mouse CP (137,138), while P-gp has been localized apically or subapically in CP of rats and pigs (64,143). Since BCRP and P-gp are efflux transporters, their location at the apical membrane of CPE cells would imply a paradoxical role of mediating blood-to-brain transport, which is opposite to their functions at the BBB. Limited functional studies have been conducted using *in vitro* systems. Transport of calcein-AM, a P-gp probe, was sensitive to the P-gp inhibitor valspodar, in rat and human cultured cell

lines (62,144). Apical to basolateral transport of the P-gp substrate ^{99m}Tc-sestamibi increased with elacridar in rat CPE primary cell lines cultured in a transwell system, suggesting P-gp activity at the apical, CSF-facing membrane (64). However, two other P-gp substrates, rhodamine123 and verapamil, were not actively transported in porcine primary CP cells (143). Evidence of BCRP function at the blood-CSF barrier is even more limited; a single study demonstrated transport of the BCRP substrate BODIPY FL-Prazosin was sensitive to the BCRP specific inhibitor Ko143 in cultured human choroid plexus papilloma cells (144). However, no directional difference in transport was observed when the cells were grown in a Transwell system (144). Broadly, primary CPE cell cultures and CP cell lines have been shown to have altered transporter expression and tight junction formation as compared to CP tissue (62). Thus, there is an impetus to study P-gp and Bcrp transport mechanisms in a more physiologically relevant system.

Our laboratory recently developed and validated a quantitative fluorescence microscopy approach to study transcellular transport mechanisms of organic cations and organic anions at the murine blood-CSF barrier (117). This approach enables the study of real-time transport processes in freshly isolated intact choroid plexus tissues and can distinguish between transport processes at the apical and basolateral membranes (200). In this study, we first determine the relative mRNA expression of *Abcb1a/b* (P-gp) and *Abcg2* (Bcrp) in murine lateral ventricle CP tissues. Using quantitative fluorescence microscopy, we investigated the functional role of P-gp and Bcrp at the blood-CSF barrier using fluorescent probes in freshly isolated murine CP tissues. The contribution of P-gp and Bcrp were evaluated using established inhibitors and mouse models with targeted deletion of the *Abcb1a/b* or *Abcg2* genes.

4.3 MATERIALS AND METHODS

4.3.1 *Chemicals and Materials*

All chemicals purchased and used were of 95% or greater purity. Calcein-AM was purchased from Enzo Life Sciences (ENZ-52002, Farmingdale, NY). BODIPY FL-Prazosin was purchased from ThermoFisher Scientific (B7433, Waltham, MA). Ko143 was purchased from Medchemexpress (HY-10010, Monmouth Junction, NJ). Unless otherwise specified, all other chemicals were purchased from Sigma-Aldrich (St. Louis, MO). Animal handling supplies, PCR plates, confocal dishes, and other plastic wares were purchased from VWR (Radnor, PA).

4.3.2 *Animals and Choroid Plexus Tissue Collection*

Animal experiments were carried out in accordance with the Guide for the Care and Use of Laboratory Animals as adopted and promulgated by the U.S. National Institutes of Health and in accordance with animal protocols approved by the Institutional Animal Care and Use Committee at the University of Washington. Animals were housed in the specific pathogen free facility at the University of Washington and maintained under standard conditions, with food and water available ad libitum. FVB wild-type (FVB-M), FVB Bcrp$^{-/-}$ (2767-M), and Mdr1a/1b$^{-/-}$ (1487-M) mice were obtained from Taconic Biosciences (Germantown, NY). Generation and physiological characteristics of the transgenic strains have been described previously (221,222).

Adult (8-13 week old) male FVB wild-type and transgenic mice were euthanized by CO_2 inhalation, followed by decapitation. Mouse brain was isolated and maintained in ice cold artificial CSF (aCSF: 119 mM NaCl, 26.2 mM $NaHCO_3$, 2.5 mM KCl, 1 mM NaH_2PO_4, 1.3 mM $MgCl_2$, 2.5 mM $CaCl_2$, 10 mM glucose, previously gassed with 95% O_2/5% CO_2 for tissue isolation.

Lateral ventricle CP and 4th ventricle CP were isolated from mouse brain under a dissecting microscope using an approach previously described (200). CP tissue used for uptake experiments were then transferred into pre-gassed, ice-cold aCSF immediately after removal, while tissues used for real-time PCR were immediately flash frozen in LN_2 and stored in a -80°C freezer until further processing.

4.3.3 *Quantification of Transporter mRNA Expression by Real Time PCR*

Frozen CP tissue was homogenized by bead disruptor, and total RNA was extracted by RNeasy Mini Kit (Qiagen, Germantown, NY). Total RNA was then converted to cDNA by reverse transcription using the High-Capacity cDNA Reverse Transcription Kit (Applied Biosystems, Waltham, MA). Expression at the mRNA level of transporters at the CP was quantified using TaqMan Real-Time PCR Master Mix (Applied Biosystems, Waltham, MA) as described previously (96,117). The relative mRNA levels of these transporters in CP were normalized to glyceraldehyde-3-phosphate dehydrogenase (*Gapdh*).

4.3.4 *Transport Studies in Freshly Isolated CP tissues from FVB wildtype and KO mice*

Transport imaging studies using freshly isolated mouse lateral ventricle CP were performed using an approach previously described (117,200). Isolated CP tissues maintain vitality and transport activity for up to 2-3 hours after isolation, and all transport studies were performed within 2 hours after isolation (200). Single time-point transport studies were initiated by adding the fluorescent compound in the presence or absence of an inhibitor into the aCSF. Incubations were carried out for 20 min in sealed Ziploc bags containing 95% O_2/5% CO_2. One to three undamaged observation areas containing both CPE cells and adjacent subepithelial region were selected, and

the fluorescent signals were recorded. To record real-time transport of fluorescent substrate, a specific observation area containing intact CPE cells and adjacent subepithelial region was selected and immobilized in pregassed aCSF. The experiment was initiated by adding a specified concentration of fluorescent compound, and fluorescent signals were recorded every minute for 20 minutes. Additional observation areas containing CPE cells and adjacent subepithelial region were recorded after 20 minutes of uptake.

4.3.5 *Confocal Image Acquisition and Analysis*

Image acquisition and analysis were performed using procedures previously described (200). Briefly, imaging was performed using a Zeiss LSM 710 confocal microscope fitted with a Zeiss 40x, NA 1.3 oil immersion objective (total magnification: 400x). Brightfield imaging was used to identify observation areas containing CPE cells with adjacent blood capillaries. Samples containing BODIPY FL-Prazosin or calcein-AM were illuminated using a 488nm fixed wavelength argon laser, with appropriate corresponding dichroic and emission filters used to detect the emission of the fluorescent probes. Low laser intensity (5% of maximum) was used to minimize sample photobleaching. Laser gain and offset was set such that autofluorescence of tissue was minimally detectable, with the pinhole set to 36.8 μm. Confocal images were captured as 15 sec scans at 1024×1024 resolution, 16 frames line-averaged, with a pixel dwell of 0.79 μsec. Replicate studies were performed using the same objective lens, identical laser power, and identical detector settings.

Digital image analysis was performed using Fiji ImageJ (1.53t) (184) and performed as described previously (200).

$CPEI_{20min}$ was calculated according to the following formula (200):

$$CPEI_{20min}(\%) = \frac{\sum pixel\ intensity_{se}}{\sum pixel\ intensity_{cells+se}}$$

$CPEI_{20min}$ is expressed as a percentage, where Σpixel $intensity_{se}$ is the sum average pixel intensity in the subepithelial region at 20 minutes from three segmentations, and Σpixel $intensity_{cells+se}$ is the combined sum average pixel intensity in the subepithelial and CPE cell regions at 20 minutes from three segmentations.

4.3.6 *Statistical Analysis*

All imaging experiments were carried out with CP tissue isolated from at least 3 animals. Calculated intensity values were presented as mean ± SD. Statistical significance was determined by using a one-way ANOVA followed by Dunnett's test or by an unpaired Student's t-test. P value less than 0.05 indicated a statistically significant difference.

4.4 RESULTS

4.4.1 *mRNA Expression of Abcb1a (Mdr1a), Abcb1b (Mdr1b), and Abcg2 (Bcrp) in FVB mouse CP*

Previous studies have suggested that P-gp and Bcrp are expressed apically at the blood-CSF barrier (137), implying a paradoxical function, opposite of the BBB, to mediate a blood-to-CSF transport of xenobiotics and endobiotics. However, functional studies on P-gp and Bcrp activity at the blood-CSF barrier are limited and have not been investigated in freshly isolated, intact CP tissue. In mice, there are two isoforms of P-gp, Mdr1a and Mdr1b. We initially determined the mRNA expression the two murine isoforms of P-gp, *Abcb1a* (Mdr1a) and *Abcb1b*

(Mdr1b), as well as *Abcg2* (Bcrp) in the lateral ventricle CP of wild-type FVB mice using RT-qPCR (**Figure 4.1**). *Abcg2* mRNA is expressed at higher levels than *Abcb1a*, while *Abcb1b* is minimally expressed. The higher expression of *Abcb1a* over *Abcb1b* in choroid plexus is similar to previous findings in whole brain homogenates (223).

4.4.2 *Calcein-AM accumulation in wild-type and Mdr1a/1b$^{-/-}$ CP tissues*

To test the activity of P-gp at the apical CPE cell membrane, real-time uptake of calcein-AM, a P-gp substrate, was performed in CP tissues of wild-type and Mdr1a/1b$^{-/-}$ mice in different inhibitory conditions. Calcein-AM is a non-fluorescent, lipophilic P-gp substrate. After entering the cell, the compound is cleaved by intracellular esterases to yield the hydrophilic, fluorescent molecule calcein (224,225). When calcein-AM was incubated alone in CP tissues of wild-type mice, the fluorescent calcein was primarily retained intracellularly in the CPE cells (**Figure 4.2**), with a $CPEI_{20min}$ of 18.9±4.1%. When co-incubated with the dual inhibitor elacridar, calcein accumulation increased 468% in the CPE cells compared to the control group (**Figure 4.2**; **Figure 4.3**). Curiously, coincubation with the Bcrp inhibitor Ko143 also enhanced CPE cell accumulation of calcein, with an increase of 358% compared to treatment with calcein-AM alone (**Figure 4.2**; **Figure 4.3**). However, cellular accumulation of calcein did not increase in Mdr1a/1b$^{-/-}$ CP tissues compared to wild-type controls (**Figure 4.2**; **Figure 4.3**). No apparent changes to subepithelial accumulation were observed across treatment groups. Taken together, the data does not confirm P-gp transport activity at the blood-CSF barrier but does suggest a P-gp independent, Ko143- and elacridar-sensitive transport mechanism contributing to the apical efflux of calcein-AM at the murine blood-CSF barrier. As Bcrp is also expressed apically and is sensitive to the same inhibitors

(131), we hypothesized that Bcrp is functionally active at the blood-CSF barrier which may be contributing to calcein-AM efflux.

4.4.3 *Transport of BODIPY FL-Prazosin is sensitive to Bcrp inhibitor Ko143 in mouse CP*

To test the functional activity of Bcrp on the apical membrane, we incubated freshly isolated CP tissues with an established Bcrp substrate, BODIPY FL-Prazosin, in the presence and absence of the Bcrp inhibitor Ko143. When incubated alone in CP tissues, BODIPY FL-Prazosin accumulated primarily in the CPE cells with minimal accumulation in the subepithelial space (**Figure 4.4**), with a $CPEI_{20min}$ of 20.5±3.6%. Coincubation with Ko143 increased the CPE cell accumulation of BODIPY FL-Prazosin by 165% (**Figure 4.4**), while subepithelial accumulation did not change (data not shown). The data demonstrates that Ko143 inhibits apical transport of BODIPY FL-Prazosin in CPE cells, suggesting Bcrp is functionally active at the apical membrane of the blood-CSF barrier.

4.4.4 *Transport of BODIPY FL-Prazosin in wild-type and Bcrp$^{-/-}$ CP tissues*

Studies conducted using *ex vivo* tissue samples are advantageous in that they reflect the *in vivo* conditions more closely compared to *in vitro* cell-based systems (174). However, the *ex vivo* system is also more complex, expressing the full spectrum of transporters present *in vivo*. As BODIPY FL-Prazosin has also been reported as a P-gp substrate (226), we performed transport studies in CP tissues isolated from wild-type and Bcrp$^{-/-}$ mice. BODIPY FL-Prazosin was incubated in CP tissues of wild-type and Bcrp$^{-/-}$ mice in the presence and absence of elacridar, a dual inhibitor of Bcrp and P-gp (227) (**Figure 4.5**). With the dual inhibitor elacridar, we observed a 220% increase in CPE cell accumulation of BODIPY FL-Prazosin in wild-type tissues (**Figure**

4.5). In the Bcrp$^{-/-}$ group with no elacridar, we observed a 43% increase in CPE cell accumulation compared to the wild-type CP (**Figure 4.5**), suggesting Bcrp protein is expressed and functionally active at the blood-CSF barrier apical membrane. BODIPY FL-Prazosin accumulation was further increased in CP tissues of Bcrp$^{-/-}$ mice coincubated with elacridar, with a 116% increase in CPE cell accumulation compared to wild-type tissues with no inhibitor (**Figure 4.5**). This data suggests, ancillary to Bcrp, P-gp may also contribute to apical efflux of BODIPY FL-prazosin at the murine blood-CSF barrier. To examine if Bcrp$^{-/-}$ mice exhibited any compensatory expression of P-gp at the CP, we additionally tested and compared mRNA expression of the murine P-gp isoforms, the *Abcb1a* and *Abcb1b* genes, in CP of wild-type and Bcrp$^{-/-}$ mice. No significant change in mRNA expression of either isoform of P-gp was observed (**Figure 4.6**).

4.5 DISCUSSION

Earlier research has suggested that Bcrp and P-gp are expressed apically or subapically at the blood-CSF barrier (64,137). This CSF-facing localization implies an inward transport function to the brain, which is opposite to their role of restricting brain entry of xenobiotics at the luminal membrane of the BBB. Functional studies on Bcrp and P-gp at the blood-CSF barrier are limited and have only been conducted using cultured CPE cells that do not preserve the physiology and transporter expression at the blood-CSF barrier (62). Thus, further exploration of Bcrp and P-gp activity at the blood-CSF barrier in a more physiologically relevant system is warranted. In this study, we demonstrated functional activity of Bcrp at the apical membrane of the blood-CSF barrier using quantitative fluorescence microscopy in freshly isolated CP tissues from wild-type and Bcrp$^{-/-}$ mice. Our results also suggested an additional Bcrp-independent, elacridar-sensitive apical efflux mechanism at the blood-CSF barrier possibly mediated by P-gp or an unknown efflux transporter.

In this study, BODIPY FL-Prazosin, a fluorescent BCRP substrate (131), was utilized to probe for Bcrp activity at the apical membrane of the blood-CSF barrier. We observed a 43% increase in CPE cell accumulation of BODIPY FL-Prazosin in Bcrp$^{-/-}$ mice compared to wild-type controls (**Figure 4.5**), demonstrating that Bcrp is indeed expressed and functionally active at the apical membrane. Accumulation of BODIPY FL-Prazosin in the CPE cells of Bcrp$^{-/-}$ was further increased with elacridar coincubation, suggesting additional contribution from a Bcrp-independent, elacridar-sensitive efflux mechanism at the apical membrane. As BODIPY FL-Prazosin is also transported by P-gp, and elacridar is also an inhibitor of P-gp (228), P-gp may additionally contribute to BODIPY FL-Prazosin efflux.

For a dual Bcrp and P-gp substrate, it is likely that the loss of one transporter can be functionally compensated by another. At the BBB, P-gp and Bcrp are known to 'cooperate' to limit the entry of chemotherapeutic and other shared substrates into the brain (220). When only a single transporter is inhibited or knockout, little or no increase in brain penetration was observed for several dual substrates (136,229–232). For these compounds, large increases in brain concentrations are only observed when both P-gp and Bcrp are inhibited or knocked out. One example is topotecan, an antineoplastic substrate of both Bcrp and P-gp (229). Brain exposure of topotecan was only marginally (< 1.5 fold) increased in Bcrp$^{-/-}$ mice or Mdr1a/1b$^{-/-}$ mice but increased over 12-fold in P-gp and Bcrp double KO mice (229). Our study shares some similarities with a previous study by Lee et al. (233). In their study, the authors conducted an *in situ* brain perfusion of [^{3}H]mitoxantrone in wild-type, P-gp KO, and Bcrp KO mice. Brain uptake was enhanced with elacridar inhibition, but mitoxantrone brain uptake did not increase in either P-gp or Bcrp KO mice (233). The authors initially concluded that Bcrp played a minor role in mitoxantrone efflux out of the brain (233) . However, in a follow up study, the authors observed a

large increase in brain penetration of mitoxantrone by ~8-fold in mice lacking both P-gp and Bcrp transporters (234).

We noted an interesting observation that wildtype CP incubated with Ko143 showed a higher increase of BODIPY FL-Prazosin accumulation compared to Bcrp$^{-/-}$ CP tissues (165% increase vs 43% increase) (**Figure 4.4**, **Figure 4.5**). This could be attributed to a few potential reasons. One potential explanation would be a compensatory increase in P-gp expression in the CP of Bcrp$^{-/-}$ mice. However, this is unlikely, as we found no significant increase in mRNA expression of either isoform of P-gp in Bcrp$^{-/-}$ CP tissues (**Figure 4.6**). Additionally, a previous study has demonstrated no changes in BBB expression of P-gp in Bcrp$^{-/-}$mice (235). A potential explanation is Ko143 is acting as a dual inhibitor similar to elacridar, rather than a Bcrp specific inhibitor. Although early studies demonstrate that Ko143 is much more potent for human BCRP compared to human P-gp (236), some evidence suggests that Ko143 can inhibit murine Mdr1a at micromolar concentrations (237), and that Ko143 is transported by Mdr1a at the murine BBB (238).

Another intriguing observation we found was that both elacridar and Ko143 inhibited calcein-AM efflux, while knockout of P-gp had no impact (**Figure 4.3**), suggesting a P-gp independent, but elacridar- and Ko143- sensitive efflux mechanism for calcein-AM. While calcein-AM is not a substrate for human BCRP (239,240), to our knowledge calcein-AM has not been specifically tested with the mouse Bcrp homolog. More research is needed to confirm whether this transport is mediated by Bcrp or by another transporter. Broadly, transporter isoforms of preclinical species are poorly characterized relative to their human counterparts, yet academics and the pharmaceutical industry heavily utilize preclinical models to inform and interpret human clinical pharmacokinetics. Further studies characterizing species differences in

transporter function are needed to improve the translational utility of preclinical models towards assessing and interpreting human PK.

The apical localization of Bcrp at the blood-CSF barrier implies the transporter mediates entry of compounds into the CSF from the blood. While this localization is peculiar with respect to the barrier function of the blood-CSF barrier, another blood-CSF barrier function is to provide nourishment and maintain healthy brain homeostasis (174). For example, the CP actively transports vitamin C from blood into CSF via the sodium-dependent vitamin C transport system-1 (13). Several endogenous compounds are substrates of BCRP, including dehydroepiandrosterone sulfate, riboflavin, and folic acid (241). Thus, the apical localization of BCRP may imply a role of BCRP in transporting certain nutrients into the CSF. This function may be especially relevant during early development, as the choroid plexuses receive higher relative blood supply during this period (242).

In summary, studies performed in this work demonstrated a functional presence of the drug efflux transporter Bcrp at the blood-CSF barrier. CSF fluid remains the only accessible fluid to sample drug concentrations in the human CNS. However, prediction of free brain concentrations from CSF is challenging and depends on a full understanding of the transport processes at the BBB and blood-CSF barrier. More research to understand the contribution of these transporters on brain drug disposition can help our understanding of the relationship between CSF and unbound brain concentrations and improve our predictions of CNS efficacy and toxicity in humans.

4.6 CONCLUSIONS

In this study we demonstrated functional activity of Bcrp at the murine blood-CSF barrier using quantitative fluorescence microscopy and genetic knockout mouse model of Bcrp. An

additional Bcrp-independent, elacridar-sensitive apical efflux mechanism at the blood-CSF barrier was detected, which is possibly mediated by P-gp. Findings from this study contribute to the understanding of transport mechanisms that regulate CSF drug concentrations, which is relevant for the prediction and interpretation of CNS pharmacokinetics and pharmacodynamics for CNS drug candidates.

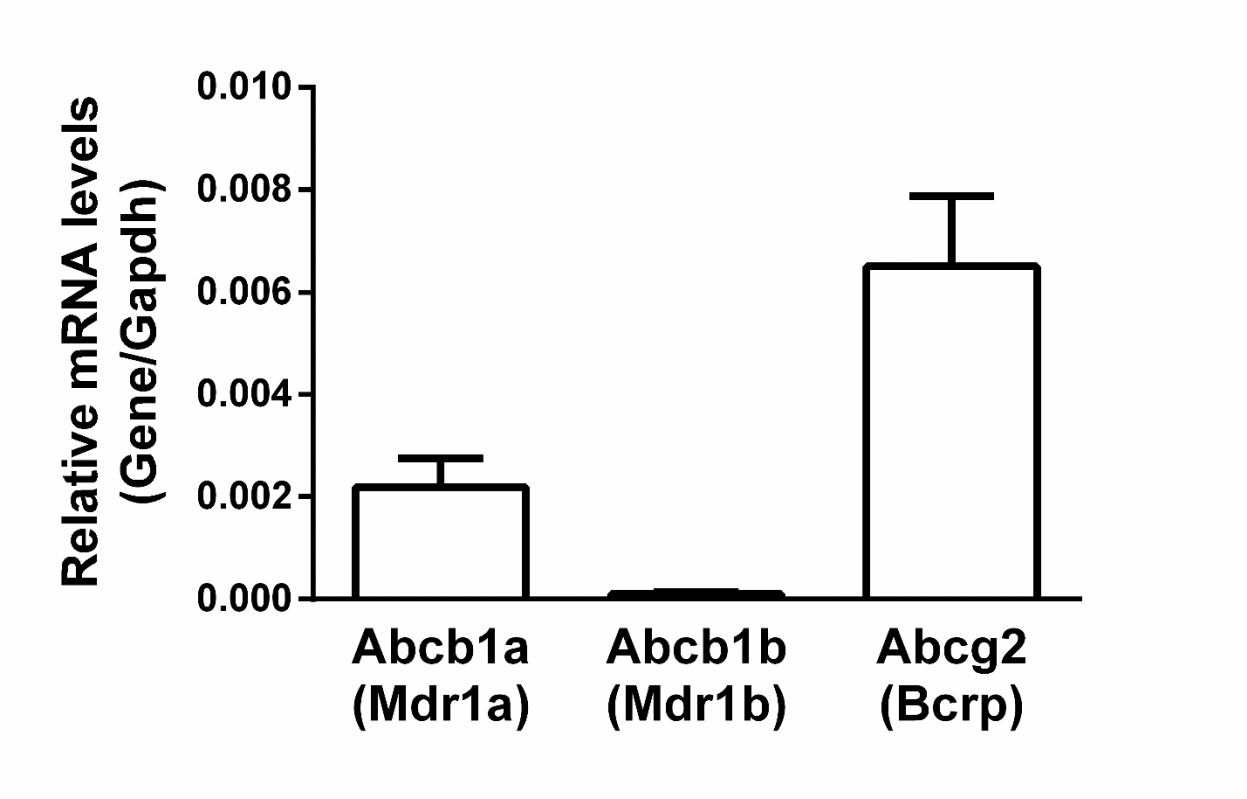

Figure 4.1. Relative mRNA expression of *Abcb1a* (Mdr1a), *Abcb1b* (Mdr1b), and *Abcg2* (Bcrp) transporters

Relative mRNA expression of *Abcb1a* (Mdr1a), *Abcb1b* (Mdr1b), and *Abcg2* (Bcrp) transporters in FVB mouse lateral ventricle CP tissues (n=9, pooled groups of 3). Expression levels are normalized to the housekeeping gene *Gapdh*

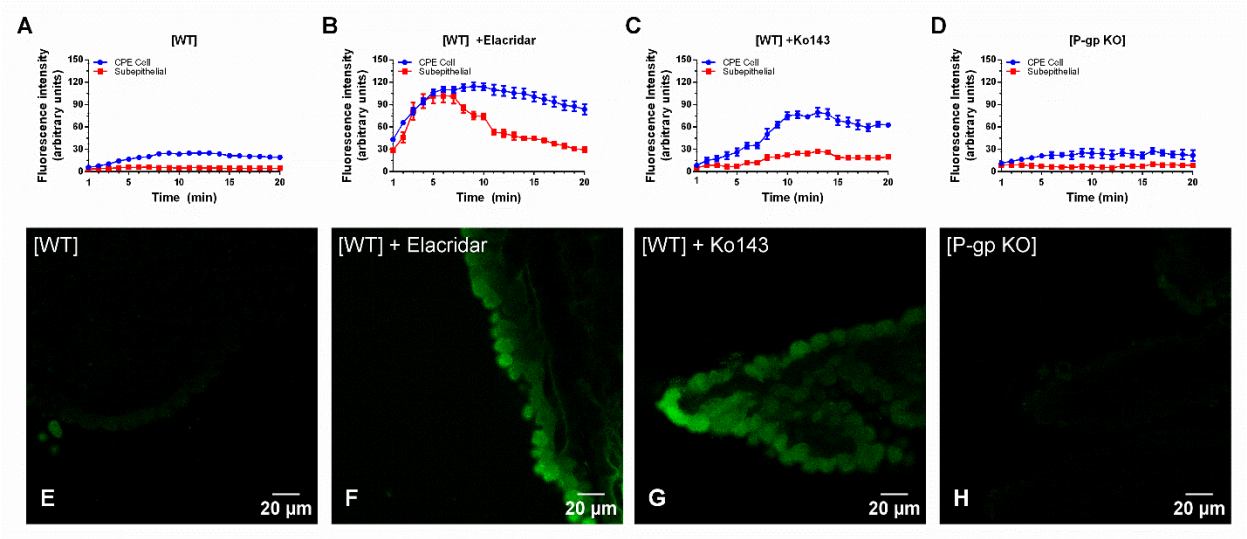

Figure 4.2. Representative time courses and confocal images at 20 minutes of calcein-AM in CP of WT and P-gp KO mice

CP tissues were incubated with 2 µM Calcein-AM for 20 minutes in different experimental conditions. Shown are representative time courses of quantified Calcein accumulation in CPE cell and subepithelial compartments from CP obtained from wild-type mice in the (A) absence of inhibitor, the (B) presence of 2 µM elacridar, the (C) presence of 1 µM Ko143, and from CP obtained from (D) Mdr1a/b$^{-/-}$ mice in the absence of inhibitor. Representative confocal images of Calcein accumulation after 20 minutes in CP tissues from wild-type mice in the (E) absence of inhibitor, the (F) presence of 2 µM elacridar, the (G) presence of 1 µM Ko143, and from CP obtained from (H) Mdr1a/b$^{-/-}$ mice in the absence of inhibitor.

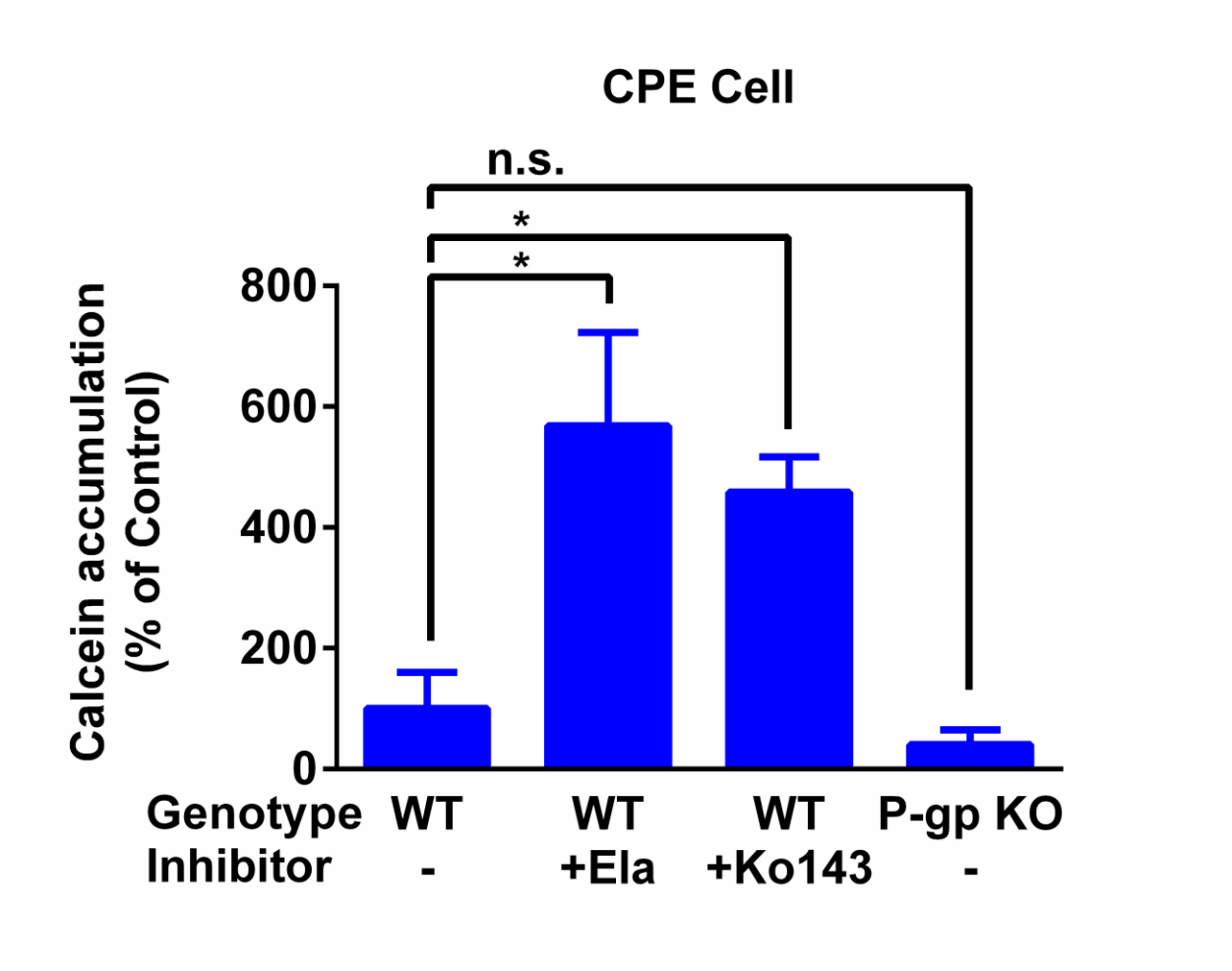

Figure 4.3. Changes in CPE cell accumulation in WT and P-gp KO mice

Quantified changes in CPE cell accumulation under different inhibitory conditions and between CP tissues of wild-type and Mdr1a/b$^{-/-}$ mice. Data are normalized to Calcein CPE cell accumulation with no inhibitor in wild-type tissues. Values are means ± SD across 3 biological replicates for all treatment groups. Statistical significance was determined using one-way ANOVA followed by Dunnett's test (*P<0.05).

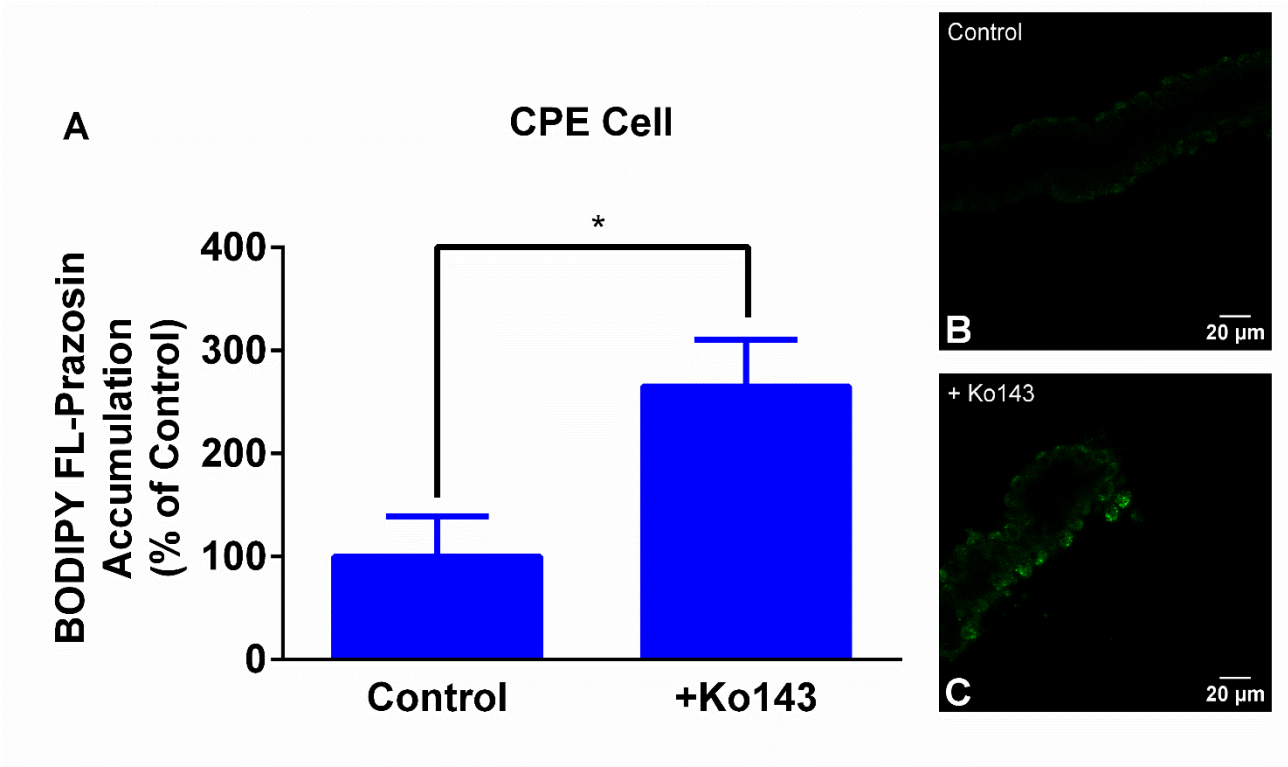

Figure 4.4. BODIPY FL-Prazosin accumulation in CPE cells after 20 minutes with and without Ko143

(A) Change in BODIPY FL-Prazosin accumulation in CPE cells after 20 minutes with and without Ko143. Tissues were incubated with BODIPY FL-Prazosin (2 µM) in the presence or absence of Ko143 (1 µM). Data are normalized to BODIPY FL-Prazosin accumulation in tissues with no inhibitor added. Values are means ± SD across 3 biological replicates for all treatment groups. Statistical significance was determined using aqn unpaired student's *t* test (*P<0.05). Representative images of CP tissues taken at 20 minutes in the (B) absence or (C) presence of Ko143

.

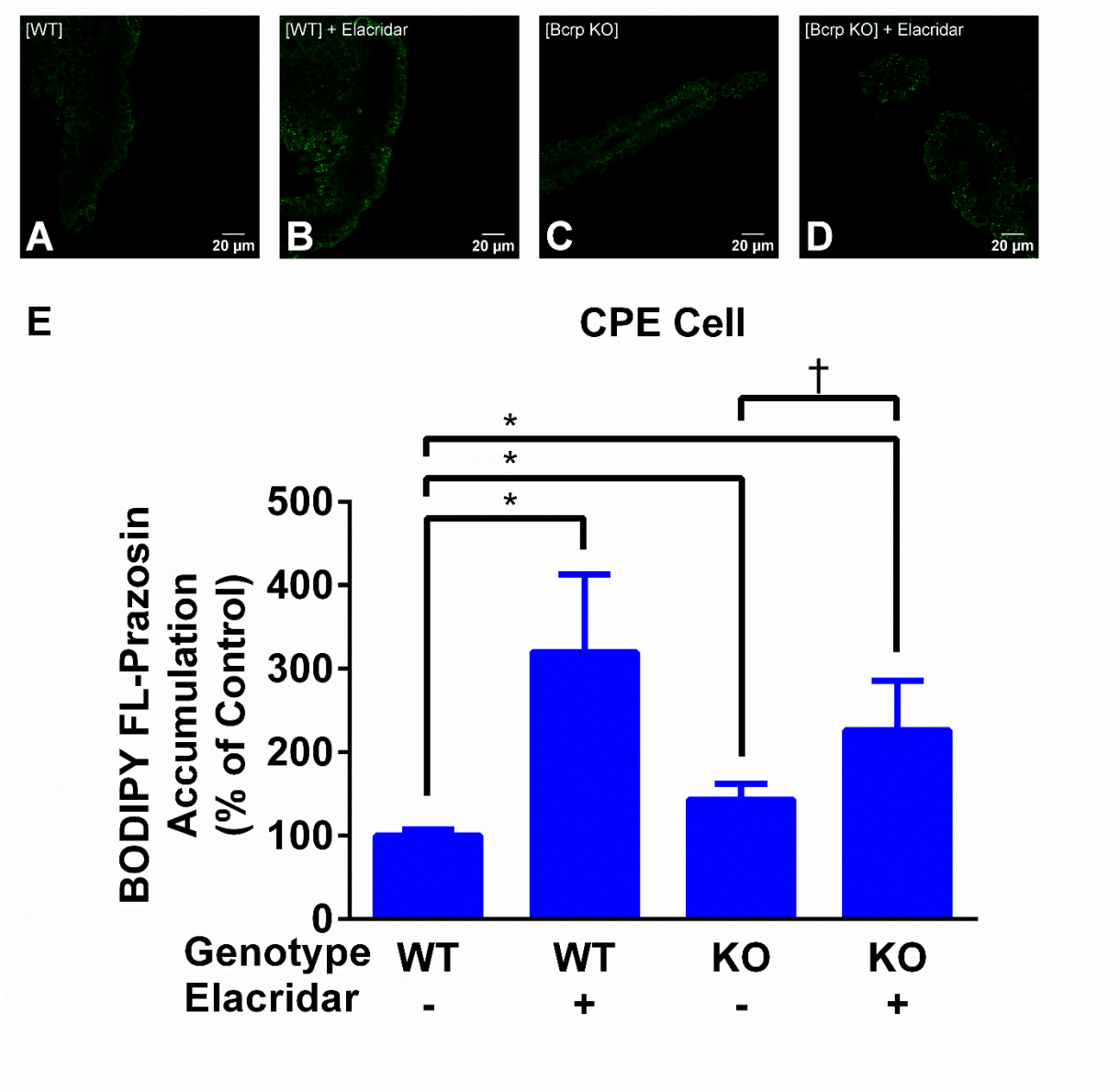

Figure 4.5. BODIPY FL-Prazosin in WT and Bcrp$^{-/-}$ mice

(A) Representative confocal images of BODIPY FL-Prazosin (2 µM) accumulation in CPE cells of wild-type mice in the (A) absence and (B) presence of elacridar (2 µM) and of Bcrp$^{-/-}$ mice in (C) absence and (D) presence of elacridar (2 µM). (E) Changes in CPE cell accumulation between treatment groups. Data are normalized to BODIPY FL-Prazosin CPE cell accumulation Data are normalized to BODIPY FL-Prazosin CPE cell accumulation with no inhibitor in wild-type tissues. BODIPY FL-Prazosin accumulation in other treatment groups were compared to

that in wild-type tissues with no elacridar (*P<0.05). Accumulation of BODIPY FL-Prazosin was also compared between knockout tissues in the absence or presence of elacridar (†P<0.05). Values are means ± SD across 3-4 biological replicates for all treatment groups. Statistical significance was determined using one-way ANOVA followed by Dunnett's test.

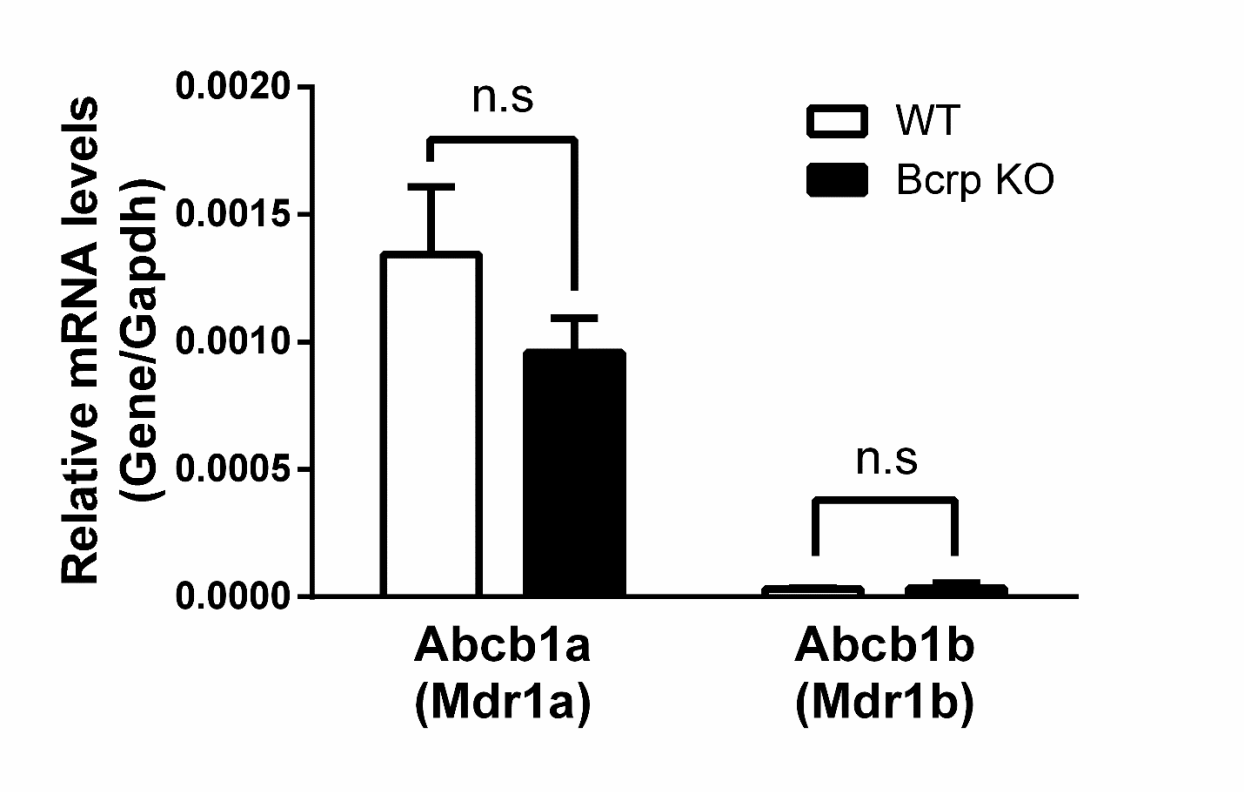

Figure 4.6. *Abcb1a* and *Abcb1b* expression in wild-type and Bcrp KO mice

Relative mRNA expression of *Abcb1a* (Mdr1a) and *Abcb1b* (Mdr1b) in 4th lateral ventricle CP of wild-type and Bcrp KO mice (n=3). Expression levels are normalized to the housekeeping gene *Gapdh*

Chapter 5. CONCLUSIONS AND FUTURE DIRECTIONS

The choroid plexus epithelial cells that form the blood-cerebrospinal fluid barrier express polyspecific transporters that contribute towards xenobiotic and endogenous compound clearance from the cerebrospinal fluid(174). However, transporters at the BCSFB are poorly understood with respect to function, activity, and pharmacokinetic significance. As brain drug concentrations cannot directly be measured in humans, understanding the transport mechanisms at the BCSFB may help the prediction of CNS pharmacokinetics and the identification of drug candidates with favorable CNS pharmacokinetic properties. This dissertation research is aimed to develop an approach to study and quantify BCSFB transport activity using quantitative fluorescence microscopy, and to utilize this approach and other biochemical approaches to elucidate the molecular and functional significance of OATP-, BCRP-, and P-gp-mediated transport at the BCSFB.

In Chapter 2, I developed and described the application of confocal microscopy to study and quantify transepithelial transport processes at the murine BCSFB in real time. This approach was shown to be consistent, reproducible, and capable of tracking real time transepithelial transport at the BCSFB with temporal and spatial resolution. Using this quantitative fluorescence microscopy approach, I visualized, quantified, and described separate processes of transport across the apical and basolateral membranes of BCSFB for organic anion and organic cation probes. I proposed a novel parameter, CPEI, or choroid plexus efflux index to distinguish between transepithelial flux and CPE cell accumulation. This approach can be used to evaluate transport mechanisms at the apical and basolateral membranes for CSF-to-blood transport, assess

potential tissue drug accumulation and toxicity, and predict potential drug-drug interaction at transporter sites at the blood-CSF barrier. Our data suggest that small organic cations may accumulate in CPE cells and may thus pose higher risk for CP tissue toxicity. Further studies are needed to validate whether low CPEI compounds are at higher risk for inducing CP toxicity. Some considerations when using this approach include the semi-quantitative nature of the approach and the limited number of naturally fluorescent clinical drugs. CP drug concentrations cannot be directly measured using fluorescence microscopy; thus, the real clearance from the CSF cannot be estimated using this approach. Therefore, while this approach provides insight on the transepithelial transport processes for broad classes of drugs (e.g. large organic anions, organic cations), characterizing and estimating the real clearance of specific drugs across the BCSFB will require alternative approaches, such as *in vitro* to *in vivo* extrapolation. For example, if a drug is known to be cleared by a specific transporter at the BCSFB, the relative expression factor approach could be utilized to estimate the transport CL_{int}. Transporter k_{cat} and K_m values can be determined using overexpressing cells, and the CL_{int} can then be scaled using the transporter abundance in CP tissues relative to that in overexpressing cells (243).

In Chapter 3, I utilized the method developed and validated in Chapter 2 alongside other biochemical approaches to characterize the molecular mechanisms of OATP-mediated organic anion clearance at the BCSFB. Through quantitative fluorescence imaging, I showed several OATP1A5 fluorescent substrates were readily transported in choroid plexus tissues of wild-type mice but not in tissues of Oatp1a/1b$^{-/-}$ mice, demonstrating that large organic anion uptake is predominantly mediated by OATP1A5 at the apical membrane of the murine BCSFB. Using OATP1A5 and OATP1A2 overexpressing cells, I showed an overlap in substrate pool across the

two transporters, suggesting an overlap in function between OATP1A5 and OATP1A2 in humans and mice. I then established the expression and localization of OATP1A2 at the apical membrane of the BCSFB using immunofluorescence on human choroid plexus tissue samples. These findings collectively identify and highlight the mechanisms of an efficient pathway for large organic anion clearance from the CSF in humans, mediated by OATP1A2 (OATP1A5 in mice) at the apical membrane and MRPs at the basolateral membrane. While our study did not examine drug substrates of OATP1A2, previous studies have shown that the antibiotic ceftriaxone is a substrate of OATPs (216) and appears to be actively cleared from the CSF (244), notably with lower concentrations in ventricular CSF compared to lumbar CSF (245,246). The significance of the OATP1A2 and MRP1/4 pathway for BCSFB clearance for ceftriaxone and other OATP substrates should be further evaluated using *in vivo* studies in preclinical animal models. A study by Smith et al. examined the role of PepT2 at the choroid plexus and other brain cells biodistribution of GlySar and Cefedroxil through intracerebroventricular injection of radiolabeled GlySar and Cefedroxil in wild-type and Pept2 knockout mice (247). A similar study design could be adopted to quantify changes in CSF clearance of ceftriaxone in wild-type and Oatp1a/1b cluster KO mice.

In Chapter 4, I utilized the approach described in Chapter 2 alongside selective inhibitors and knockout models to explore the activity, mechanisms, and potential interplay of P-gp and Bcrp at the BCSFB. Using qRT-PCR I identified the relative mRNA expression of P-gp and Bcrp. Using quantitative fluorescence microscopy in isolated CP tissues of wild-type and $Bcrp^{-/-}$ mice, I demonstrated BODIPY FL-prazosin was actively transported by Bcrp, demonstrating functional activity of apical Bcrp efflux. Moreover, I detected an additional Bcrp-independent,

elacridar-sensitive apical efflux mechanism at the BCSFB, suggested, but not confirmed, to be P-gp. We observed with calcein-AM and BODIPY FL-prazosin, similar to previous studies conducted at the blood-brain barrier, that inhibition of both or all efflux transporters is needed to observe large changes in substrate efflux when two or more efflux transport mechanisms are present on the membrane. Further studies comparing transport in Bcrp$^{-/-}$ and Bcrp/Mdr1a/b$^{-/-}$ mice would be able to confirm the functional presence of P-gp at the murine BCSFB. Alternatively, evaluating the transport kinetics and inhibitor specificity in mouse Bcrp and mouse Mdr1a overexpressing cells could also provide additional information and evidence towards P-gp function at the BCSFB. However, these studies should not be conducted in MDCK cells, as endogenous canine P-gp is expressed and may complicate the interpretation of data (248). In this study, we demonstrated BCRP activity at the murine BCSFB, and there is also some evidence of BCRP expression in other species. BCRP is expressed at the protein level in the BCSFB of rats, pigs, and a single human subject (58,60). BCRP has also been localized apically at the BCSFB in the developing human brain (249). Further study of the localization and protein quantification of BCRP at the human BCSFB in a larger adult cohort would help contextualize our findings for human adults.

In summary, this dissertation research has contributed greatly to our understanding of the molecular mechanisms mediating xenobiotic transport at the blood-CSF barrier. My research revealed a functional role of OATP1A5 in clearing large organic anions from the CSF and suggests a similar role for OATP1A2 at the human BCSFB. Furthermore, we have demonstrated functional activity of Bcrp at the apical membrane in mice. Taken together, this research provides mechanistic evidence towards several understudied transport pathways at the BCSFB

that may play an important role in CNS drug disposition and modulate the relationship between CSF and unbound brain drug concentrations. The findings of this dissertation provide strong rationales for future research to investigate the roles and significance of OATP1A2, P-gp, and BCRP transporters towards CNS drug disposition and endobiotic transport at the blood-CSF barrier in vivo. These studies are especially relevant for the development of drugs that specifically target the CSF, such as those used in the treatment of bacterial or viral meningitis. As CNS pharmacokinetics and exposure may drive drug efficacy and toxicity, this dissertation research has the potential to impact on the future outlook of CNS drug development to treat various brain disorders.

BIBLIOGRAPHY

1. Lun MP, Monuki ES, Lehtinen MK. Development and functions of the choroid plexus-cerebrospinal fluid system. Nat Rev Neurosci. 2015 Aug;16(8):445–57.
2. Fame RM, Cortés-Campos C, Sive HL. Brain Ventricular System and Cerebrospinal Fluid Development and Function: Light at the End of the Tube: A Primer with Latest Insights. Bioessays. 2020 Mar;42(3):e1900186.
3. Spector R, Keep RF, Snodgrass SR, Smith QR, Johanson CE. A balanced view of choroid plexus structure and function: Focus on adult humans. Exp Neurol. 2015;267:78–86.
4. Damkier HH, Brown PD, Praetorius J. Epithelial Pathways in Choroid Plexus Electrolyte Transport. Physiology. 2010 Aug 1;25(4):239–49.
5. Davson H, Purvis C. Cryoscopic apparatus suitable for studies on aqueous humour and cerebro-spinal fluid. J Physiol. 1954 Dec;124:1-47 12P.
6. Welch K, Sadler K. Electrical Potentials of Choroid Plexus of the rabbit. J Neurosurg. 1965 Apr;22(4):344–51.
7. Wolburg H, Paulus W. Choroid plexus: biology and pathology. Acta Neuropathol. 2010 Jan;119(1):75–88.
8. Prinz M, Priller J. The role of peripheral immune cells in the CNS in steady state and disease. Nat Neurosci. 2017;20(2):136–44.
9. Prinz M, Priller J, Sisodia SS, Ransohoff RM. Heterogeneity of CNS myeloid cells and their roles in neurodegeneration. Nat Neurosci. 2011 Sep;14(10):1227–35.
10. Schwartz M, Baruch K. The resolution of neuroinflammation in neurodegeneration: leukocyte recruitment via the choroid plexus. EMBO J. 2014 Jan 2;33(1):7–22.
11. Davson H, Welch K, Segal MB. Physiology and pathophysiology of the cerebrospinal

fluid. Edinburgh–London: Churchill Livingstone. 1987;

12. Davson H, Segal MB. Physiology of the CSF and blood-brain barriers. Boca Raton: CRC press; 1996.

13. Spector R, Robert Snodgrass S, Johanson CE. A balanced view of the cerebrospinal fluid composition and functions: Focus on adult humans. Exp Neurol. 2015;273:57–68.

14. Dawson RMC, Freinkel N. The distribution of free mesoinositol in mammalian tissues, including some observations on the lactating rat. Biochem J. 1961 Mar 1;78(3):606–10.

15. de Rougemont J, Ames A, Nesbett FB, Hofmann HF. Fluid formed by choroid plexus: A technique for its collection and a comparison of its electrolyte composition with serum and cisternal fluids. J Neurophysiol. 1960 Sep 1;23(5):485–95.

16. Johanson CE, Stopa EG, McMillan PN. The Blood–Cerebrospinal Fluid Barrier: Structure and Functional Significance. In: Nag S, editor. The Blood-Brain and Other Neural Barriers. New York: Springer; 2011. p. 101–31.

17. Herndon RM, Brumback RA. The Cerebrospinal Fluid. Boston/Dordrecht/London: Kluwer Academic Publishers; 2012.

18. Thompson EJ. The CSF Proteins: A Biochemical Approach. Amsterdam: Elsevier; 1988. 9–26 p.

19. Sakka L, Coll G, Chazal J. Anatomy and physiology of cerebrospinal fluid. Eur Ann Otorhinolaryngol Head Neck Dis. 2011;128(6):309–16.

20. Nilsson C, Stahlberg F, Thomsen C, Henriksen O, Herning M, Owman C. Circadian variation in human cerebrospinal fluid production measured by magnetic resonance imaging. Am J Physiol Integr Comp Physiol. 1992 Jan 1;262(1):R20–4.

21. Dreha-Kulaczewski S, Joseph AA, Merboldt K-D, Ludwig H-C, Gärtner J, Frahm J.

Inspiration Is the Major Regulator of Human CSF Flow. J Neurosci. 2015 Feb 11;35(6):2485 LP – 2491.

22. Bateman GA, Brown KM. The measurement of CSF flow through the aqueduct in normal and hydrocephalic children: from where does it come, to where does it go? Child's Nerv Syst. 2012;28(1):55–63.

23. Rubin RC, Henderson ES, Ommaya AK, Walker MD, Rall DP. The production of cerebrospinal fluid in man and its modification by acetazolamide. J Neurosurg. 1966 Oct;25(4):430–6.

24. Cutler RW, Page L, Galicich J, Watters G V. Formation and absorption of cerebrospinal fluid in man. Brain. 1968;91(4):707–20.

25. Lorenzo A V, Page LK, Watters G V. Relationship between cerebrospinal fluid formation, absorption and pressure in human hydrocephalus. Brain. 1970;93(4):679–92.

26. Preston JE. Ageing choroid plexus-cerebrospinal fluid system. Microsc Res Tech. 2001 Jan 1;52(1):31–7.

27. May C, Kaye JA, Atack JR, Schapiro MB, Friedland RP, Rapoport SI. Cerebrospinal fluid production is reduced in healthy aging. Neurology. 1990 Mar 1;40(3 Part 1):500 LP – 500.

28. Chen CPC, Chen RL, Preston JE. The influence of cerebrospinal fluid turnover on age-related changes in cerebrospinal fluid protein concentrations. Neurosci Lett. 2010;476(3):138–41.

29. Chiu C, Miller MC, Caralopoulos IN, Worden MS, Brinker T, Gordon ZN, et al. Temporal course of cerebrospinal fluid dynamics and amyloid accumulation in the aging rat brain from three to thirty months. Fluids Barriers CNS. 2012;9(1):3.

30. Silverberg GD, Heit G, Huhn S, Jaffe RA, Chang SD, Bronte–Stewart H, et al. The

cerebrospinal fluid production rate is reduced in dementia of the Alzheimer's type. Neurology. 2001 Nov 27;57(10):1763 LP – 1766.

31. de Leon MJ, Li Y, Okamura N, Tsui WH, Saint-Louis LA, Glodzik L, et al. Cerebrospinal Fluid Clearance in Alzheimer Disease Measured with Dynamic PET. J Nucl Med. 2017 Sep 1;58(9):1471–6.

32. Schubert JJ, Veronese M, Marchitelli L, Bodini B, Tonietto M, Stankoff B, et al. Dynamic 11C-PiB PET Shows Cerebrospinal Fluid Flow Alterations in Alzheimer Disease and Multiple Sclerosis. J Nucl Med. 2019 Oct 1;60(10):1452–60.

33. Alperin N, Lee SH, Sivaramakrishnan A, Hushek SG. Quantifying the effect of posture on intracranial physiology in humans by MRI flow studies. J Magn Reson Imaging. 2005 Nov 1;22(5):591–6.

34. Fultz NE, Bonmassar G, Setsompop K, Stickgold RA, Rosen BR, Polimeni JR, et al. Coupled electrophysiological, hemodynamic, and cerebrospinal fluid oscillations in human sleep. Science (80-). 2019 Nov 1;366(6465):628 LP – 631.

35. Grubb S, Lauritzen M. Deep sleep drives brain fluid oscillations. Science. 2019 Nov;366(6465):572–3.

36. Abbott NJ. Evidence for bulk flow of brain interstitial fluid: significance for physiology and pathology. Neurochem Int. 2004;45(4):545–52.

37. Jessen NA, Munk ASF, Lundgaard I, Nedergaard M. The Glymphatic System: A Beginner's Guide. Neurochem Res. 2015;40(12):2583–99.

38. Pardridge WM. CSF, blood-brain barrier, and brain drug delivery. Expert Opin Drug Deliv. 2016;13(7):963–75.

39. Davson H, Segal MB. The effects of some inhibitors and accelerators of sodium transport

on the turnover of 22Na in the cerebrospinal fluid and the brain. J Physiol. 1970 Jul 1;209(1):131–53.

40. Oldendorf WH, Davson H. Brain Extracellular Space and the Sink Action of Cerebrospinal Fluid: Measurement of Rabbit Brain Extracellular Space Using Sucrose Labeled With Carbon 14. Arch Neurol. 1967 Aug 1;17(2):196–205.

41. Abbott NJ, Pizzo ME, Preston JE, Janigro D, Thorne RG. The role of brain barriers in fluid movement in the CNS: is there a "glymphatic" system? Acta Neuropathol. 2018 Mar;135(3):387–407.

42. Cserr HF, Cooper DN, Suri PK, Patlak CS. Efflux of radiolabeled polyethylene glycols and albumin from rat brain. Am J Physiol Physiol. 1981 Apr 1;240(4):F319–28.

43. Cserr HF, Cooper DN, Milhorat TH. Flow of cerebral interstitial fluid as indicated by the removal of extracellular markers from rat caudate nucleus. Exp Eye Res. 1977;25:461–73.

44. Plog BA, Nedergaard M. The Glymphatic System in Central Nervous System Health and Disease: Past, Present, and Future. Annu Rev Pathol Mech Dis. 2018 Jan 24;13(1):379–94.

45. Wang M, Liao Y, Venkataraman A, Plog BA, Nedergaard M, Deane R, et al. Cerebral Arterial Pulsation Drives Paravascular CSF-Interstitial Fluid Exchange in the Murine Brain. J Neurosci. 2013;33(46):18190–9.

46. Xie L, Kang H, Xu Q, Chen MJ, Liao Y, Thiyagarajan M, et al. Sleep Drives Metabolite Clearance from the Adult Brain. Science (80-). 2013 Oct 18;342(6156):373 LP – 377.

47. Smith AJ, Yao X, Dix JA, Jin B-J, Verkman AS. Test of the "glymphatic" hypothesis demonstrates diffusive and aquaporin-4-independent solute transport in rodent brain parenchyma. Huguenard J, editor. Elife. 2017;6:e27679.

48. Mestre H, Hablitz LM, Xavier ALR, Feng W, Zou W, Pu T, et al. Aquaporin-4-dependent glymphatic solute transport in the rodent brain. Kleinfeld D, Morrison SJ, editors. Elife. 2018;7:e40070.

49. Wolak DJ, Thorne RG. Diffusion of Macromolecules in the Brain: Implications for Drug Delivery. Mol Pharm. 2013 May 6;10(5):1492–504.

50. Holter KE, Kehlet B, Devor A, Sejnowski TJ, Dale AM, Omholt SW, et al. Interstitial solute transport in 3D reconstructed neuropil occurs by diffusion rather than bulk flow. Proc Natl Acad Sci. 2017 Sep 12;114(37):9894 LP – 9899.

51. Giacomini KM, Huang S-M, Tweedie DJ, Benet LZ, Brouwer KLR, Chu X, et al. Membrane transporters in drug development. Nat Rev Drug Discov. 2010;9(3):215–36.

52. Wagner DJ, Hu T, Wang J. Polyspecific organic cation transporters and their impact on drug intracellular levels and pharmacodynamics. Pharmacol Res. 2016;111:237–46.

53. Giacomini KM, Huang S-M, Tweedie DJ, Benet LZ, Brouwer KLR, Chu X, et al. Membrane transporters in drug development. Nat Rev Drug Discov. 2010;9(3):215–36.

54. Lin L, Yee SW, Kim RB, Giacomini KM. SLC transporters as therapeutic targets: emerging opportunities. Nat Rev Drug Discov. 2015;14(8):543–60.

55. Dahlin A, Royall J, Hohmann JG, Wang J. Expression Profiling of the Solute Carrier Gene Family in the Mouse Brain. J Pharmacol Exp Ther. 2009;329(2):558–70.

56. Ho H, Dahlin A, Wang J. Expression Profiling of Solute Carrier Gene Families at the Blood-CSF Barrier. Front Pharmacol. 2012;3:154.

57. Choudhuri S, Cherrington NJ, Li N, Klaassen CD. Constitutive expression of various xenobiotic and endobiotic transporter mRNAs in the choroid plexus of rats. Drug Metab Dispos. 2003;31(11):1337–45.

58. Uchida Y, Zhang Z, Tachikawa M, Terasaki T. Quantitative targeted absolute proteomics of rat blood-cerebrospinal fluid barrier transporters: Comparison with a human specimen. J Neurochem. 2015;134(6):1104–15.

59. Braun C, Sakamoto A, Fuchs H, Ishiguro N, Suzuki S, Cui Y, et al. Quantification of Transporter and Receptor Proteins in Dog Brain Capillaries and Choroid Plexus: Relevance for the Distribution in Brain and CSF of Selected BCRP and P-gp Substrates. Mol Pharm. 2017 Oct 2;14(10):3436–47.

60. Uchida Y, Goto R, Takeuchi H, Łuczak M, Usui T, Tachikawa M, et al. Abundant Expression of OCT2, MATE1, OAT1, OAT3, PEPT2, BCRP, MDR1, and xCT Transporters in Blood-Arachnoid Barrier of Pig and Polarized Localizations at CSF- and Blood-Facing Plasma Membranes. Drug Metab Dispos. 2020 Feb 1;48(2):135–45.

61. Akanuma S, Kubo Y, Hosoya K. Techniques for Evaluating Efflux Transport of Radiolabeled Drugs and Compounds from the Cerebrospinal Fluid Across the Blood-Cerebrospinal Fluid Barrier BT - Blood-Brain Barrier. In: Barichello T, editor. Blood-Brain Barrier. New York, NY: Springer New York; 2019. p. 231–48.

62. Kläs J, Wolburg H, Terasaki T, Fricker G, Reichel V. Characterization of immortalized choroid plexus epithelial cell lines for studies of transport processes across the blood-cerebrospinal fluid barrier. Cerebrospinal Fluid Res. 2010;7(11).

63. Pellegrini L, Bonfio C, Chadwick J, Begum F, Skehel M, Lancaster MA. Human CNS barrier-forming organoids with cerebrospinal fluid production. Science (80-). 2020 Jul 10;369(6500):eaaz5626.

64. Rao V V, Dahlheimer JL, Bardgett ME, Snyder AZ, Finch RA, Sartorelli AC, et al. Choroid plexus epithelial expression of MDR1 P glycoprotein and multidrug resistance-

associated protein contribute to the blood–cerebrospinal-fluid drug-permeability barrier. Proc Natl Acad Sci. 1999 Mar 30;96(7):3900 LP – 3905.

65. Morris ME, Rodriguez-Cruz V, Felmlee MA. SLC and ABC Transporters: Expression, Localization, and Species Differences at the Blood-Brain and the Blood-Cerebrospinal Fluid Barriers. AAPS J. 2017;19(5):1317–31.

66. Pritchard JB. Intracellular alpha-ketoglutarate controls the efficacy of renal organic anion transport. J Pharmacol Exp Ther. 1995 Sep 1;274(3):1278 LP – 1284.

67. Nigam SK, Bush KT, Martovetsky G, Ahn S-Y, Liu HC, Richard E, et al. The Organic Anion Transporter (OAT) Family: A Systems Biology Perspective. Physiol Rev. 2015 Jan 1;95(1):83–123.

68. VanWert AL, Bailey RM, Sweet DH. Organic anion transporter 3 (Oat3/Slc22a8) knockout mice exhibit altered clearance and distribution of penicillin G. Am J Physiol Physiol. 2007 Oct 1;293(4):F1332–41.

69. VanWert AL, Sweet DH. Impaired Clearance of Methotrexate in Organic Anion Transporter 3 (Slc22a8) Knockout Mice: A Gender Specific Impact of Reduced Folates. Pharm Res. 2008;25(2):453–62.

70. Pappenheimer JR, Heisey SR, Jordan EF. Active transport of Diodrast and phenolsulfonphthalein from cerebrospinal fluid to blood. Am J Physiol Content. 1961 Jan 1;200(1):1–10.

71. Fishman RA. Blood-Brain and CSF Barriers to Penicillin and Related Organic Acids. Arch Neurol. 1966 Aug 1;15(2):113–24.

72. Sweet DH, Wolff NA, Pritchard JB. Expression cloning and characterization of ROAT1: The basolateral organic anion transporter in rat kidney. J Biol Chem. 1997 Nov

28;272(48):30088–95.

73. Sekine T, Watanabe N, Hosoyamada M, Kanai Y, Endou H. Expression Cloning and Characterization of a Novel Multispecific Organic Anion Transporter. J Biol Chem . 1997 Jul 25;272(30):18526–9.

74. Bode U, Magrath IT, Bleyer WA, Poplack DG, Glaubiger DL. Active Transport of Methotrexate from Cerebrospinal Fluid in Humans. Cancer Res. 1980 Jul 1;40(7):2184 LP – 2187.

75. Nagata Y, Kusuhara H, Endou H, Sugiyama Y. Expression and Functional Characterization of Rat Organic Anion Transporter 3 (rOat3) in the Choroid Plexus. Mol Pharmacol. 2002 May 1;61(5):982 LP – 988.

76. Sweet DH, Miller DS, Pritchard JB, Fujiwara Y, Beier DR, Nigam SK. Impaired Organic Anion Transport in Kidney and Choroid Plexus of Organic Anion Transporter 3 (Oat3 (Slc22a8)) Knockout Mice. J Biol Chem. 2002;277(30):26934–43.

77. Sykes D, Sweet DH, Lowes S, Nigam SK, Pritchard JB, Miller DS, et al. Organic anion transport in choroid plexus from wild-type and organic anion transporter 3 (Slc22a8)-null mice. Am J Physiol - Ren Physiol. 2004 May;286(5):F972-8.

78. Liu W, Liang R, Ramamoorthy S, Fei Y-J, Ganapathy ME, Hediger MA, et al. Molecular cloning of PEPT 2, a new member of the H+/peptide cotransporter family, from human kidney. Biochim Biophys Acta - Biomembr. 1995;1235(2):461–6.

79. Kamal MA, Keep RF, Smith DE. Role and Relevance of PEPT2 in Drug Disposition, Dynamics, and Toxicity. Drug Metab Pharmacokinet. 2008;23(4):236–42.

80. Smith DE, Clémençon B, Hediger MA. Proton-coupled oligopeptide transporter family SLC15: Physiological, pharmacological and pathological implications. Mol Aspects Med.

2013;34(2):323–36.

81. Ocheltree SM, Shen H, Hu Y, Keep RF, Smith DE. Role and Relevance of Peptide Transporter 2 (PEPT2) in the Kidney and Choroid Plexus: In Vivo Studies with Glycylsarcosine in Wild-Type and PEPT2 Knockout Mice. J Pharmacol Exp Ther. 2005;315(1):240–7.

82. Shen H, Ocheltree SM, Hu Y, Keep RF, Smith DE. Impact of genetic knockout of PEPT2 on cefadroxil pharmacokinetics, renal tubular reabsorption, and brain penetration in mice. Drug Metab Dispos. 2007;35(7):1209–16.

83. Kamal MA, Jiang H, Hu Y, Keep RF, Smith DE. Influence of genetic knockout of Pept2 on the in vivo disposition of endogenous and exogenous carnosine in wild-type and Pept2 null mice. Am J Physiol Integr Comp Physiol. 2009 Apr 1;296(4):R986–91.

84. Shu C, Shen H, Teuscher NS, Lorenzi PJ, Keep RF, Smith DE. Role of PEPT2 in Peptide/Mimetic Trafficking at the Blood-Cerebrospinal Fluid Barrier: Studies in Rat Choroid Plexus Epithelial Cells in Primary Culture. J Pharmacol Exp Ther. 2002 Jun 1;301(3):820 LP – 829.

85. Shen H, Smith DE, Keep RF, Brosius FC. Immunolocalization of the Proton-Coupled Oligopeptide Transporter PEPT2 in Developing Rat Brain. Mol Pharm. 2004;1(4):248–56.

86. Shen H, Smith DE, Keep RF, Xiang J, Brosius FC. Targeted Disruption of the PEPT2 Gene Markedly Reduces Dipeptide Uptake in Choroid Plexus. J Biol Chem. 2003 Feb 14;278(7):4786–91.

87. Shen H, Keep RF, Hu Y, Smith DE. PEPT2 (Slc15a2)-Mediated Unidirectional Transport of Cefadroxil from Cerebrospinal Fluid into Choroid Plexus. J Pharmacol Exp Ther. 2005 Dec 1;315(3):1101 LP – 1108.

88. Chen X, Keep RF, Liang Y, Zhu H-J, Hammarlund-Udenaes M, Hu Y, et al. Influence of peptide transporter 2 (PEPT2) on the distribution of cefadroxil in mouse brain: A microdialysis study. Biochem Pharmacol. 2017;131:89–97.

89. Engel K, Zhou M, Wang J. Identification and Characterization of a Novel Monoamine Transporter in the Human Brain. J Biol Chem. 2004 Nov 26;279(48):50042–9.

90. Wang J. The Plasma Memebrane Monoamine Transporter (PMAT): Structure, Function, and Role in Organic Cation Disposition. Clin Pharmacol Ther. 2016;100(5):489–99.

91. Foti RS, Swaan PW, Wang J, Duan H, Pan Y, Hu T. Potent and Selective Inhibition of Plasma Membrane Monoamine Transporter by HIV Protease Inhibitors. Drug Metab Dispos. 2015;43(11):1773–80.

92. Zhou M, Xia L, Wang J. Metformin Transport by a Newly Cloned Proton-Stimulated Organic Cation Transporter (Plasma Membrane Monoamine Transporter) Expressed in Human Intestine. Drug Metab Dispos. 2007 Oct 1;35(10):1956 LP – 1962.

93. Itagaki S, Ganapathy V, Ho HTB, Zhou M, Babu E, Wang J. Electrophysiological Characterization of the Polyspecific Organic Cation Transporter Plasma Membrane Monoamine Transporter. Drug Metab Dispos. 2012 Jun 1;40(6):1138 LP – 1143.

94. Duan H, Wang J. Selective Transport of Monoamine Neurotransmitters by Human Plasma Membrane Monoamine Transporter and Organic Cation Transporter 3. J Pharmacol Exp Ther. 2010 Dec 1;335(3):743–53.

95. Xia L, Engel K, Zhou M, Wang J. Membrane localization and pH-dependent transport of a newly cloned organic cation transporter (PMAT) in kidney cells. Am J Physiol Physiol. 2007 Feb 1;292(2):F682–90.

96. Duan H, Wang J. Impaired monoamine and organic cation uptake in choroid plexus in

mice with targeted disruption of the plasma membrane monoamine transporter (Slc29a4) gene. J Biol Chem. 2013;288(5):3535–44.

97. Sweet DH, Miller DS, Pritchard JB. Ventricular choline transport: A role for organic cation transporter 2 expressed in choroid plexus. J Biol Chem. 2001 Nov 9;276(45):41611–9.

98. Miller DS, Villalobos AR, Pritchard JB. Organic cation transport in rat choroid plexus cells studied by fluorescence microscopy. Am J Physiol Physiol. 1999 Apr 1;276(4):C955–68.

99. Cole SP, Bhardwaj G, Gerlach JH, Mackie JE, Grant CE, Almquist KC, et al. Overexpression of a transporter gene in a multidrug-resistant human lung cancer cell line. Science (80-). 1992 Dec 4;258(5088):1650 LP – 1654.

100. Cole SPC. Targeting Multidrug Resistance Protein 1 (MRP1, ABCC1): Past, Present, and Future. Annu Rev Pharmacol Toxicol. 2014 Jan 6;54(1):95–117.

101. Lu JF, Pokharel D, Bebawy M. MRP1 and its role in anticancer drug resistance. Drug Metab Rev. 2015 Oct 2;47(4):406–19.

102. Semsei AF, Erdelyi DJ, Ungvari I, Csagoly E, Hegyi MZ, Kiszel PS, et al. ABCC1 polymorphisms in anthracycline-induced cardiotoxicity in childhood acute lymphoblastic leukaemia. Cell Biol Int. 2012 Jan 1;36(1):79–86.

103. Krause MS, Oliveira Jr LP, Silveira EMS, Vianna DR, Rossato JS, Almeida BS, et al. MRP1/GS-X pump ATPase expression: is this the explanation for the cytoprotection of the heart against oxidative stress-induced redox imbalance in comparison to skeletal muscle cells? Cell Biochem Funct. 2007 Jan 1;25(1):23–32.

104. Leszek W, Bettina K, Markus S, Gregor S, Albrecht S, Albert R, et al. NAD(P)H Oxidase

and Multidrug Resistance Protein Genetic Polymorphisms Are Associated With Doxorubicin-Induced Cardiotoxicity. Circulation. 2005 Dec 13;112(24):3754–62.

105. Gazzin S, Strazielle N, Schmitt C, Fevre-Montange M, Ostrow JD, Tiribelli C, et al. Differential expression of the multidrug resistance-related proteins ABCb1 and ABCc1 between blood-brain interfaces. J Comp Neurol. 2008 Oct 10;510(5):497–507.

106. Wijnholds J, de Lange ECM, Scheffer GL, van den Berg D-J, Mol CAAM, van der Valk M, et al. Multidrug resistance protein 1 protects the choroid plexus epithelium and contributes to the blood-cerebrospinal fluid barrier. J Clin Invest. 2000 Feb 1;105(3):279–85.

107. Kool M, De Haas M, Scheffer GL, Scheper RJ, Van Eijk MJT, Juijn JA, et al. Analysis of expression of cMOAT (MRP2), MRP3, MRP4, and MRP5, homologues of the multidrug resistance-associated protein gene (MRP1), in human cancer cell lines. Cancer Res. 1997 Aug 15;57(16):3537–47.

108. Russel FGM, Koenderink JB, Masereeuw R. Multidrug resistance protein 4 (MRP4/ABCC4): a versatile efflux transporter for drugs and signalling molecules. Trends Pharmacol Sci. 2008;29(4):200–7.

109. Nies AT, Jedlitschky G, König J, Herold-Mende C, Steiner HH, Schmitt H-P, et al. Expression and immunolocalization of the multidrug resistance proteins, MRP1–MRP6 (ABCC1–ABCC6), in human brain. Neuroscience. 2004;129(2):349–60.

110. Zamek-Gliszczynski MJ, Taub ME, Chothe PP, Chu X, Giacomini KM, Kim RB, et al. Transporters in Drug Development: 2018 ITC Recommendations for Transporters of Emerging Clinical Importance. Clin Pharmacol Ther. 2018 Nov 1;104(5):890–9.

111. Leggas M, Adachi M, Scheffer GL, Sun D, Wielinga P, Du G, et al. Mrp4 Confers

Resistance to Topotecan and Protects the Brain from Chemotherapy. Mol Cell Biol. 2004 Sep 1;24(17):7612–21.

112. Reichel V, Kläs J, Fricker G, Masereeuw R. Fluo-cAMP is transported by multidrug resistance-associated protein isoform 4 in rat choroid plexus. J Neurochem. 2010;115(1):200–8.

113. Flores K, Manautou JE, Renfro JL. Gender-specific expression of ATP-binding cassette (Abc) transporters and cytoprotective genes in mouse choroid plexus. Toxicology. 2017 Jul 1;386:84–92.

114. Hagenbuch B, Stieger B. The SLCO (former SLC21) superfamily of transporters. Mol Aspects Med. 2013;34(2):396–412.

115. Kalliokoski A, Niemi M. Impact of OATP transporters on pharmacokinetics. Br J Pharmacol. 2009 Oct 1;158(3):693–705.

116. Mayerl S, Müller J, Bauer R, Richert S, Kassmann CM, Darras VM, et al. Transporters MCT8 and OATP1C1 maintain murine brain thyroid hormone homeostasis. J Clin Invest. 2014 May 1;124(5):1987–99.

117. Hu T, Zha W, Sun A, Wang J. Live Tissue Imaging Reveals Distinct Transcellular Pathways for Organic Cations and Anions at the Blood-Cerebrospinal Fluid Barrier. Mol Pharmacol. 2022 Jan 1;101(5):334–42.

118. Sugiyama D, Kusuhara H, Taniguchi H, Ishikawa S, Nozaki Y, Aburatani H, et al. Functional Characterization of Rat Brain-specific Organic Anion Transporter (Oatp14) at the Blood-Brain Barrier: HIGH AFFINITY TRANSPORTER FOR THYROXINE *. J Biol Chem. 2003 Oct 31;278(44):43489–95.

119. Roberts LM, Woodford K, Zhou M, Black DS, Haggerty JE, Tate EH, et al. Expression of

the Thyroid Hormone Transporters Monocarboxylate Transporter-8 (SLC16A2) and Organic Ion Transporter-14 (SLCO1C1) at the Blood-Brain Barrier. Endocrinology. 2008 Dec 1;149(12):6251–61.

120. Huber RD, Gao B, Pfa MS, Zhang-fu W, Leuthold S, Hagenbuch B, et al. Characterization of two splice variants of human organic anion transporting polypeptide 3A1 isolated from human brain. Am J Physiol Physiol. 2007;292(2):C795–806.

121. Bakos É, Német O, Kucsma N, Tőkési N, Stieger B, Rushing E, et al. Cloning and characterization of a novel functional organic anion transporting polypeptide 3A1 isoform highly expressed in the human brain and testis. Front Pharmacol. 2022 Sep 2;13.

122. Gao B, Stieger B, Noé B, Fritschy J-M, Meier PJ. Localization of the Organic Anion Transporting Polypeptide 2 (Oatp2) in Capillary Endothelium and Choroid Plexus Epithelium of Rat Brain. J Histochem Cytochem. 1999 Oct 1;47(10):1255–63.

123. Ohtsuki S, Takizawa T, Takanaga H, Terasaki N, Kitazawa T, Sasaki M, et al. In Vitro Study of the Functional Expression of Organic Anion Transporting Polypeptide 3 at Rat Choroid Plexus Epithelial Cells and Its Involvement in the Cerebrospinal Fluid-to-Blood Transport of Estrone-3-Sulfate. Mol Pharmacol. 2003 Mar 1;63(3):532–7.

124. Cattori V, Montfoort JE, Stieger B, Landmann L, Meijer DK, Winterhalter KH, et al. Localization of organic anion transporting polypeptide 4 (Oatp4) in rat liver and comparison of its substrate specificity with Oatp1, Oatp2 and Oatp3. Pflügers Arch. 2001;443(2):188–95.

125. Kikuchi R, Kusuhara H, Abe T, Endou H, Sugiyama Y. Involvement of Multiple Transporters in the Efflux of 3-Hydroxy-3-methylglutaryl-CoA Reductase Inhibitors across the Blood-Brain Barrier. J Pharmacol Exp Ther. 2004 Dec 1;311(3):1147 LP –

1153.

126. Kikuchi A, Nozawa T, Wakasawa T, Maeda T, Tamai I. Transporter-mediated Intestinal Absorption of Fexofenadine in Rats. Drug Metab Pharmacokinet. 2006;21(4):308–14.

127. Shirasaka Y, Suzuki K, Nakanishi T, Tamai I. Differential Effect of Grapefruit Juice on Intestinal Absorption of Statins Due to Inhibition of Organic Anion Transporting Polypeptide and/or P-glycoprotein. J Pharm Sci. 2011;100(9):3843–53.

128. Liu H, Yu N, Lu S, Ito S, Zhang X, Prasad B, et al. Solute Carrier Family of the Organic Anion-Transporting Polypeptides 1A2–Madin-Darby Canine Kidney II: A Promising In Vitro System to Understand the Role of Organic Anion-Transporting Polypeptide 1A2 in Blood-Brain Barrier Drug Penetration. Drug Metab Dispos. 2015;43(7):1008–18.

129. Robey RW, Pluchino KM, Hall MD, Fojo AT, Bates SE, Gottesman MM. Revisiting the role of ABC transporters in multidrug-resistant cancer. Nat Rev Cancer. 2018;18(7):452–64.

130. Kim RB. Drugs as P-glycoprotein substrates, inhibitors, and inducers. Drug Metab Rev. 2002 Jan 1;34(1–2):47–54.

131. Mao Q, Unadkat JD. Role of the Breast Cancer Resistance Protein (BCRP/ABCG2) in Drug Transport—an Update. AAPS J. 2015;17(1):65–82.

132. Mizutani T, Masuda M, Nakai E, Furumiya K, Togawa H, Nakamura Y, et al. Genuine Functions of P-Glycoprotein (ABCB1). Curr Drug Metab. 2008;9(2).

133. Vlaming MLH, Lagas JS, Schinkel AH. Physiological and pharmacological roles of ABCG2 (BCRP): Recent findings in Abcg2 knockout mice. Adv Drug Deliv Rev. 2009;61(1):14–25.

134. Jonker JW, Merino G, Musters S, van Herwaarden AE, Bolscher E, Wagenaar E, et al.

The breast cancer resistance protein BCRP (ABCG2) concentrates drugs and carcinogenic xenotoxins into milk. Nat Med. 2005;11(2):127–9.

135. Fuchs H, Kishimoto W, Gansser D, Tanswell P, Ishiguro N. Brain Penetration of WEB 2086 (Apafant) and Dantrolene in Mdr1a (P-Glycoprotein) and Bcrp Knockout Rats. Drug Metab Dispos. 2014 Oct 1;42(10):1761 LP – 1765.

136. Polli JW, Olson KL, Chism JP, John-Williams L St., Yeager RL, Woodard SM, et al. An Unexpected Synergist Role of P-Glycoprotein and Breast Cancer Resistance Protein on the Central Nervous System Penetration of the Tyrosine Kinase Inhibitor Lapatinib (N-{3-Chloro-4-[(3-fluorobenzyl)oxy]phenyl}-6-[5-({[2-(methylsulfonyl)ethyl]amino}meth. Drug Metab Dispos. 2009 Feb 1;37(2):439 LP – 442.

137. Tachikawa M, Watanabe M, Hori S, Fukaya M, Ohtsuki S, Asashima T, et al. Distinct spatio-temporal expression of ABCA and ABCG transporters in the developing and adult mouse brain. J Neurochem. 2005 Oct 1;95(1):294–304.

138. Zhuang Y, Fraga CH, Hubbard KE, Hagedorn N, Panetta JC, Waters CM, et al. Topotecan Central Nervous System Penetration Is Altered by a Tyrosine Kinase Inhibitor. Cancer Res. 2006 Dec 4;66(23):11305–13.

139. Ek CJ, Wong A, Liddelow SA, Johansson PA, Dziegielewska KM, Saunders NR. Efflux mechanisms at the developing brain barriers: ABC-transporters in the fetal and postnatal rat. Toxicol Lett. 2010;197(1):51–9.

140. Daood M, Tsai C, Ahdab-Barmada M, Watchko JF. ABC transporter (P-gp/ABCB1, MRP1/ABCC1, BCRP/ABCG2) expression in the developing human CNS. Neuropediatrics. 2009/01/22. 2008 Aug;39(4):211–8.

141. Roberts LM, Black DS, Raman C, Woodford K, Zhou M, Haggerty JE, et al. Subcellular

localization of transporters along the rat blood–brain barrier and blood–cerebral-spinal fluid barrier by in vivo biotinylation. Neuroscience. 2008 Aug 13;155(2):423–38.

142. Verscheijden LFM, van Hattem AC, Pertijs JCLM, de Jongh CA, Verdijk RM, Smeets B, et al. Developmental patterns in human blood–brain barrier and blood–cerebrospinal fluid barrier ABC drug transporter expression. Histochem Cell Biol. 2020;154(3):265–73.

143. Baehr C, Reichel V, Fricker G. Choroid plexus epithelial monolayers – a cell culture model from porcine brain. Cerebrospinal Fluid Res. 2006;3(1):13.

144. Bernd A, Ott M, Ishikawa H, Schroten H, Schwerk C, Fricker G. Characterization of efflux transport proteins of the human choroid plexus papilloma cell line HIBCPP, a functional in vitro model of the blood-cerebrospinal fluid barrier. Pharm Res. 2015;32(9):2973–82.

145. Hammarlund-Udenaes M. Microdialysis in CNS PKPD Research: Unraveling Unbound Concentrations BT - Microdialysis in Drug Development. In: Müller M, editor. New York, NY: Springer New York; 2013. p. 83–102.

146. Watson J, Wright S, Lucas A, Clarke KL, Viggers J, Cheetham S, et al. Receptor Occupancy and Brain Free Fraction. Drug Metab Dispos. 2009 Apr 1;37(4):753 LP – 760.

147. Lin JH. CSF as a Surrogate for Assessing CNS Exposure: An Industrial Perspective. Curr Drug Metab. 2008;9(1):46–59.

148. Nagaya Y, Katayama K, Kusuhara H, Nozaki Y. Impact of P-Glycoprotein–Mediated Active Efflux on Drug Distribution into Lumbar Cerebrospinal Fluid in Nonhuman Primates. Drug Metab Dispos. 2020 Nov 1;48(11):1183–90.

149. Yaguchi Y, Tachikawa M, Zhang Z, Terasaki T. Organic Anion-Transporting Polypeptide 1a4 (Oatp1a4/Slco1a4) at the Blood–Arachnoid Barrier is the Major Pathway of

Sulforhodamine-101 Clearance from Cerebrospinal Fluid of Rats. Mol Pharm. 2019;4:acs.molpharmaceut.9b00005.

150. Kido Y, Nanchi I, Fusamae Y, Matsuzaki T, Akazawa T, Sawada H, et al. Species difference in brain penetration of P-gp and BCRP substrates among monkey, dog and mouse. Drug Metab Pharmacokinet. 2022;42:100426.

151. Lange ECM de, Chang HY, Shah D. Approaches Towards Prediction of CNS PK and PD BT - Drug Delivery to the Brain: Physiological Concepts, Methodologies and Approaches. In: de Lange ECM, Hammarlund-Udenaes M, Thorne RG, editors. Cham: Springer International Publishing; 2022. p. 353–86.

152. Betts JG, Young KA, Wise JA, Johnson E, Poe B, Kruse DH, et al. Circulation and the Central Nervous System. In: Anatomy and Physiology. Houston: OpenStax; 2013.

153. Cha SH, Sekine T, Fukushima J, Kanai Y, Kobayashi Y, Goya T, et al. Identification and Characterization of Human Organic Anion Transporter 3 Expressing Predominantly in the Kidney. Mol Pharmacol. 2001 May 1;59(5):1277 LP – 1286.

154. Matsumoto S, Yoshida K, Ishiguro N, Maeda T, Tamai I. Involvement of Rat and Human Organic Anion Transporter 3 in the Renal Tubular Secretion of Topotecan [(S)-9-Dimethylaminomethyl-10-hydroxy-camptothecin hydrochloride]. J Pharmacol Exp Ther. 2007 Sep 1;322(3):1246 LP – 1252.

155. Takeda M, Khamdang S, Narikawa S, Kimura H, Kobayashi Y, Yamamoto T, et al. Human Organic Anion Transporters and Human Organic Cation Transporters Mediate Renal Antiviral Transport. J Pharmacol Exp Ther. 2002 Mar 1;300(3):918 LP – 924.

156. Tahara H, Shono M, Kusuhara H, Kinoshita H, Fuse E, Takadate A, et al. Molecular Cloning and Functional Analyses of OAT1 and OAT3 from Cynomolgus Monkey Kidney.

Pharm Res. 2005;22(4):647–60.

157. Ueo H, Motohashi H, Katsura T, Inui K. Human organic anion transporter hOAT3 is a potent transporter of cephalosporin antibiotics, in comparison with hOAT1. Biochem Pharmacol. 2005;70(7):1104–13.

158. Yin J, Wagner DJ, Prasad B, Isoherranen N, Thummel KE, Wang J. Renal secretion of hydrochlorothiazide involves organic anion transporter 1/3, organic cation transporter 2, and multidrug and toxin extrusion protein 2-K. Am J Physiol Physiol. 2019 Jul 19;317(4):F805–14.

159. Ebner T, Ishiguro N, Taub ME. The Use of Transporter Probe Drug Cocktails for the Assessment of Transporter-Based Drug-Drug Interactions in a Clinical Setting - Proposal of a Four Component Transporter Cocktail. J Pharm Sci. 2015 Sep 1;104(9):3220–8.

160. Mimura Y, Yasujima T, Ohta K, Inoue K, Yuasa H. Functional Identification of Plasma Membrane Monoamine Transporter (PMAT/SLC29A4) as an Atenolol Transporter Sensitive to Flavonoids Contained in Apple Juice. J Pharm Sci. 2017 Sep 1;106(9):2592–8.

161. Song F, Hu Y, Jiang H, Smith DE. Species Differences in Human and Rodent PEPT2-Mediated Transport of Glycylsarcosine and Cefadroxil in Pichia Pastoris Transformants. Drug Metab Dispos. 2017 Feb 1;45(2):130 LP – 136.

162. Li M, Anderson GD, Phillips BR, Kong W, Shen DD, Wang J. Interactions of amoxicillin and cefaclor with human renal organic anion and peptide transporters. Drug Metab Dispos. 2006 Apr 1;34(4):547 LP – 555.

163. Zaman GJ, Flens MJ, van Leusden MR, de Haas M, Mülder HS, Lankelma J, et al. The human multidrug resistance-associated protein MRP is a plasma membrane drug-efflux

pump. Proc Natl Acad Sci. 1994 Sep 13;91(19):8822 LP – 8826.

164. Zeng H, Chen Z-S, Belinsky MG, Rea PA, Kruh GD. Transport of Methotrexate (MTX) and Folates by Multidrug Resistance Protein (MRP) 3 and MRP1. Cancer Res. 2001 Oct 1;61(19):7225 LP – 7232.

165. Knauer MJ, Urquhart BL, Meyer zu Schwabedissen HE, Schwarz UI, Lemke CJ, Leake BF, et al. Human skeletal muscle drug transporters determine local exposure and toxicity of statins. Circ Res. 2010 Feb;106(2):297–306.

166. van der Sandt IC, Vos CM, Nabulsi L, Blom-Roosemalen MC, Voorwinden HH, de Boer AG, et al. Assessment of active transport of HIV protease inhibitors in various cell lines and the in vitro blood-brain barrier. AIDS. 2001 Mar;15(4):483–91.

167. de Waart DR, van de Wetering K, Kunne C, Duijst S, Paulusma CC, Oude Elferink RPJ. Oral availability of cefadroxil depends on ABCC3 and ABCC4. Drug Metab Dispos. 2012 Mar;40(3):515–21.

168. Chen Z-S, Lee K, Walther S, Raftogianis RB, Kuwano M, Zeng H, et al. Analysis of methotrexate and folate transport by multidrug resistance protein 4 (ABCC4): MRP4 is a component of the methotrexate efflux system. Cancer Res. 2002 Jun;62(11):3144–50.

169. Tian Q, Zhang J, Chan SY, Chin Tan, Theresa M., Duan W, et al. Topotecan Is a Substrate for Multidrug Resistance Associated Protein 4. Curr Drug Metab. 2006;7(1):105–18.

170. Chen ZS, Lee K, Kruh GD. Transport of cyclic nucleotides and estradiol 17-beta-D-glucuronide by multidrug resistance protein 4. Resistance to 6-mercaptopurine and 6-thioguanine. J Biol Chem. 2001 Sep;276(36):33747–54.

171. Imaoka T, Kusuhara H, Adachi M, Schuetz JD, Takeuchi K, Sugiyama Y. Functional

Involvement of Multidrug Resistance-Associated Protein 4 (MRP4/ABCC4) in the Renal Elimination of the Antiviral Drugs Adefovir and Tenofovir. Mol Pharmacol. 2007 Feb 1;71(2):619 LP – 627.

172. Ci L, Kusuhara H, Adachi M, Schuetz JD, Takeuchi K, Sugiyama Y. Involvement of MRP4 (ABCC4) in the luminal efflux of ceftizoxime and cefazolin in the kidney. Mol Pharmacol. 2007 Jun;71(6):1591–7.

173. Hasegawa M, Kusuhara H, Adachi M, Schuetz JD, Takeuchi K, Sugiyama Y. Multidrug Resistance–Associated Protein 4 Is Involved in the Urinary Excretion of Hydrochlorothiazide and Furosemide. J Am Soc Nephrol. 2007 Jan 1;18(1):37 LP – 45.

174. Sun A, Wang J. Choroid Plexus and Drug Removal Mechanisms. AAPS J. 2021;23(3):61.

175. Hurley J V, McD. Anderson R, Sexton PT. The fate of plasma protein which escapes from blood vessels of the choroid plexus of the rat–an electron microscope study. J Pathol. 1981 May 1;134(1):57–70.

176. Ghersi-Egea J-F, Gorevic PD, Ghiso J, Frangione B, Patlak CS, Fenstermacher JD. Fate of Cerebrospinal Fluid-Borne Amyloid β-Peptide: Rapid Clearance into Blood and Appreciable Accumulation by Cerebral Arteries. J Neurochem. 1996 Aug 1;67(2):880–3.

177. Ocheltree SM. Mechanisms of Cefadroxil Uptake in the Choroid Plexus: Studies in Wild-Type and PEPT2 Knockout Mice. J Pharmacol Exp Ther. 2004;308(2):462–7.

178. Duan H, Hu T, Foti RS, Pan Y, Swaan PW, Wang J. Potent and Selective Inhibition of Plasma Membrane Monoamine Transporter by HIV Protease Inhibitors. Drug Metab Dispos. 2015 Nov 1;43(11):1773–80.

179. Miller DS. Confocal imaging of xenobiotic transport across the choroid plexus. Adv Drug Deliv Rev. 2004;56(12):1811–24.

180. Yasuda K, Ganguly S, Schuetz EG. Pheophorbide A: Fluorescent Bcrp Substrate to Measure Oral Drug-Drug Interactions in Real-Time In Vivo. Drug Metab Dispos. 2018 Nov 1;46(11):1725 LP – 1733.

181. Ryan JC, Dunn KW, Decker BS. Effects of chronic kidney disease on liver transport: quantitative intravital microscopy of fluorescein transport in the rat liver. Am J Physiol Integr Comp Physiol. 2014 Oct 22;307(12):R1488–92.

182. Breen CM, Sykes DB, Fricker G, Miller DS. Confocal imaging of organic anion transport in intact rat choroid plexus. Am J Physiol Physiol. 2002 May 1;282(5):F877–85.

183. Baehr CH, Fricker G, Miller DS. Fluorescein-methotrexate transport in dogfish shark (Squalus acanthias) choroid plexus. Am J Physiol Integr Comp Physiol. 2006 Aug 1;291(2):R464–72.

184. Schindelin J, Arganda-Carreras I, Frise E, Kaynig V, Longair M, Pietzsch T, et al. Fiji: an open-source platform for biological-image analysis. Nat Methods. 2012;9(7):676–82.

185. Patik I, Kovacsics D, Német O, Gera M, Várady G, Stieger B, et al. Functional expression of the 11 human Organic Anion Transporting Polypeptides in insect cells reveals that sodium fl uorescein is a general OATP substrate. Biochem Pharmacol. 2015;98(4):649–58.

186. Izumi S, Nozaki Y, Komori T, Takenaka O, Maeda K, Kusuhara H, et al. Investigation of Fluorescein Derivatives as Substrates of Organic Anion Transporting Polypeptide (OATP) 1B1 to Develop Sensitive Fluorescence-Based OATP1B1 Inhibition Assays. Mol Pharm. 2016;13(2):438–48.

187. Bednarczyk D. Fluorescence-based assays for the assessment of drug interaction with the human transporters OATP1B1 and OATP1B3. Anal Biochem. 2010;405(1):50–8.

188. Székely V, Patik I, Ungvári O, Telbisz Á, Szakács G, Bakos É, et al. Fluorescent probes for the dual investigation of MRP2 and OATP1B1 function and drug interactions. Eur J Pharm Sci. 2020;151:105395.

189. Pritchard JB, Sweet DH, Miller DS, Walden R. Mechanism of Organic Anion Transport across the Apical Membrane of Choroid Plexus. J Biol Chem. 1999 Nov 19;274(47):33382–7.

190. Breen CM, Sykes DB, Baehr C, Fricker G, Miller DS. Fluorescein-methotrexate transport in rat choroid plexus analyzed using confocal microscopy. Am J Physiol Physiol. 2004 Sep 1;287(3):F562–9.

191. Karlgren M, Vildhede A, Norinder U, Wisniewski JR, Kimoto E, Lai Y, et al. Classification of inhibitors of hepatic organic anion transporting polypeptides (OATPs): influence of protein expression on drug-drug interactions. J Med Chem. 2012 May;55(10):4740–63.

192. Syvänen S, Lindhe Ö, Palner M, Kornum BR, Rahman O, Långström B, et al. Species Differences in Blood-Brain Barrier Transport of Three Positron Emission Tomography Radioligands with Emphasis on P-Glycoprotein Transport. Drug Metab Dispos. 2009 Mar 1;37(3):635 LP – 643.

193. Gaigalas AK, Li L, Henderson O, Vogt R, Barr J, Marti G, et al. The Development of Fluorescence Intensity Standards. J Res Natl Inst Stand Technol. 2001 Apr 1;106(2):381–9.

194. Shipley FB, Dani N, Xu H, Deister C, Cui J, Head JP, et al. Tracking Calcium Dynamics and Immune Surveillance at the Choroid Plexus Blood-Cerebrospinal Fluid Interface. Neuron. 2020;108(4):623-639.e10.

195. Babbey CM, Ryan JC, Gill EM, Ghabril MS, Burch CR, Paulman A, et al. Quantitative intravital microscopy of hepatic transport. IntraVital. 2012 Jul 1;1(1):44–53.

196. Feigin VL, Vos T, Nichols E, Owolabi MO, Carroll WM, Dichgans M, et al. The global burden of neurological disorders: translating evidence into policy. Lancet Neurol. 2020 Mar 1;19(3):255–65.

197. Gribkoff VK, Kaczmarek LK. The need for new approaches in CNS drug discovery: Why drugs have failed, and what can be done to improve outcomes. Neuropharmacology. 2017;120:11–9.

198. de Lange ECM. The mastermind approach to CNS drug therapy: translational prediction of human brain distribution, target site kinetics, and therapeutic effects. Fluids Barriers CNS. 2013;10(1):12.

199. de Lange ECM. Utility of CSF in translational neuroscience. J Pharmacokinet Pharmacodyn. 2013;40(3):315–26.

200. Sun A, Wang J. Evaluation of Blood-CSF Barrier Transport by Quantitative Real Time Fluorescence Microscopy. Pharm Res. 2022;39(7):1469–80.

201. van de Steeg E, Wagenaar E, van der Kruijssen CMM, Burggraaff JEC, de Waart DR, Elferink RPJO, et al. Organic anion transporting polypeptide 1a/1b–knockout mice provide insights into hepatic handling of bilirubin, bile acids, and drugs. J Clin Invest. 2010 Aug 2;120(8):2942–52.

202. López Quiñones AJ, Wagner DJ, Wang J. Characterization of Meta-Iodobenzylguanidine (mIBG) Transport by Polyspecific Organic Cation Transporters: Implication for mIBG Therapy. Mol Pharmacol. 2020 Aug 1;98(2):109–19.

203. Bakos É, Német O, Patik I, Kucsma N, Várady G, Szakács G, et al. A novel fluorescence-

based functional assay for human OATP1A2 and OATP1C1 identifies interaction between third-generation P-gp inhibitors and OATP1A2. FEBS J. 2020 Jun 1;287(12):2468–85.

204. Csanaky IL, Lu H, Zhang Y, Ogura K, Choudhuri S, Klaassen CD. Organic anion–transporting polypeptide 1b2 (Oatp1b2) is important for the hepatic uptake of unconjugated bile acids: Studies in Oatp1b2-null mice. Hepatology. 2011 Jan 1;53(1):272–81.

205. Kimura T, Allen PB, Nairn AC, Caplan MJ. Arrestins and Spinophilin Competitively Regulate Na+,K+-ATPase Trafficking through Association with a Large Cytoplasmic Loop of the Na+,K+-ATPase. Mol Biol Cell. 2007 Sep 5;18(11):4508–18.

206. Praetorius J, Nielsen S. Distribution of sodium transporters and aquaporin-1 in the human choroid plexus. Am J Physiol Physiol. 2006 Jul 1;291(1):C59–67.

207. Mayerl S, Visser TJ, Darras VM, Horn S, Heuer H. Impact of Oatp1c1 Deficiency on Thyroid Hormone Metabolism and Action in the Mouse Brain. Endocrinology. 2012 Mar 1;153(3):1528–37.

208. Thompson BJ, Sanchez-Covarrubias L, Slosky LM, Zhang Y, Laracuente M, Ronaldson PT. Hypoxia/Reoxygenation Stress Signals an Increase in Organic Anion Transporting polypeptide 1a4 (Oatp1a4) at the Blood–Brain Barrier: Relevance to CNS Drug Delivery. J Cereb Blood Flow Metab. 2014 Jan 29;34(4):699–707.

209. Reichel V, Miller DS, Fricker G. Texas Red transport across rat and dogfish shark (Squalus acanthias) choroid plexus. Am J Physiol Integr Comp Physiol. 2008 Oct 1;295(4):R1311–9.

210. Kullak-Ublick G-A, Fisch T, Oswald M, Hagenbuch B, Meier PJ, Beuers U, et al. Dehydroepiandrosterone sulfate (DHEAS): identification of a carrier protein in human

liver and brain. FEBS Lett. 1998;424(3):173–6.

211. Maninger N, Wolkowitz OM, Reus VI, Epel ES, Mellon SH. Neurobiological and neuropsychiatric effects of dehydroepiandrosterone (DHEA) and DHEA sulfate (DHEAS). Front Neuroendocrinol. 2009 Jan 1;30(1):65–91.

212. Corpéchot C, Robel P, Axelson M, Sjövall J, Baulieu EE. Characterization and measurement of dehydroepiandrosterone sulfate in rat brain. Proc Natl Acad Sci. 1981 Aug 1;78(8):4704–7.

213. Roth M, Obaidat A, Hagenbuch B. OATPs, OATs and OCTs: the organic anion and cation transporters of the SLCO and SLC22A gene superfamilies. Br J Pharmacol. 2012 Mar 1;165(5):1260–87.

214. Leib SL, Täuber MG. PATHOGENESIS OF BACTERIAL MENINGITIS. Infect Dis Clin North Am. 1999;13(3):527–48.

215. Lutsar I, Friedland IR. Pharmacokinetics and Pharmacodynamics of Cephalosporins in Cerebrospinal Fluid. Clin Pharmacokinet. 2000;39(5):335–43.

216. Yamaguchi H, Takeuchi T, Okada M, Kobayashi M, Unno M, Abe T, et al. Screening of Antibiotics That Interact with Organic Anion-Transporting Polypeptides 1B1 and 1B3 Using Fluorescent Probes. Biol Pharm Bull. 2011;34(3):389–95.

217. Cheng Z, Liu H, Yu N, Wang F, An G, Xu Y, et al. Hydrophilic anti-migraine triptans are substrates for OATP1A2, a transporter expressed at human blood-brain barrier. Xenobiotica. 2012 Sep 1;42(9):880–90.

218. Whyte-Allman S-K, Bendayan R. HIV-1 Sanctuary Sites—the Role of Membrane-Associated Drug Transporters and Drug Metabolic Enzymes. AAPS J. 2020;22(5):118.

219. Aragon-Ching JB, Zujewski JA. CNS Metastasis: An Old Problem in a New Guise. Clin

Cancer Res. 2007 Mar 15;13(6):1644–7.

220. Agarwal S, Hartz AMS, Elmquist WF, Bauer B. Breast cancer resistance protein and P-glycoprotein in brain cancer: two gatekeepers team up. Curr Pharm Des. 2011;17(26):2793–802.

221. Schinkel AH, Mayer U, Wagenaar E, Mol CAAM, van Deemter L, Smit JJM, et al. Normal viability and altered pharmacokinetics in mice lacking mdr1-type (drug-transporting) P-glycoproteins. Proc Natl Acad Sci. 1997 Apr 15;94(8):4028–33.

222. Jonker JW, Buitelaar M, Wagenaar E, van der Valk MA, Scheffer GL, Scheper RJ, et al. The breast cancer resistance protein protects against a major chlorophyll-derived dietary phototoxin and protoporphyria. Proc Natl Acad Sci. 2002 Nov 26;99(24):15649–54.

223. Cui YJ, Cheng X, Weaver YM, Klaassen CD. Tissue Distribution, Gender-Divergent Expression, Ontogeny, and Chemical Induction of Multidrug Resistance Transporter Genes (Mdr1a, Mdr1b, Mdr2) in Mice. Drug Metab Dispos. 2009 Jan 1;37(1):203 LP – 210.

224. Holló Z, Homolya L, Davis CW, Sarkadi B. Calcein accumulation as a fluorometric functional assay of the multidrug transporter. Biochim Biophys Acta - Biomembr. 1994;1191(2):384–8.

225. Glavinas H, von Richter O, Vojnits K, Mehn D, Wilhelm I, Nagy T, et al. Calcein assay: a high-throughput method to assess P-gp inhibition. Xenobiotica. 2011 Aug 1;41(8):712–9.

226. Dey S, Ramachandra M, Pastan I, Gottesman MM, Ambudkar S V. Evidence for two nonidentical drug-interaction sites in the human P-glycoprotein. Proc Natl Acad Sci. 1997 Sep 30;94(20):10594–9.

227. de Bruin M, Miyake K, Litman T, Robey R, Bates SE. Reversal of resistance by

GF120918 in cell lines expressing the ABC half-transporter, MXR. Cancer Lett. 1999;146(2):117–26.

228. Hyafil F, Vergely C, Du Vignaud P, Grand-Perret T. In Vitro and in Vivo Reversal of Multidrug Resistance by GF120918, an Acridonecarboxamide Derivative. Cancer Res. 1993 Oct 1;53(19):4595–602.

229. de Vries NA, Zhao J, Kroon E, Buckle T, Beijnen JH, van Tellingen O. P-Glycoprotein and Breast Cancer Resistance Protein: Two Dominant Transporters Working Together in Limiting the Brain Penetration of Topotecan. Clin Cancer Res. 2007 Nov;13(21):6440–9.

230. Chen Y, Agarwal S, Shaik NM, Chen C, Yang Z, Elmquist WF. P-glycoprotein and Breast Cancer Resistance Protein Influence Brain Distribution of Dasatinib. J Pharmacol Exp Ther. 2009 Sep 1;330(3):956 LP – 963.

231. Agarwal S, Sane R, Gallardo JL, Ohlfest JR, Elmquist WF. Distribution of Gefitinib to the Brain Is Limited by P-glycoprotein (ABCB1) and Breast Cancer Resistance Protein (ABCG2)-Mediated Active Efflux. J Pharmacol Exp Ther. 2010 Jul 1;334(1):147 LP – 155.

232. Lagas JS, van Waterschoot RAB, Sparidans RW, Wagenaar E, Beijnen JH, Schinkel AH. Breast Cancer Resistance Protein and P-glycoprotein Limit Sorafenib Brain Accumulation. Mol Cancer Ther. 2010 Feb 9;9(2):319–26.

233. Lee Y-J, Kusuhara H, Jonker JW, Schinkel AH, Sugiyama Y. Investigation of Efflux Transport of Dehydroepiandrosterone Sulfate and Mitoxantrone at the Mouse Blood-Brain Barrier: A Minor Role of Breast Cancer Resistance Protein. J Pharmacol Exp Ther. 2005 Jan 1;312(1):44 LP – 52.

234. Kodaira H, Kusuhara H, Ushiki J, Fuse E, Sugiyama Y. Kinetic Analysis of the

Cooperation of P-Glycoprotein (P-gp/Abcb1) and Breast Cancer Resistance Protein (Bcrp/Abcg2) in Limiting the Brain and Testis Penetration of Erlotinib, Flavopiridol, and Mitoxantrone. J Pharmacol Exp Ther. 2010 Jun 1;333(3):788 LP – 796.

235. Agarwal S, Uchida Y, Mittapalli RK, Sane R, Terasaki T, Elmquist WF. Quantitative Proteomics of Transporter Expression in Brain Capillary Endothelial Cells Isolated from P-Glycoprotein (P-gp), Breast Cancer Resistance Protein (Bcrp), and P-gp/Bcrp Knockout Mice. Drug Metab Dispos. 2012 Jun 1;40(6):1164 LP – 1169.

236. Allen JD, van Loevezijn A, Lakhai JM, van der Valk M, van Tellingen O, Reid G, et al. Potent and Specific Inhibition of the Breast Cancer Resistance Protein Multidrug Transporter in Vitro and in Mouse Intestine by a Novel Analogue of Fumitremorgin C1. Mol Cancer Ther. 2002 Apr 1;1(6):417–25.

237. Weidner LD, Zoghbi SS, Lu S, Shukla S, Ambudkar S V, Pike VW, et al. The Inhibitor Ko143 Is Not Specific for ABCG2. J Pharmacol Exp Ther. 2015 Sep 1;354(3):384–93.

238. Mairinger S, Zoufal V, Wanek T, Traxl A, Filip T, Sauberer M, et al. Influence of breast cancer resistance protein and P-glycoprotein on tissue distribution and excretion of Ko143 assessed with PET imaging in mice. Eur J Pharm Sci. 2018;115:212–22.

239. Mao Q. Role of the breast cancer resistance protein (ABCG2) in drug transport. AAPS J. 2005;7(1):E118–33.

240. Litman T, Brangi M, Hudson E, Fetsch P, Abati A, Ross DD, et al. The multidrug-resistant phenotype associated with overexpression of the new ABC half-transporter, MXR (ABCG2). J Cell Sci. 2000 Jun 1;113(11):2011–21.

241. Jani M, Ambrus C, Magnan R, Jakab KT, Beéry E, Zolnerciks JK, et al. Structure and function of BCRP, a broad specificity transporter of xenobiotics and endobiotics. Arch

Toxicol. 2014;88(6):1205–48.

242. Ghersi-Egea J-F, Vasiljevic A, Blondel S, Strazielle N. Neuroprotective Mechanisms at the Blood-CSF Barrier of the Developing and Adult Brain BT - Role of the Choroid Plexus in Health and Disease. In: Praetorius J, Blazer-Yost B, Damkier H, editors. New York, NY: Springer US; 2020. p. 193–207.

243. Storelli F, Yin M, Kumar AR, Ladumor MK, Evers R, Chothe PP, et al. The next frontier in ADME science: Predicting transporter-based drug disposition, tissue concentrations and drug-drug interactions in humans. Pharmacol Ther. 2022;238:108271.

244. Spector R. Ceftriaxone pharmacokinetics in the central nervous system. J Pharmacol Exp Ther. 1986 Feb 1;236(2):380 LP – 383.

245. Nau R, Prange HW, Muth P, Mahr G, Menck S, Kolenda H, et al. Passage of cefotaxime and ceftriaxone into cerebrospinal fluid of patients with uninflamed meninges. Antimicrob Agents Chemother. 1993;37(7):1518–24.

246. Chandrasekar PH, Rolston KVI, Smith BR, LeFrock JL. Diffusion of ceftriaxone into the cerebrospinal fluid of adults. J Antimicrob Chemother. 1984 Oct 1;14(4):427–30.

247. Smith DE, Hu Y, Shen H, Nagaraja TN, Fenstermacher JD, Keep RF. Distribution of glycylsarcosine and cefadroxil among cerebrospinal fluid, choroid plexus, and brain parenchyma after intracerebroventricular injection is markedly different between wild-type and Pept2 null mice. J Cereb Blood Flow Metab. 2011 Jan;31(1):250–61.

248. Goh L-B, Spears KJ, Yao D, Ayrton A, Morgan P, Roland Wolf C, et al. Endogenous drug transporters in in vitro and in vivo models for the prediction of drug disposition in man. Biochem Pharmacol. 2002;64(11):1569–78.

249. Møllgård K, Dziegielewska KM, Holst CB, Habgood MD, Saunders NR. Brain barriers

and functional interfaces with sequential appearance of ABC efflux transporters during human development. Sci Rep. 2017;7(1):11603.